



Universitat Autònoma de Barcelona

**ADVERTIMENT.** L'accés als continguts d'aquesta tesi queda condicionat a l'acceptació de les condicions d'ús establertes per la següent llicència Creative Commons:  [http://cat.creativecommons.org/?page\\_id=184](http://cat.creativecommons.org/?page_id=184)

**ADVERTENCIA.** El acceso a los contenidos de esta tesis queda condicionado a la aceptación de las condiciones de uso establecidas por la siguiente licencia Creative Commons:  <http://es.creativecommons.org/blog/licencias/>

**WARNING.** The access to the contents of this doctoral thesis it is limited to the acceptance of the use conditions set by the following Creative Commons license:  <https://creativecommons.org/licenses/?lang=en>



Departamento de Química  
Facultad de Ciencias

Julio 2019

# **Clinical diagnosis and pathogen detection with a novel multiplexed nanophotonic point-of-care biosensor**

Tesis Doctoral

**Nuria Fabri Faja**  
Autora

**Prof. Laura M. Lechuga**

**Dr. M<sup>a</sup>Carmen Estévez**

Directoras

**Dr. Julian Alonso Chamarro**

Tutor





Memòria presentada per aspirar al Grau de Doctor per Nuria Fabri Faja

Vist i plau:

Prof. Laura M. Lechuga  
Nanobiosensors and Bioanalytical Applications  
Instituto Catalán de Nanociencia y Nanotecnología (ICN2)

M<sup>a</sup>Carmen Estévez  
Nanobiosensors and Bioanalytical Applications  
Instituto Catalán de Nanociencia y Nanotecnología (ICN2)

Julian Alonso Chamarro  
Departament de Química  
Universitat Autònoma de Barcelona

Bellaterra, 11 de Julio de 2019



A mis padres



# Abstract

This Doctoral Thesis focuses on a novel point-of-care device based on a nanophotonic microarray biosensor for the direct and label-free quantification of multiple clinical biomarkers for clinical diagnosis and pathogen detection directly on patient's sample. The recently developed biosensor is a new large-field-of-view interferometric microscope which measures phase shifts upon changes in refractive indexes.

Firstly, the optical physics behind the novel device and its feasibility to be used for biomolecules detection and quantification have been evaluated. Then, several analytical assays based on the use antibodies as bioreceptors have been developed and their performance evaluated. Finally, with the aim of using it as a specific biosensor, the immunoassay that showed the best performance has been applied to actual biomarker detection. Specifically, the biomarkers selected are related with the diagnosis of sepsis, a clinical condition characterized for a grave whole-body inflammatory response caused by an infection. There is an urgent need for fast diagnosis of sepsis because this condition is currently the main cause of death in Intensive Care Units and its incidence is increasing worldwide with a mortality rate between 40 to 50% in developed countries.

The work in this Thesis combines the wide knowledge of the research group in the design and creation of biofunctionalised surfaces and the implementation of bioanalytical techniques to achieve cheap, fast and robust biosensors that overcome current challenges related to costly and time-consuming clinical analysis.





## Resumen

El trabajo que recoge esta tesis doctoral se centra en el estudio y aplicación de un nuevo biosensor nanofotónico con configuración de *microarray* en formato *point-of-care* para la detección y cuantificación directa y sin marcaje de varios biomarcadores clínicos y microorganismos patógenos. Este nuevo biosensor está basado en un microscopio interferométrico con un campo visual amplio que mide cambios en la fase en la luz producidos por variaciones en índices de refracción.

Para ello, primero, se ha profundizado en la óptica del dispositivo para evaluar el potencial del dispositivo para la detección y cuantificación de biomoléculas. Posteriormente, se han desarrollado varios inmunoensayos en formato directo (usando anticuerpos como bioreceptores) basados en diferentes técnicas de biofuncionalización. A partir de las mejores condiciones, se ha desarrollado una estrategia reproducible que ha sido empleada para la detección de un panel de biomarcadores de interés clínico. Estos biomarcadores están relacionados con el diagnóstico de sepsis, una afección médica grave que se caracteriza por una reacción inflamatoria sistémica producida por una infección. Actualmente existe la necesidad urgente de establecer un diagnóstico rápido de la sepsis puesto que se trata de la principal causa de muerte en las unidades de cuidados intensivos de los hospitales (tasas de mortalidad entre un 40 y 50% en países desarrollados).

Esta Tesis Doctoral combina los conocimientos del grupo de investigación en el ámbito del diseño y preparación de superficies biofuncionalizadas y en su implementación en el desarrollo de biosensores sencillos, rápidos y económicos como técnicas bioanalíticas competitivas con las técnicas convencionales usadas actualmente en diagnóstico clínico.



## Acknowledgments

This is my favourite section in thesis manuscripts. In my opinion this is the most honest part and the one that tells you how the PhD years have gone through the life of the student. A PhD is not only an academic degree but also an obstacle race against deadlines, non-expected issues, learning new skills, acquiring new knowledge and above all, knowing yourself better.

Para empezar me gustaría dar las gracias a la **Profesora Laura Lechuga** por darme la oportunidad de hacer este doctorado. Gracias por confiar en mí desde el primer momento, por apoyarme y por ayudarme durante toda esta aventura. Gracias por los congresos, los viajes y todas las experiencias que hemos vivido juntas a lo largo y ancho de este mundo. Gracias porque he podido aprender muchísimo de ti, no solo como científica si no, también, en muchos otros ámbitos de la vida.

Para continuar tengo que también darle infinitas gracias a **Mari Carmen** por ser mi guía y supervisora durante el proyecto y el doctorado. Gracias por enseñarme tanto y por tener tanta paciencia conmigo. Gracias por exigirme tanto para, finalmente, poder sacar lo mejor de mí.

Quiero dar las gracias a todo **el equipo del RAIS**, especialmente a Josselin, a Pieterjan y a Roland. Gracias también al resto de integrantes del proyecto por poner su granito de arena o dinamita, de todos ellos he aprendido algo y me llevo una lección a casa. También dar las gracias a la Unión Europea por crear el programa de financiación Horizonte 2020 que promueve la investigación e innovación para asegurar la competitividad global de Europa.

I want to thank all my colleagues from the **nanob2a group**: Patri, Cristina, Berto, Roger, Blanca, Jessica and Alejandro. Very special thanks to Olalla and Priyanka for working together and supporting and understanding each other along the project. Also, big thanks to all the people that have been in the group throughout these years whether it was a research stay or an internship: Cris Kurachi, Rafa, Toni, Iraís, Miquel, Crispin, Óscar, etc and many more that perhaps I forgot to include.

Muchas gracias a **César** y a **María** por escucharme y ser mi voz consejera siempre que se lo pedía.

Además, dentro del **ICN2** hay muchas personas que hacían que mi día a día tuviera un valor añadido. Gracias a Raúl por enseñarme a usar la evaporadora y estar siempre disponible para cualquier cosa que pudiera surgir. También a Ainhoa por nuestras charlas y nuestros “solo tengo 10 minutos” cafés/tés. Gracias a Pau, a José y a Anabel, y sobre todo a las “chicas de la limpieza” por tener siempre un “buenos días” y unas palabras amables. Y gracias a nuestros vecinos de enfrente del laboratorio de Biosensors, sobre todo a Dani Quesada y a José Fran.

Me gustaría hacer una mención más que especial a **mis compañeros de vagón** por las mañanas: el grupo *quetrén quetrén*. Gracias por estar cada mañana en el tren, riéndonos y preparándonos para un día de trabajo, gracias por hacer que los trayectos fueran más divertidos y sociables. Veros por las mañanas y estar un ratito en la cafetería al llegar al ICN2 ha sido mi motivación para seguir durante mucho tiempo. Gracias a Civan, Ceren, Fabian, Fede, Dani y Marianna. Y sobre todo, y por encima de todo gracias a Kumara, gracias por TODO, eres una gran amiga, la mejor hermana y una gran persona. Te mereces lo mejor en la vida y espero de corazón que lo consigas.

También me gustaría agradecer a mis **amigos** dispersados por diferentes partes del mundo (sobre todo en Alicante y Bélgica) los cuáles siempre me preguntaban cómo iba todo y me mandaban ánimos desde sus respectivos lugares. Además, gracias a mis **tíos, tías, primos y primas** por siempre consultarme sus dudas científicas y animarme con todo esto. Y a mi abuela, que aunque no ha podido verme acabar estoy segura que desde el cielo me estará mirando bien acompañada.

Muchísimas gracias a **Rubén**. Gracias cariño por acompañarme en esta etapa final, gracias por apoyarme, abrazarme y estar ahí siempre que lo he necesitado. Gracias por tus consejos y tus reflexiones que siempre me aportan tanto. Una parte de este trabajo también es tuya. También gracias por traer a Syrah a mi vida, no sabes lo feliz que me ha hecho poder estar sentada con ella en mi regazo mientras escribía tantos días delante del ordenador.

Y por último, gracias a mi **Familia: mis padres y mi hermano Pablo**. Ellos son lo mejor que me ha pasado en la vida. Somos un equipo, y puedo decir orgullosamente que estoy rodeada de los mejores. Gracias Mamá y Papá por siempre siempre siempre apoyarme en todas y cada una de mis decisiones, gracias por tener siempre una palabra de ánimo, de apoyo, de consejo. Os quiero muchísimo. Esto no habría sido posible sin vosotros.

*Enamórate de tus ideas,  
trabaja con ilusión,  
recuerda que siempre, siempre, siempre,  
sale el sol*

- Un cojín



## Motivation and Objectives

Sepsis is a potential fatal whole-body inflammatory reaction caused by severe infection. Its mortality rate is around 35% causing 20.000 deaths per day worldwide. Moreover, the cost of sepsis is high and rising. In 2009 more than US\$15.4 billion were spent on hospitalizations both in USA and Europe.<sup>1</sup> Quantification of the cost of sepsis patients in developing countries is more complicated as the early symptoms are the same than in other diseases, which makes even more difficult its fast detection without an intensive laboratory analysis. In addition, detection of the infection-causing agent usually takes hours or even days which increases the mortality and reduces the survival rate.

During the last decades, the scientific and medical community are changing the paradigm of diagnosis moving from laboratory analysis to point-of-care (POC) tests, which are fast, easy to handle and use and, in many cases, less expensive. The compactness and autonomy of a POC device to diagnose sepsis will be very useful to pave the way towards its application in different decentralized environments. For example, a POC can be placed in the hospital benchtop at the physician desk or even at ICU unit for sepsis diagnosis or for other diseases as well as fast-settled hospitals in developed countries. Furthermore, sepsis requires identification of many biomarkers to be diagnosed. Hence, multiplex detection and quantification of these indicators can be very useful for proper and early diagnosis, thus, allowing early start of the treatment.

In order to achieve early diagnosis of sepsis a POC device was proposed within the framework of a European Project called RAIS (Horizon 2020). The overall objective of the RAIS project ([www.rais-project.eu](http://www.rais-project.eu)) was developing a nanophotonic point-of-care biosensor that can detect and quantify, in label-free conditions, multiple biomarkers in human serum or plasma simultaneously in an easy and simple way by using a new microarray technology (**Figure 1**). Several sepsis biomarkers were initially selected to demonstrate the capability of this novel POC biosensor to detect this condition in less than 30 minutes



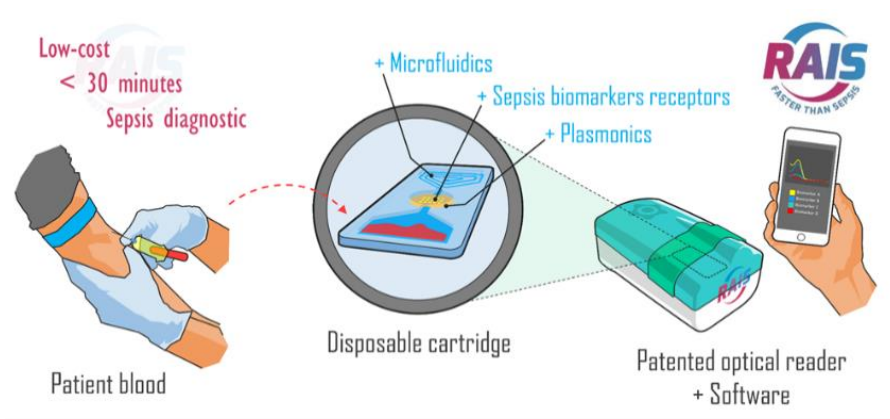


**Figure 1:** Scheme of the RAIS project goals.

The main aim of this thesis is to evaluate the performance of the novel point-of-care biosensor and to demonstrate its feasibility to be applied for the detection of clinical biomarkers commonly related to sepsis. This involves the following specific objectives:

- Characterization of the POC biosensor for its application with biological samples (liquid solutions, proteins layers, etc.).
- Development of biofunctionalization strategies compatible with the microarray format to anchor antibodies as specific receptors for the detection of protein biomarkers and bacteria.
- Development and characterization of direct assays for protein and bacteria detection and quantification.
- Validation of the POC and the developed assays with real human samples





## Table of Contents

Abstract .....	i
Resumen .....	iii
Acknowledgments .....	v
Motivation and Objectives .....	ix
1. Introduction .....	1
1.1 Clinical diagnosis: From analytical laboratories to point-of-care platforms.....	1
1.1.1 Conventional clinical diagnostic techniques .....	2
1.1.2 Biosensors and Point-of-Care devices.....	4
1.2 Optical biosensors .....	10
1.2.1 Plasmonic biosensors .....	11
1.2.2 Multiplexed biosensors .....	14
1.3 Microarrays .....	16
1.3.1 Array fabrication technologies .....	17
1.4 Biofunctionalization of solid surfaces: the biorecognition layer .....	20
1.4.1 Bioreceptors .....	20
1.5 Sepsis.....	24
1.5.1 Current biomarkers for sepsis diagnosis and detection methods	26
1.5.2 Commercially available systems for Sepsis diagnosis .....	30
1.5.3 Sepsis diagnosis in the frame of RAIS H2020 project.....	32
2. Materials and Methods.....	37
2.1 Optical POC device .....	37
2.1.1 Nanoplasmonic sensor chip fabrication .....	38
2.1.2 Signal processing and Data analysis .....	39
2.1.3 Characterization of the POC for sensor measurements.....	39
2.2 Fabrication of Microarrays with Dip-pen Nanolithography .....	40
2.3 Chemical and Biological Reagents .....	40
2.3.1 Chemical Reagents and Buffers Composition .....	40
2.3.2 Biological compounds.....	41

2.4	Biofunctionalization Strategies .....	42
2.4.1	Glass surface functionalization by dip-pen nanolithography ...	42
2.4.2	Gold surface functionalization by dip-pen nanolithography ....	42
2.5	Immunoassays for protein biomarkers and bacteria (Chapters 5 and 6)	44
2.5.1	Calibration curves .....	44
2.5.2	Hospital samples and clinical validation .....	45
3.	Nanophotonic microarray-based biosensor.....	49
3.1	POC nanophotonic biosensor .....	49
3.2	Custom-designed nanoplasmonic structures for signal enhancement.	54
3.3	Characterization of the POC for biosensing applications .....	59
3.3.1	Signal enhancement due to the Nanoplasmonic chip.....	59
3.3.2	Influence of the evaluation medium.....	60
3.3.3	POC device applied to biosensing.....	61
3.4	Conclusions .....	63
4.	Optimization of antibody immobilization.....	67
4.1	Biofunctionalization strategies for gold and glass surfaces .....	67
4.2	Initial study of the attachment of antibodies over different surfaces compatible with the POC biosensor .....	75
4.2.1	Functionalized glass surfaces .....	75
4.2.2	Gold surfaces.....	76
4.3	Optimization of antibody immobilization on Au-NHAs chips .....	81
4.3.1	Direct antibody binding.....	81
4.3.2	Antibody binding through Protein G orientation .....	83
4.3.3	Antibody binding through avidin/biotin interaction.....	87
4.4	Conclusions .....	95
5.	Evaluation of Protein Biomarkers for Sepsis.....	99
5.1	Introduction .....	99
5.2	Design, optimization and analytical evaluation of the protein biomarkers in buffer .....	102
5.2.1	Interleukin-6.....	110
5.2.2	Procalcitonin.....	113

5.3	Multiplex measurement of CRP and IL-6 .....	116
5.4	Design, optimization and analytical evaluation of proteins in plasma 120	
5.4.1	Effect of the plasma in the CRP assay .....	121
5.4.2	Plasma effect in the IL-6 assay .....	127
5.5	Validation with real samples .....	129
5.6	Conclusions .....	133
6.	Evaluation of Bacteria Biomarkers for Sepsis diagnosis .....	137
6.1	Introduction .....	137
6.2	Design, optimization and analytical evaluation of <i>P. aeruginosa</i> .....	137
6.3	<i>E coli</i> detection and quantification with the POC .....	142
6.3.1	Multiplexed measurements of <i>P. aeruginosa</i> and <i>E. coli</i> in buffer 144	
6.4	Analysis of <i>P. aeruginosa</i> and <i>E. coli</i> in blood plasma .....	147
6.5	Validation with Clinical Plasma samples .....	149
6.6	Conclusions .....	156
	General Conclusions and Future Perspectives .....	159
	Abbreviations and Acronyms .....	165
	List of publications .....	169
	References .....	173



# Chapter 1

# Introduction

This chapter provides a general introduction to the topic of the Thesis. It begins with an insight about current clinical diagnosis and its evolution towards point-of-care platforms. We review the traditional techniques that have been used and how this has evolved to the need of faster and more user-oriented devices. After this, we explain optical biosensors and how their easiness for integration makes them ideal candidates for point-of-care devices. Then, protein microarray technology and several techniques to generate microarrays are explained. Later, we provide some information about the use of bioreceptors for biomolecular identification. Finally, we describe the sepsis as a representative clinical complication to assess the new POC device for diagnostics. Sepsis is a severe blood infection which can lead to organ failure and death. This is a clinical condition whose diagnosis is still challenging and has become a major public health issue.





# 1. Introduction

## 1.1 Clinical diagnosis: From analytical laboratories to point-of-care platforms

Successful prevention of and therapies against diseases can only be achieved by having a proper diagnosis. Conventional diagnostic techniques are based on clinical imaging or in bodily fluids analysis (such as blood, urine or other fluids). Imaging techniques for diagnosis require advanced infrastructures with trained personnel and can be relatively costly and complex. In addition, collection of human samples implies later shipment to a specialised laboratory and waiting for several hours, days or weeks for the results. In this case, the process of diagnosis involves sample pretreatment, detection and identification of the pathology and determination of its severity which will finally serve as a basis for the medical doctor to make the selection of the more suitable therapy or medical treatment. Afterwards, the physiological status of the patients must be followed up to check their evolution during the therapy and assess their health improvement.<sup>2,3</sup>

During the last decades there have been strong advancements in medicine and in clinical research; however, the mortality associated with diseases not treated on time or not monitored correctly is still high. This is also aggravated in low resource settings, where there is a limited access to advanced equipment, such as in developing countries.<sup>2</sup> Many efforts have been conducted to develop novel ways to diagnose in cheaper, faster and more user-friendly conditions. Biosensors are analytical tools that employ biomolecules which act as receptors to recognize and capture the analyte of interest (commonly a biomarker that has a role in the suspected disease or condition). Biosensors are user-friendly, easy to move and provide fast results. Consequently, many hospitals bet on including biosensors in their clinical laboratories to achieve faster diagnosis.

In addition, improvement of healthcare management and disease monitoring at the hospital or at home can be done by placing the biosensors near the patient (i.e. at the point-of-care). Therefore, novel biosensors with special features such as compactness, smaller size, portability and easy-to-use

have arisen. They are called point-of-care (POC) devices and they should perform accurate and fast diagnosis where the patient is located.<sup>4</sup>

### 1.1.1 Conventional clinical diagnostic techniques

Medical decisions nowadays mainly rely on acquiring biomolecular information through imaging techniques (magnetic resonance imaging, X-rays, TAC, PET, etc.) or through analysis of biofluids (i.e. blood, urine, saliva, tears, sputum) from the patient (*in vitro* diagnosis). Currently, bodily fluids analysis is preferred rather than imaging techniques because is cheaper and less invasive. Detection and quantification of the biomarkers present in the sample have been used throughout many years. Therefore, many routine techniques are widely used in laboratories.

Common standard techniques to identify biomarkers are Enzyme-Linked Immunosorbent Assay (ELISA), chromatography, flow cytometry and mass spectrometry. Currently, detection of specific biomarkers (such as proteins) in a high throughput screening is mostly based on ELISA. This method involves the use of antibodies for a specific biomarker and a chromogenic reporter that signals its detection. Detection with higher sensitivity is achieved by adding fluorescence and electrochemiluminescence labels. ELISA is a sensitive and well established methodology, however it is labourious as it needs many reagents and trained personnel to perform it.<sup>5</sup> Mass spectrometry is highly used for proteomic patterns search. This technology enables high throughput analysis of hundreds of clinical samples per day. Despite mass spectrometric patterns may be very useful, only well-defined and highly validated clinical biomarkers are eventually useful in this type of tests. Thus, the wide mass pattern search is limited by the availability of well-established biomarkers.<sup>6</sup> Flow cytometry is another technique employed which relies on the analysis of the physical and chemical characteristics of a big population of cells (or particles). The cells present in a sample are previously stained with a dye whose absorption spectrum matches the wavelength of a light beam. When passing through the focus of the light, each cell emits a pulse of fluorescence and the scattered light is collected by lenses and directed onto sensitive detectors (photomultiplier tubes). These detectors transform the light pulses into an equivalent electrical signal. The

light scattering of the cells gives information on their size, shape and structure and cell mass.<sup>7-9</sup> This means that in a single-channel cytometer we can acquire approximately 1000 images of cells per second. Thanks to the labelling of the cells with specific fluorochromes or fluorescent conjugates that bind with high specificity to one given cellular constituent, it is possible to measure a wide variety of cell surface biomolecules like proteins, carbohydrates, or enzymes. Although initially developed for eukaryotic cells, flow cytometry has also been adapted for bacteria. Flow cytometry is a powerful technique but, besides being a very costly equipment, it lacks reproducibility which is required to produce consistent data.<sup>10</sup>

Clinical conditions related with pathogen infection have another plethora of techniques that can be complementary to the previously explained.<sup>5,11</sup> Pathogen identification traditionally depends on microscopic analysis, the growth of the microorganism (cell culture) and staining. These techniques are reliable but time consuming. Culture-based diagnosis (culture and later visual inspection) remains as the reference standard method. This method takes up to 72 h and may vary depending on the growth speed of the bacteria/microorganism. However, this technique is not convenient for infections when the infection causing pathogen cannot be cultured in the lab or when an antibiotic treatment started before the sampling.<sup>12</sup>

The evolution of molecular biology and in particular the development of amplification methods like polymerase chain reaction (PCR) have resulted in a faster solution than culture growth. This technique is highly sensitive although it also has disadvantages. The main one is the need of having a pure sample (to avoid cross-contamination and measuring DNA of foreign species) which implies several complex previous steps before the analysis. This delays the process several hours and increases the overall cost. Recent advances in the technology, for example digital PCR, quantitative PCR or microfluidic PCR, can reduce the assay time, the sample and reagent volumes, and give a better performance. However, these novel techniques need dyes or labeled probes which also increases the overall cost and complexity of the assay.<sup>12,13</sup>

All these clinical laboratory techniques are applied broadly to different types of biomolecules or microorganisms and, in general, are highly effective processing large number of samples. However, these advantages come with a

significant commercial cost and often the speed of analysis is reduced because the technology is confined to small laboratories, which limits the availability. Moreover costly equipment cannot be afforded in resource-constrained areas such as hospitals in developing countries.<sup>14</sup>

Current challenges in the diagnostics field are to create cheaper, simpler and de-centralized tests which can deliver faster results. Biosensors devices are pointed-out to improve the diagnosis and follow-up of therapies and to help in the near future opening the door to a global health access.

### 1.1.2 Biosensors and Point-of-Care devices

Biosensors (**Figure 1.1**) are devices in which the recognition system employs a biorecognition element that has affinity for the target or that has catalytic activity over the target. This biorecognition can be carried out by enzymes, proteins, nucleic acids, tissues, organelles or whole cells. Upon interaction among the bioreceptor and the target, a series of physicochemical changes in the medium or the transducer surface occurs. This change is detected and converted into discrete or continuous signals. Depending on the signal change experimented by the transducer, different types of biosensors can be defined being electrochemical, mechanical or optical biosensors the most common ones.<sup>15–17</sup>

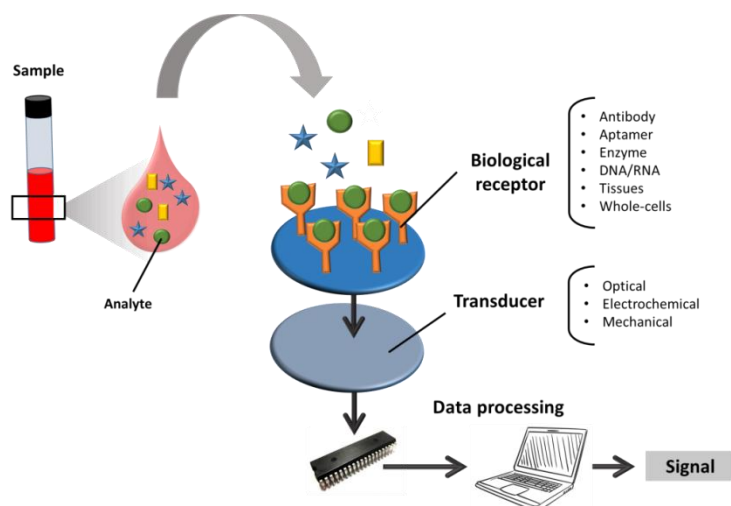


**Figure 1.1: Biosensor Scheme:** Representation of a biosensor including a heterogeneous sample, the biological receptor, the transducer and the data processing for achieving a signal.

The merge of the bioreceptors layer together with the transducer gives the ability to selectively detect the target analyte with high sensitivity. Biosensors have been widely used in many fields like medicine, food, safety, water control, compliance with regulations (drug testing or doping), public health and security.<sup>18</sup> They offer several advantages over conventional methods, including low limit of detection, real-time analysis, label-free detection, and low sample consumption.

The most representative biosensor is the glucose biosensor. This device was invented in 1962 by Clark and Lyon<sup>19</sup> and since then it is used for self-testing the levels of glucose in blood in diabetic people. Initially it was developed for measuring glucose and urea levels. It consisted on an electrode system that combined with a specific enzyme (glucose oxidase or urease) embedded in a membrane was able to detect the analyte. Later, in 1965, Kadish and Hall<sup>20</sup> described a similar method in which an oxygen electrode was in contact with glucose oxidase and by oxidation of glucose, reduction of oxygen was monitored. All these works culminated on a patent<sup>21</sup> followed by its commercialisation by the company Yellow Springs Instruments from 1975.

Nowadays, with the advances in microelectronics, the glucose biosensor or glucose-meter measures the electrochemical signals generated by the redox reaction produced by the enzymes glucose oxidase or glucose dehydrogenase in contact with the glucose (**Figure 1.2**). Glucose-meter sensors display the result in 5 seconds and use 300 nL of blood which are collected by puncturing, commonly on a fingerstick. Recently, the company Abbot released the FreeStyle® Libre glucose-meter which is a wearable sensor located at the back of the upper arm (directly on skin) that provides real-time glucose readings for up to 10 days.

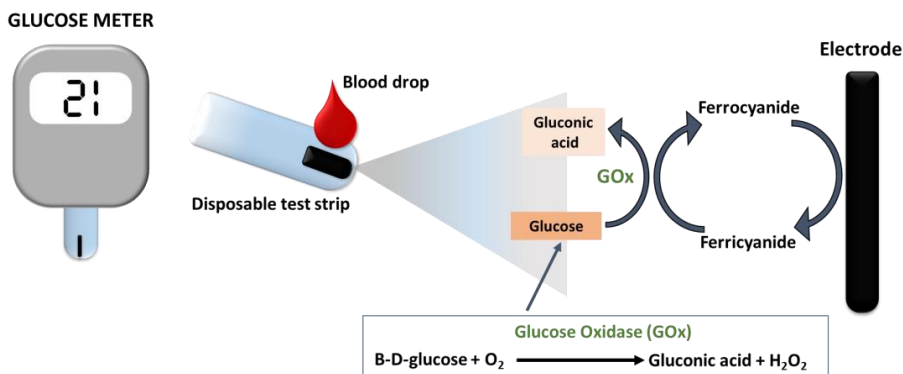


**Figure 1.2: Glucose meter.** The glucose meter is a device in which disposable test strips with a blood drop is inserted. The glucose in the blood reacts with an enzyme electrode containing the glucose oxidase (GOx). The enzyme is reoxidized with an excess of a mediator reagent, ferricyanide. The mediator in turn is reoxidized by reaction at the electrode, which generates an electric current. The total charge passing through the electrode is proportional to the amount of glucose in the blood that has reacted with the enzyme.

However, not all biosensors are as simple as the glucose-meter. Some are difficult to integrate and to reduce its size ending in bulky and expensive devices limited to specialized laboratories. The trend followed during the last decades is to develop compact, fully-integrated, user-friendly and portable biosensors to be used as POC devices. These devices aim at performing the analysis near the site of the patient (i.e. point-of-care). They should provide results in a fast way and without the need of laboratory staff or specialized facilities.<sup>22</sup> The test should be easy-to-use requiring only elementary instructions and if possible or needed, should measure more than one parameter at a time (multiplex measurement). Also, interpretation of the results should be easy and clear, adequate to the final user. POC devices for clinical diagnosis should eventually be used by medical doctors either at the hospital or in their office, or at home by the patient to track health, monitor therapies and manage disease (**Figure 1.3**). Thus, ideally, they should be developed considering the analysis of common bodily fluids such as blood, saliva or urine.<sup>23–25</sup>

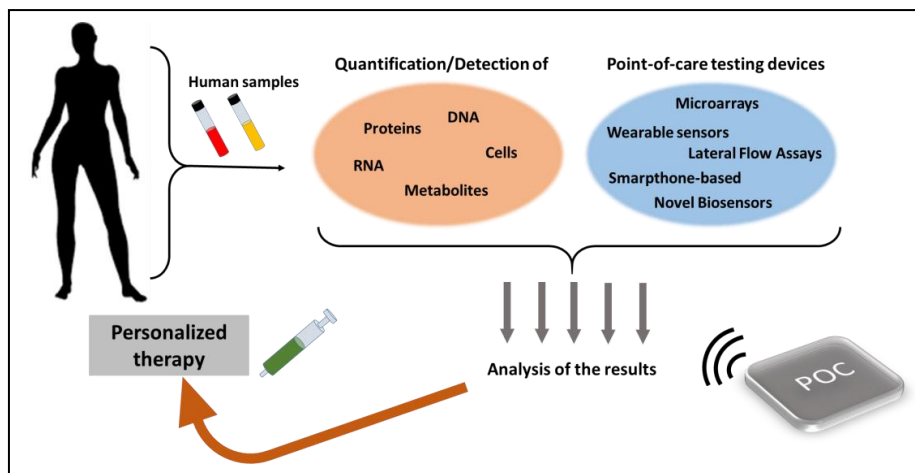


**Figure 1.3: Scheme showing the application of POC devices in health diagnosis.** Human samples such as urine or blood are withdrawn from the patient and inserted in a POC and different substances are measured. Upon reception of the results the doctor will choose the most appropriate therapy for the patient. Adapted from <sup>26</sup>

Ideal POC devices should require small sample volumes (nL up to 1 mL),<sup>27</sup> should be affordable or use disposable chips or cartridges that (if needed) incorporate microfluidics with features to provide and control sample preparation, flow rate, mixture of reagents, filtration or separation.<sup>28–30</sup> Commonly, POCs devices include a strip, chip or cartridge that interacts with the sample and is disposable. Additional components, such as secondary dyes, optics, electrodes or thermal control components might be also incorporated in this part if required. Often, a reduction of economic cost is associated with POCs due to the avoidance of sample mislabelling or mishandling. Furthermore, by providing quicker results, POC systems enable for the earlier treatment to start and eventually could improve the patient outcome.

Also, portable POC devices may help the physicians with the follow-up of therapies by connecting remotely to the device. It has been appointed that higher patient compliance is achieved by making patients more responsible for managing their own condition(s).<sup>31</sup> As a consequence, the doctor can track the results online, which reduces hospital visits frequency, thus, reducing travel expenses for the patient.<sup>32</sup>

Currently, one of the most successful and robust POC devices available is the pregnancy test. It is a test based on Lateral Flow Assay (LFA) or lateral



flow immunochromatographic assay which detects the presence of human chorionic gonadotropin (hCG), whose level increases during pregnancy (**Figures 1.4**). LFA devices incorporate porous membranes, antibodies, and a visible signal-generating system. The fluid sample migrates through the test strip and generates a response signal that begins when an antibody (usually labelled with colloidal gold particles or dyed polystyrene or latex spheres) flows through the adsorbent pad and binds the analyte. Due to the colour label on the antibodies, upon binding, a colour line appears on the strip showing a positive result. This example of POC system illustrates the feasibility of giving qualitative results in a short time with a portable device.

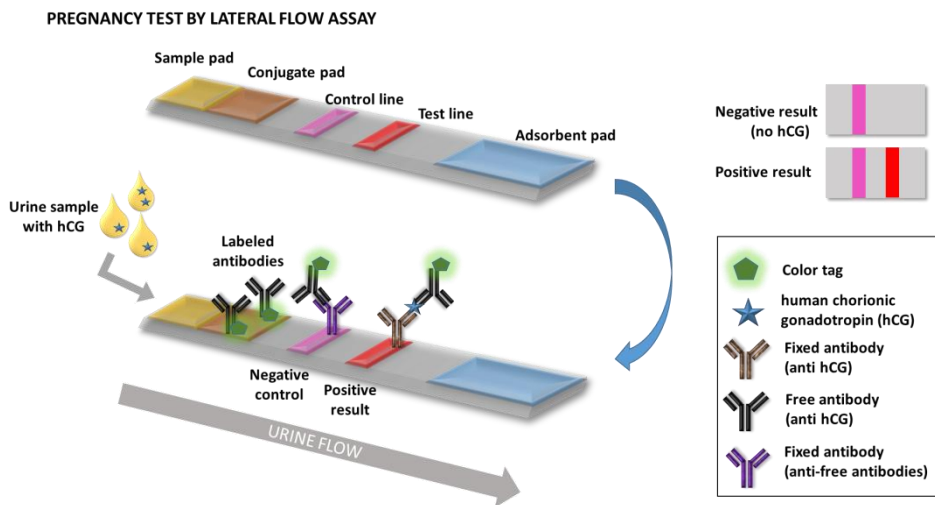


**Figure 1.4: Pregnancy test.** Urine migrates through a test stripe in which several antibodies are located: free tagged antibodies anti-hCG on the conjugated pad, fixed anti-antibodies on the negaiv control line and fixed antibodies anti-hCG on the test line. Free tagged antibodies on the conjugated pad migrate when urine is applied on the sample pad. If urine does not contain hCG the antibodies will react only in the control line area (negative result), however, if hCG is present, binding of the labelled antibody will occur in the test line, giving two coloured lines (positive result).

The LFA has also being exploited to measure other analytes different than hormones. For example, the product Rapid Analyte Measurement Platform (RAMP, from Response Biomedical Corp., BC, Canada, [www.responsebio.com](http://www.responsebio.com)) requires a sample, which is mixed and incubated with a label and buffer and then applied on the strip, to quantify several analytes with interest in the cardiovascular response, infectious disease

response, biodefense control and even environmental monitoring.<sup>33</sup> Latest advances in the LFA field include 3D pore structures to control the pore-size, thus, having better control of the fluid flow rates.<sup>28</sup>

During the last years, advances in microfluidics, smart materials, data analytics, and web based connectivity have allowed the use of more sophisticated technologies for the development of POCs.<sup>4</sup> For example, a large number of devices based on coupling the readout system to a smartphone or including the POC in fabrics (wearable sensors and e-textiles) have been explored. As most of the population has at least one mobile phone this is seen as an opportunity to couple the POC to a smartphone implementing some of the tools that they normally carry such as a camera, a light sensor, power source, movement detector, wireless connection (Wi-Fi), Bluetooth, near-field communication (NFC), infra-red sensor and global positioning system (GPS). For example, camera has been used as an imaging tool such as a spectrometer,<sup>34</sup> as a bright field and fluorescent microscope<sup>35</sup> or an automated cell counter.<sup>36</sup>

In addition, in-situ continuous monitoring of health parameters remotely is slowly being achieved by the use of wearable sensors. These non-invasive devices offer to the user valuable real-time information that can be useful on tracking wearer's health, tracking exercise activity or assessing human performance. This allows the individuals to change their lifestyle for maintaining optimal health status.<sup>37</sup> Some examples of wearable sensors are saliva based-sensors which are placed in tooth for controlling the plaque pH or the fluoride activity.<sup>38,39</sup> Advances in flexible polymers and materials have allowed the development of new wearable POCs that are incorporated as textiles or tattoos.<sup>40-42</sup> These flexible polymers can be engineered to different shapes and structures that can be mounted on surfaces of the human body for enhanced monitoring. Also, they have special characteristics like not liquid adsorption (which allows better detection through time), transparency, electro-chemical resistance or thermal-electrical conductivity that allows its incorporation in the sensing systems.<sup>40,42</sup>

In conclusion, different requisites are needed depending on the final application of the POC. Therefore, based on this, World Health Organization stated the ASSURED criteria. This is a list of suggestions of which characteristics an ideal POC should have. ASSURED stands for: Affordable

(for those who need the POC), Sensitive (low false negatives), Specific (low false positives), User-friendly (easy and simple to use by a non-trained person), Rapid (fast results) or robust (for example not requiring refrigerated storage), Equipment-free (no extra equipment is needed) and Delivered to those who need it.<sup>22,43,44</sup>

New technologies which can revolutionize diagnosis with POCs are emerging every day. These new devices promise adding cutting edge sensors that can solve diagnosis problems in source-limited areas as well as in hospital near the patient bed. Not only by shortening work time for the doctors and the patients, but also reducing elevated hospital economical expenses.

## 1.2 Optical biosensors

As seen in previous section, point-of-care platforms are currently of utmost important in diagnosis. Many biosensor technologies have been exploited to create robust, compact and reliable POCs, however, optical biosensors are especially adequate for this purpose. Optical biosensors afford outstanding characteristics as excellent levels of sensitivity, immunity to electromagnetic interferences, miniaturization and integration capabilities, and portability, among others. Therefore, they are excellent analytical tools to move the analysis from centralized laboratories to the point-of-care. Often, their design offers fast delivery of results, easy-to-handle features and in some cases, simultaneous detection capabilities.<sup>3</sup>

Optical biosensors measure variations of the optical properties of the propagated light (i.e. absorption, fluorescence, polarization, intensity, wavelength, dispersion or refractive index) due to the interaction between the bioreceptor and the analyte.<sup>45,46</sup> Most of them are based on the evanescent field detection. Evanescent field is an oscillating electric and/or magnetic field that does not propagate as an electromagnetic wave but whose energy is spatially concentrated in the vicinity of the source (oscillating charges and currents) with an exponential decay. In the evanescent wave mechanism, a bioreceptor layer is immobilized onto the surface of a waveguide; the exposure to the partner analyte produces a biomolecular interaction affecting the guiding properties of the waveguide (specifically, a variation of the

refractive index) via the modification through the evanescent field. This evanescent field is affected by RI changes caused by a biological interaction, so no labels or special tags are required.<sup>47</sup> The variation of the RI can be measured by any of the waveguiding optical properties and this variation can be correlated with the concentration of the analyte resulting in a quantitative value of the interaction (see **Figure 1.5**).<sup>17,48</sup>

Plasmonic biosensors, interferometers and resonators are examples of the most common evanescent wave biosensors. They have high detection sensitivities in a short response time and they can operate in real-time.<sup>17,49</sup>

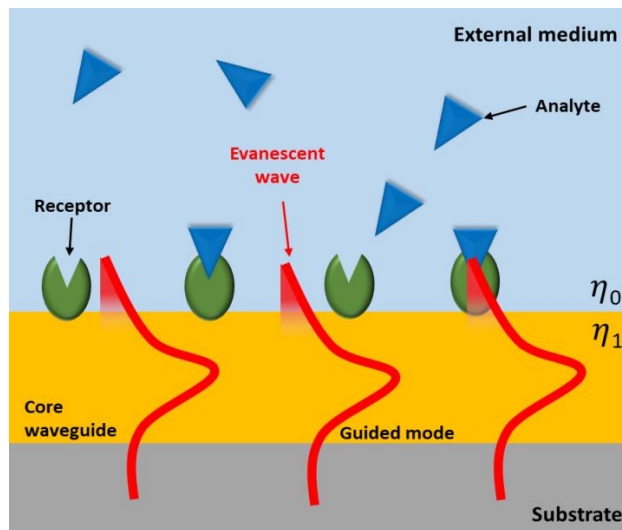


**Figure 1.5:** Scheme of the evanescent field sensing. A refractive index change is induced by a biomolecular interaction that takes place at the wave-guide surface within the evanescent region.

### 1.2.1 Plasmonic biosensors

Plasmonics is the field that studies the interaction of light with noble metals. Surface Plasmon Polaritons (SPPs) or surface plasma waves (SPW) are classically described as electromagnetic waves formed by electrons coherent oscillation at the surface of a metal when excited by an incident light. They are special modes of electromagnetic field which can exist at the interface between a dielectric and a metal that behaves like nearly-free electron plasma.<sup>50,51</sup> They contribute to one or more optical phenomena depending on the geometry of the sensor surface. The first biosensing

technique that employed SPPs was Surface Plasmon Resonance (SPR).<sup>52–54</sup> Conventionally, SPR measurements are conducted on thin metal films and the excitation triggers the propagating SPPs, which run through the sensor surface (the metal–dielectric interface) and the corresponding electromagnetic field is highly sensitive to the RI of the surrounding medium. As a result, SPR measurements can detect analytes with very low limits of detection.<sup>55–57</sup>

Simultaneously, and as the nanofabrication capabilities have improved, nanoplasmonics have emerged in order to expand sensing capabilities. Nanoplasmonic sensors take advantage of the optical phenomenon that appears when the dimensions of metallic nanostructures become smaller than the wavelength of the incident light. In this case, additional types of plasmon oscillations are observed which are locally confined within the nanostructure. Depending on the metallic nanostructure (i.e., nanoparticles of different shape and size or nanoholes) these phenomena are usually classified as localized surface plasmon resonance (LSPR) or extraordinary optical transmission (EOT), respectively (see **Figure 1.6**).<sup>58</sup>

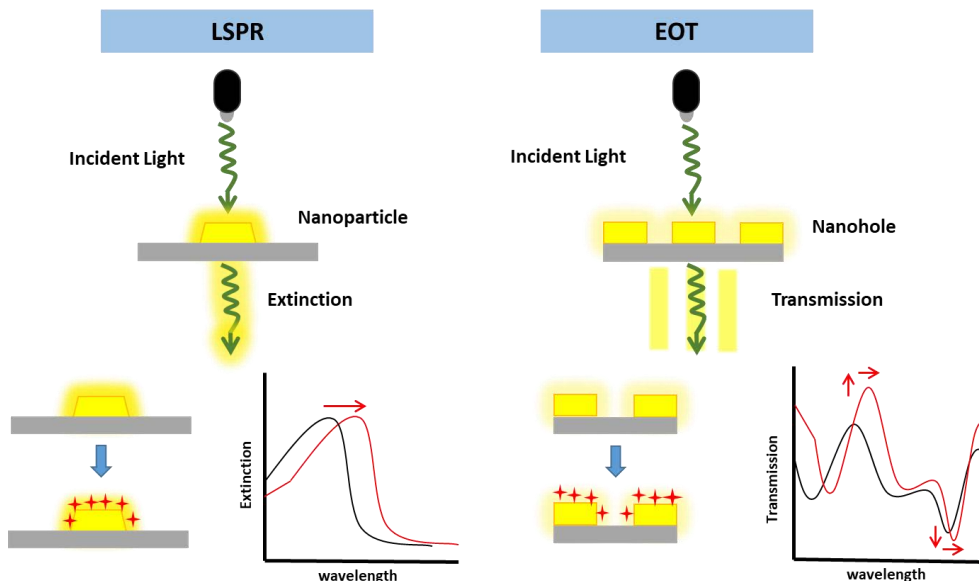


**Figure 1.6:** Schematic illustration of the working principles, nanostructures architectures and spectral information obtained from nanoplasmonic sensors based on localized surface plasmon resonance (LSPR) and extraordinary optical transmission (EOT) phenomena, respectively. Adapted from<sup>59</sup>.

LSPR generation occurs from the interaction of light with subwavelength size nanostructures instead of thin metallic layers. In this case, particular electronic modes can be excited when light strikes the metallic nanostructures, so that free electrons oscillate collectively. As a result of these resonance oscillations (i.e. localized surface plasmons), the nanostructures strongly scatters light at a specific wavelength range.<sup>48</sup> As the field is strongly confined in the surrounding of the nanostructure, the sensitivity at the surface is commonly higher than in SPR configuration, being the decay length of the electromagnetic field around 10–30 nm. At the same time, the sensitivity to bulk refractive index changes (i.e. shift of the extinction peak per unit change in the refractive index of the surrounding medium) is lower so the measurements are more stable and less susceptible to environmental fluctuations, which usually happens in SPR technique.<sup>48,60–62</sup>

EOT is a related optical phenomenon that arises from the interaction of light with periodic arrays of nanoholes, involving a combination of propagating and localized surface plasmons. The enhanced transmission is caused by the interplay of localized modes associated with individual nanoholes with coupling to propagating surface modes due to the periodicity along the cavities of the surface. As a consequence, the EOT spectral signatures exhibit wavelength-dependent transmission enhancement, resulting in multiple transmission minima and maxima.<sup>63–66</sup> In general, the transmission spectra of nanohole arrays show at least two transmission maxima ( $\lambda_{SP}$ ) and their spectral positions can be predicted based on the relationship to the lattice constant of the array (periodicity,  $p$ ), the scattering orders of the nanohole array ( $i$  and  $j$ ), and the real parts of the dielectric constant of the surrounding medium and the metal ( $\epsilon_{out}$  and  $\epsilon_r(\lambda)$ , respectively). The metal dielectric constant depends on the light wavelength ( $\lambda$ ).<sup>67</sup> This is described by the following **Equation 1.1**<sup>66</sup>:

$$\lambda_{SP} (i, j) = \frac{p}{\sqrt{i^2 + j^2}} \sqrt{\frac{\epsilon_r(\lambda)\epsilon_{out}}{\epsilon_r(\lambda) + \epsilon_{out}}} \quad (1.1)$$

The general design of an EOT-based sensing platform requires the choice of the (i) plasmonic material, (ii) geometrical properties of the nanoholes,

(iii) fabrication method, (iv) surface coating, and (v) flow conditions.<sup>59</sup>

### 1.2.2 Multiplexed biosensors

Usually, biosensors are designed to perform individual analysis. Increasing the multiplexing capabilities adds significant value to these devices, although it usually requires upgrades in the optical and microfluidics part. Moreover, it is also necessary to place different bioreceptors in defined locations over the sensing surface. Monitoring of these multiple locations (i.e. different bioreceptors) could be done by connecting a specific sensor to each location (multi-channel sensing) or by generating an image of the surface (imaging techniques). The optimal way to allocate many bioreceptors on reduced sensing surface (required for POC platforms) is by means of microarray-based designs, where tens to thousands of spots can be generated, ideally with different bioreceptors in each spot.

Several optical devices based on microarray formats have been already proposed. Commonly, fluorescent labels are used for the detection of the interaction. Typically, one of the elements involved in the recognition is tagged with a fluorescent reporter/molecule. This enables few molecules and even single-molecule detection. However, an extrinsic tag always could affect the properties of the tagged molecule and can affect the interaction. In addition, some pre-treatment of the samples is usually required prior target labelling. As a consequence, label-free detection techniques in a microarray format, with adequate sensitivities to compete with fluorescent-based detection methods, are arising as an alternative.<sup>68</sup> Some of these label-free microarray methods are: Reflectometric Interference Spectroscopy (RIFS), Total Internal Reflection Fluorescence (TIRF), Oblique-Incidence Reflectivity Difference Microscopy (OI-RD), Imaging Surface Plasmon Resonance Spectroscopy (SPRi), Imaging Optical Ellipsometry (OE) or Arrayed Imaging Reflectometry (AIR).<sup>69-74</sup>

Many of these techniques have been used mainly in applications that require high-throughput analysis. For example, Kemmler et al.<sup>71</sup> proposed a device for sepsis diagnosis based on a microarray using TIRF. The microarray device was employed to evaluate several sepsis biomarkers but required fluorescent labels and involved several fluid handling steps such as

dilution, mixing, separation, pre-incubation and incubation to carry on sandwich and inhibition assays. In addition, the biochip required internal calibration to prevent inaccuracy.

Mace et al.<sup>75</sup> developed a platform based on AIR to detect various cytokine proteins involved in the body inflammatory response. This technology relies on the interferences created on a polarized light beam that strikes on a silicon sensor chip. Initially, the sensor chip made of silicon oxide contains a protein adhesion layer and bioreceptors, which are tuned to an appropriate optical thickness. Upon binding of the target molecule to the bioreceptor, the spot where the incident light is located no longer fulfils the antireflective criteria. A different light reflection may be observed of intensity that is proportional to the amount of targets bound. This system does not required moving parts and a CCD camera is used to track the changes on antireflection.<sup>76</sup> Specific antibody-based macroarrays (i.e. 1.5  $\mu\text{L}$  spot volume) were manually generated. The design of the device allowed visualization and tracking of up to 8 differentiated spots, which limited its multiplexing potential and produced a high variability among measurements. This technology was also applied for autoantibodies detection for the diagnosis of autoimmune diseases<sup>76</sup> or for environmental monitoring.<sup>77</sup>

SPRI has been widely used since many years for evaluating affinity systems, including nucleic acids interactions, DNA binding proteins to DNA, antibody/antigen, carbohydrate/protein or enzyme/substrate, among others.<sup>73</sup> For example Jeong *et al.*<sup>78</sup> tested different cysteine tag lengths attached to Protein G. A holed sticker was used to create wells (diameter = 2.5 mm) that contained the different modified Protein Gs. The antibody binding efficiency was studied on bare gold and series of cysteine-tagged protein G layers. This technique was also used by Gorodkiewicz et al.<sup>79</sup> to study the effect of an inhibitor (MARS-115 CatG peptidyl inhibitor) that affects the enzymatic activity of cathepsin G. Moreover, Nelson *et al.*<sup>80</sup> detected the 16S ribosomal RNA from *E. coli* cells by its hybridization to a complementary DNA probe immobilized over a gold sensor surface. The limit of detection was 10 nm and the DNA array contained squared areas with the immobilized DNA probes.

As these optical technologies have gradually evolved and improved their performance, significant progress in microarray generation techniques have



also arisen as a matter of improving the allocation of multiple probes on a specific surface and especially in small-size surfaces. This may be very valuable for creating POCs which can include single-use portable sensing surfaces.

### 1.3 Microarrays

Microarrays commonly involve large ordered arrangements of molecules distributed in rows and columns in a defined area with spots size  $<250\ \mu\text{m}$ .<sup>81</sup> Immobilization of molecules can be done passively (adsorption) or actively (covalent bonding) depending on the chemical nature of the substrate. Most frequently substrates employed to generate microarrays are microscope glass slides, silicon or synthetic-polymer based materials. The recognition probes are chosen depending on the target, which commonly are nucleic acids, proteins or carbohydrates, among others.<sup>82,83</sup>

Using microarrays has made possible the development of a wide range of applications related to drug screening, vaccines development, enzyme substrates profiling and immuno-profiling, disease diagnosis, mapping of biochemical pathways and evaluation of protein-protein interactions.<sup>84</sup> Protein microarrays are widely used as proteomics tools to provide information on proteins, ligand, analyte, receptor, and antibody affinity based interactions and high-throughput analysis. Their main advantages over classical protein separation/identification techniques such as ELISAs or western blots are: (i) better detectability with improved sensitivity and specificity of proteins at lower concentration range in complex media; (ii) multiplex capabilities by detection of several proteins on a single platform (rational design); (iii) less reagents and sample consumption.<sup>84,85</sup> However, protein microarrays also face challenges especially when moving from research to clinical diagnosis. Printed microspots can have non-uniform morphologies that end in inconsistent quantification (i.e. poor coefficient of variation for spot-to-spot, assay-to-assay, substrate-to-substrate and lab-to-lab comparisons).<sup>84</sup> Complex immobilization protocols, contaminations during the microarray generation, and static (no flow) mass transport conditions lead to low signal-to-noise ratios (variability in assay kinetics and/or endpoints).<sup>86</sup> Also, the use of non-optimal (unfavourable) protocols conditions like pH,

temperature or desiccation of the surface or poor antibody compatibility with surface chemistry can hinder sensitivity of the assays. This may end in poor storage shelf-life of microarray chips.<sup>87-89</sup>

### 1.3.1 Array fabrication technologies

Specialized technology is required for spotting small volumes of biomolecules with the required control and according to the design parameters of the array (i.e.: spot diameter, separation between spots, volume of spot). Several techniques are commercially available to generate microarrays in a controlled mode and they are mainly classified according to whether there is contact or not between the substrate and the tool that carries the spotting solution, commonly called “ink”.

#### *Contact printing methods*

Nowadays, the most used method for microarray printing is contact pin printing. The spotters based on this technology use solid pins, split or quill pins, tweezers or other liquid transfer/deposition pin types to carry and deliver the droplets onto solid surfaces (**Figure 1.7A**). A robot head that is controlled electronically incorporates one to several fluid-dispensing tips/pins that are periodically dipped into wells of a microtiter plate containing the spotting solution. The robot captures a specific volume of solution from each well through the pins, which dispense droplets when contacting the surface. Surface energy between the surface, the solution and the pin, liquid wetting and interfacial tensions are important parameters to control the deposition and to have a reliable release of volume.<sup>84</sup> Printing additives are frequently added to the solution to maintain protein stability and tune the surface energy of the solution. Some examples are glycerol, concentrated sugars or high molecular weight polymers.<sup>90,91</sup> Due to the contact nature of this technology there is the possibility that the array surface suffers some damage during the deposition process.<sup>92</sup> Normally, the spot diameter is between 10 to 100  $\mu\text{m}$  but this may vary depending on the pin and the contact time.

Microcontact printing or soft lithography<sup>84</sup> is another technique which requires the use of microstamps to transfer the solution to the surface. It consists on a more parallel deposition method where several stamp features are soaked or sprayed in ink (i.e. printing solution) and then the stamp is

finally transferred to the array surface by physical contact (**Figure 1.7B**). Generally, the stamps are made of an elastomeric polymer, such as polydimethylsiloxane (PDMS) which allows tuning its hydrophilic or hydrophobic properties for better transfer from stamp to substrate and also prevents reagent adsorption or aggregation. Serial deposition can be achieved by iterative loading of reagents and cleaning of the stamp. Arrays printed with microstamps tend to be highly reproducible.<sup>84</sup> Stamp tips smaller than 100 nm buckle and deform under stamping forces, thus, spots are usually limited to sizes larger than that.<sup>93</sup>

Dip-pen nanolithography (DPN) (**Figure 1.7C**) is another method for the generation of microarrays. It consists on a modified atomic force microscopy (AFM) tip that is immersed in the spotting solution and then it is transferred to the surface creating the array in a write/drawing mode.<sup>94</sup> It can perform spots and also lines if using rastering mode. DPN has been also used to study layer growth and fabrication of nanostructures. The mechanism of ink transport is complex and likely to be influenced by numerous parameters, but it highly relies in the meniscus shape and size, temperature, humidity and deposition conditions (rate, surface hydrophobicity and tip hydrophobicity).<sup>95,96</sup> The size of the DPN tip varies from 10 to 60  $\mu\text{m}$ . Thus, the technique is very useful not only for protein microarray fabrication but also for the monitoring of biorecognition processes from molecular to cellular level,<sup>97</sup> such as the study of cellular adhesion processes.<sup>95</sup>

#### *Non-contact printing methods*

Contrary to the techniques described in the previous section, in these methods there is no physical contact between the printing tool and the surface to be spotted. Instead, the solution is ejected as a droplet from a specific distance. The working principle is similar to ink-jet printers but adapted to the deposition of biomolecules. There are three types of printings according to the mechanism used for the drop ejection: thermal ink-jet, piezo actuation and valve-jet. In thermal ejection a bubble is created in the reservoir with the use of a heating element (**Figure 1.7D**). As the bubble propagates, the liquid is squeezed out the orifice. When the bubble collapses the sample is ejected. In piezo actuation the liquid is squeezed (volumetric change) by the deformation of the reservoir causing the ejection of the droplet (**Figure 1.7E**). Finally, in valve-jet technologies there is a valve that opens and closes

the reservoir under computer control and high pressure (**Figure 1.7F**). In each cycle of open-closing the valve produces a droplet.<sup>84</sup>

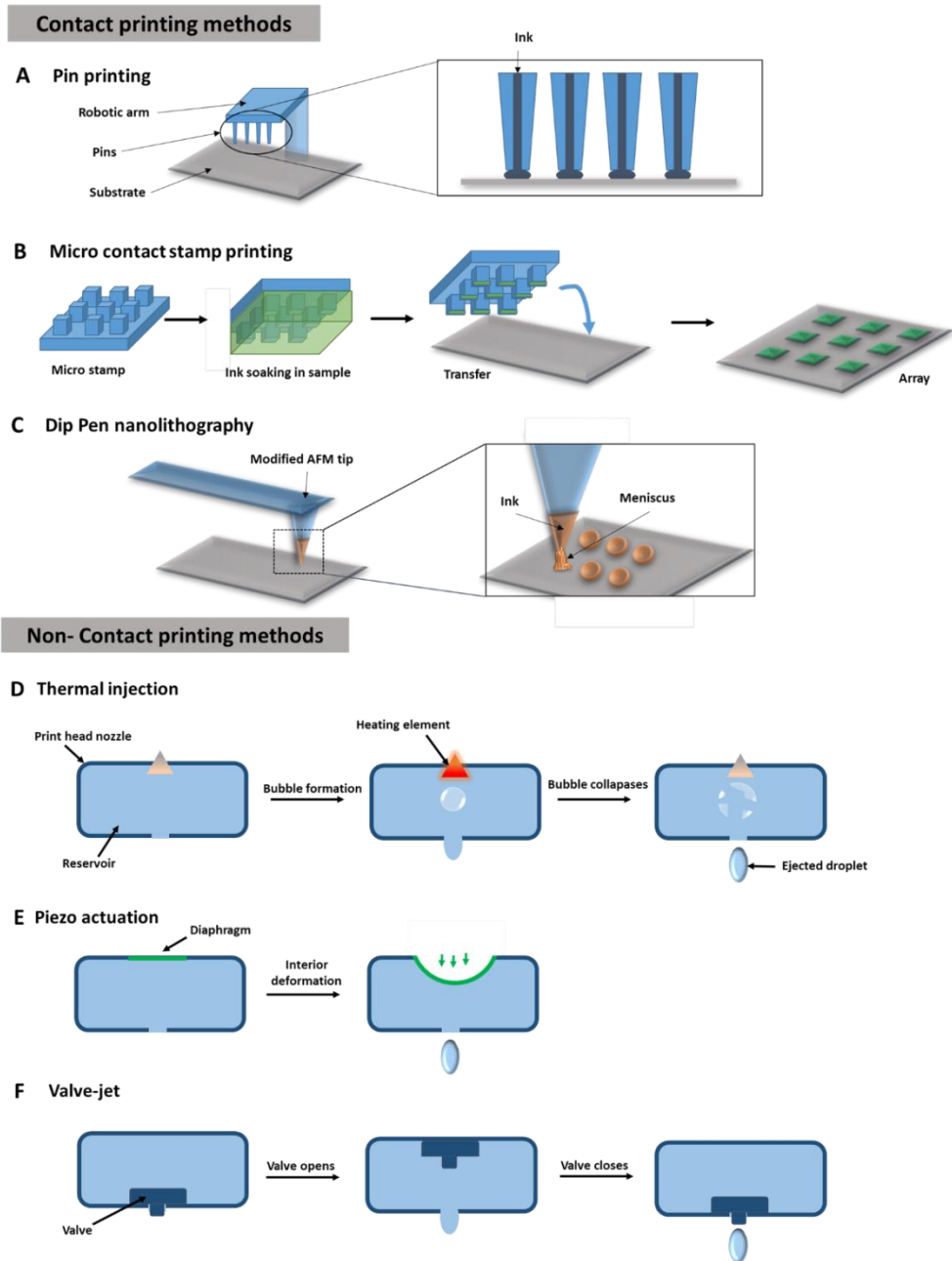


**Figure 1.7:** Scheme of contact and non-contact printing. **A:** Pin printing technology. **B:** Microcontact stamp printing. **C:** Dip-pen nanolithography. **D:** Thermal injection. **E:** Piezo actuation. **F:** Valve-jet. Adapted from<sup>84</sup>

## 1.4 Biofunctionalization of solid surfaces: the biorecognition layer

The analytical sensitivity and selectivity of any assay strongly depends on the biorecognition element anchored to the sensor surface and also on the surrounding area. Knowing and controlling this interaction, favouring the specific capture of the analyte and minimizing non-specific adsorptions, is the key element for a successful and reliable biosensor device.

### 1.4.1 Bioreceptors

Bioreceptors are classified according to its interaction with the analyte. If they introduce a change in the chemical structure of the analyte they are called catalytic bioreceptors and the most commonly used are enzymes. **Enzymes** are proteins that reduce the activation energy of a specific reaction that happens physically in their structure when the analyte is present. The analyte acts as a substrate for the reaction that is catalysed by the enzyme and transforms it into a product (**Figure 1.8A**). Commonly, the signal produced by reduction of substrate or detection of product of the reaction is evaluated.

Bioreceptors that binds specifically to the analyte are called affinity bioreceptors. They show extraordinary specificity to certain analytes, thus, permitting the selective capture of the analyte with extreme sensitivity. Commonly, affinity bioreceptors are nucleic acids, cell membrane receptor proteins, and antibodies. **Nucleic acids** show exceptional recognition properties because of the hybridization of complementary nucleotide sequences by Watson-Crick pairing (**Figure 1.8B**). Nucleotides possess amino groups that form specific hydrogen bonds that allow complementary binding with high specificity. DNA and RNA are easy to synthesize, and they are stable (DNA more than RNA) and reusable. Moreover, they can be chemically modified and tailored with additional groups at the ends (5' or 3') that make easier their immobilization or conjugation to other biomolecules. Recently, nucleic acids with new synthetic oligonucleotides have been added to improve the interaction among the nucleic acid probe and the target sequence.<sup>98</sup> Some examples of these synthetic oligonucleotides are peptide nucleic acids (PNA), locked nucleic acids (LNAs) or triplex-base pairing nucleic acids. For example, stronger bonding between the target sequence

and the protein backbone of the PNA is created due to the lack of electrostatic repulsion. This expands the pH range where the interaction remains strong compared to conventional DNA/DNA interaction. LNAs have very high thermal stability when hybridized to a complementary DNA or RNA strand. All these different forms can be also used as a bioreceptor on solid surfaces.<sup>99,100</sup> Another type of nucleic acid-based bioreceptors are the **aptamers**. They are functional oligonucleotide sequences of single-stranded DNA or RNA that fold in a unique intricate structure that allows recognition of a specific analyte with high affinity and specificity through electrostatic interactions and hydrogen bond formation (**Figure 1.8C**).<sup>101</sup> Aptamers are selected by a process called Systematic Evolution of Ligands by Exponential Enrichment (SELEX) which starts from a large aptamer library that is placed *in vitro* together with the target that fishes the most suitable aptamers out of the pool. This cycle is repeated several times with different assay conditions stringency (normally the closest ones to the final application). The best aptamers are selected and then sequenced by reverse transcription. Once the optimal aptamer sequence is known, the large-scale production of aptamers is easy and non-expensive. Some advantages of aptamers are their high affinity for the target (sometimes even higher than antibodies), their small size, and that they can be chemically modified in a precise and defined way. In addition, they can be easily stored and delivered as well as reversibly heat-denatured. However, aptamers with high affinities are still low in number compared to antibodies and their experimental sensitivities are also lower.<sup>102,103</sup>

Finally, the most frequently used bioreceptors due to their exceptional affinity and specificity are the **antibodies** (**Figure 1.8D**). These are proteins that are produced by the immune system and that recognise and bind to specific antigens.

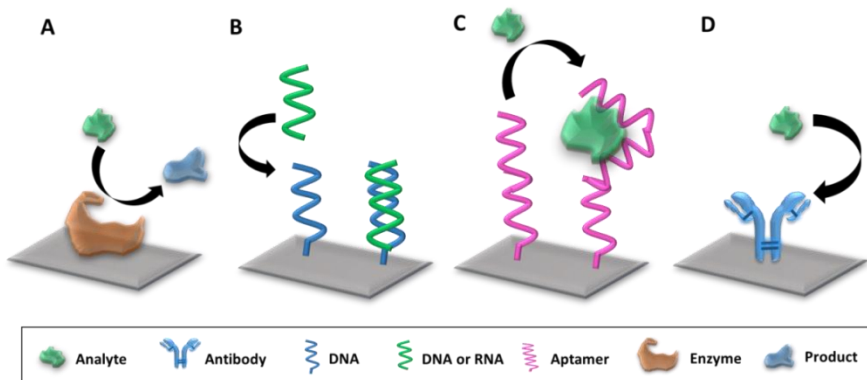


**Figure 1.8: Summary of some bioreceptors commonly used in biosensors.** A: Enzymes. B: DNA probes with complementary sequence of the target nucleic acid. C: Aptamers. D: Antibody.

### *Antibodies as bioreceptors*

Antibodies are immunoglobulin (Ig) molecules derived from the immune system and that possess highly specific ligand binding activity. They are used by the immune system as a surveillance mechanism against infectious organisms and/or their toxic products.<sup>104</sup>

We can find five different types of antibodies according to the structure of their heavy chains: IgA, IgG, IgM, IgD and IgE. IgG is the most predominant class produced during an immune response and it is the most widely used as a bioreceptors in immunoassays. The modular structure of a IgG antibody (**Figure 1.9A**) consists of 2 heavy chains (50 kDa) and 2 light chains (25 kDa), the former contains 3 constant domains ( $C_H$ ) and one variable domain ( $V_H$ ), and the latter one a constant domain ( $C_L$ ) and one variable domain ( $V_L$ ). The light chain and the constant chain are bound *via* disulphide bonds. The variable domains contain three different regions called complementary determining regions (CDRs) which have hypervariable amino acid sequences. These regions modulate the binding specificity of a certain antibody to a molecule. The rest of the antibody structure (constant domains) is highly conserved among species including certain oligosaccharide chains.<sup>105</sup>

According to the way of producing antibodies for biorecognition purposes they are classified in polyclonal, monoclonal, and recombinants antibodies, respectively.

- Animals such as rabbits, mice, goats or sheep are used as hosts for the production of polyclonal antibodies. The process begins with the injection of the target antigen or with bacterial cells or heat-treated cells (in the case of bacterial pathogens antigens) together with the presence of suitable adjuvants. The immune system of the host reacts to the antigen and its B cells start producing antibodies (pAb) against the antigen. These antibodies present in the blood of the animal are reactive to different epitopes of the same antigen. This mixture is known as **polyclonal** antiserum. When high specificity against a unique epitope is required, the production of monoclonal antibodies is more advisable.
- To produce **monoclonal antibodies** (mAb), B cells from the spleen (or the bone marrow or the primary lymph nodes) of the host animal are selected. Each B cell produces a specific type of antibody. These selected B cells are fused to an immortal myeloma cell resulting in a hybrid cell called hybridoma. This hybridoma is harvested and used to create an immortal cell culture line that secretes full-length antibodies directed towards a single epitope.<sup>106</sup>
- Moreover, **fragments of antibodies** produced by enzymatic or chemical cleavage such as F(ab')<sub>2</sub> and Fab (**Figure 1.9B**) can be also used. Later, when recombinant DNA technology evolved, **recombinant antibodies** (rAb) emerged as solutions with improved or modulated affinity and specificity. The production of rAb can be done by *de novo* design or by refinement of the gene sequence. Once the sequence is defined and synthesized, it is transferred to a cell culture that will express the sequence, thus, the recombinant antibody. Finally the antibodies are collected and purified. The newly created rAb not always have affinity levels as high as antibodies, which sometimes is a drawback<sup>105</sup>

In research, antibodies are the key molecules used for recognition. They are not only highly used in the clinical field but also in food analysis, environmental monitoring of soils and water, etc. The choice of the type of antibody will depend on the final application. Finally, the production cost should be also taken into account, monoclonal and recombinant antibodies are more costly since it requires more complex production steps.



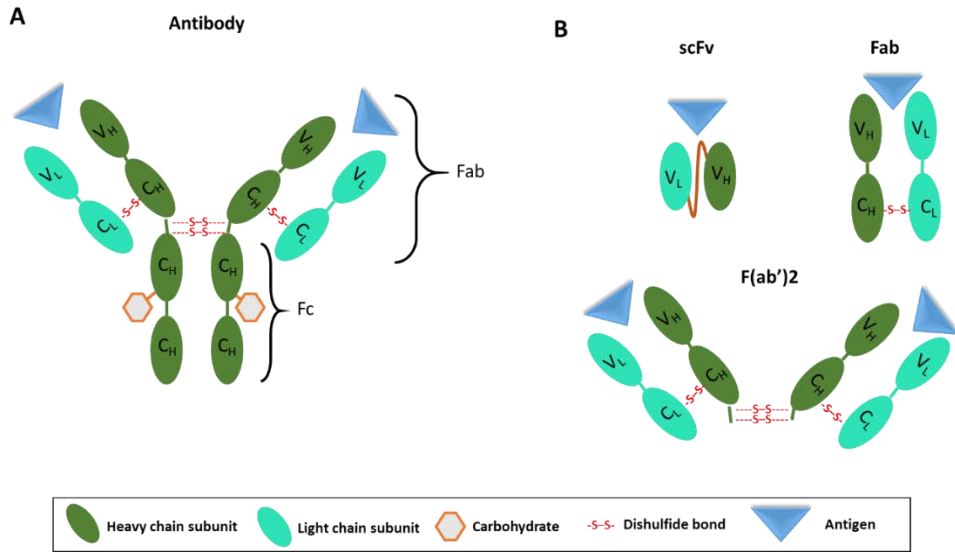


**Figure 1.9:** A: Basic structure of an antibody (IgG). B: Recombinant antibody formats. scFv is a Fv with a flexible linker. Fab is the Fv with both constant heavy and light chains. F(ab')<sub>2</sub> is the fragment with the two Fabs linked with disulphide bonds.

## 1.5 Sepsis

Sepsis is a clinical condition characterized for a grave whole-body inflammatory response due to an infection in blood. In 1992, the definition of sepsis was stated as the presence of infection and SIRS (systemic inflammatory response syndrome), which is established when two out of the four criteria listed in **Table 1.1** are met. When a patient with sepsis suffers of organ dysfunction (liver, kidney, lung and heart, mainly) the disease is called “severe sepsis”. If the disease advances, ending in hypotension of the body which does not react to fluid resuscitation, the patient will face a “septic shock” which will end up with the patient’s death.<sup>107,108</sup> Currently, sepsis affects nearly 1 out of every 23 hospitalized patients and the clinical significance of death by sepsis is hard to understate, especially in developing countries. Sepsis is the main cause of death in Intensive Care Units (ICU) and its incidence is increasing worldwide.<sup>107–109</sup> The occurrence rate was 146, 68 and 52 cases per 100.000 population for sepsis, severe sepsis and septic shock, respectively.<sup>110</sup> Clinical studies have shown that mortality rate from septic shock is between 40 to 50% in hospitals.<sup>107,110,111</sup> More alarmingly, between 2000 and 2015 sepsis has increased (17%) and sepsis related deaths

have grown 31% between 1999 and 2014.<sup>112</sup>

The mortality rate increases with a delayed diagnosis or an inappropriate antibiotic therapy, which implies a high economic cost for the health care system.<sup>111</sup> Only in the US is currently the most expensive condition treated at hospitals. For example, in Spain the yearly national total cost of hospitalization due to sepsis increased from 652 M € in 2000 to over 2.500 M € after 2010. This can be explained with the significant upward trend in average cost per patient that has been observed from 6.991€ (2000–2004) to 9.096€ (2005–2009) to 10.029€ (2010–2013).<sup>113</sup> Only in the US, the aggregated cost was US \$15.4 billions in 2009, whereas non-specific diagnosis of sepsis account for US \$23.7 billion per year.<sup>1</sup> Besides this, the global sepsis diagnostics market was valued at US \$ 367.9 Million in 2017 and is expected to reach US \$ 613.9 Million by 2023.<sup>114</sup>

The high costs are related to the hospitalization process which most of the times takes place at the Intensive Care Units (ICU). The current treatments for sepsis are fluid revival, antibiotic therapy, vasoactive mediation and/or a supportive therapy for organ dysfunction. Fast recognition of the septic patient and early location of the stage of the illness (sepsis, severe sepsis or septic shock) is critical. This helps define the proper treatment and reduce mortality risk.<sup>110,115</sup>

**Table 1.1: SIRS criteria**

<b>Presence of ≥ 2 criteria to establish a SIRS diagnosis</b>			
Temperature	Heart rate	Respiratory rate	White blood cell count
>38 °C	> 90	>20	>12.0 x10 <sup>9</sup> cells/L
<36 °C	beats/min	breaths/min	< 4.0 x10 <sup>9</sup> cells/L

### 1.5.1 Current biomarkers for sepsis diagnosis and detection methods

The evolution of an infection to sepsis usually involves changes in concentrations of endogenous inflammatory and coagulations mediators and variation in metabolism.<sup>116</sup> Many different biomarkers have been proposed for sepsis diagnosis and further treatment monitoring (**Table 1.2**). However, currently there is not a specific biomarker for sepsis which can be solely used to diagnose this condition. On the contrary, some of them can be very helpful for triaging critically ill patients.<sup>115</sup>

**Table 1.2:** Some examples of proposed biomarkers for sepsis. List retrieved from <sup>115,117,118</sup>

Proposed sepsis biomarkers	
• Lactate	• Procalcitonin (PCT)
• Macrophage inhibitory protein-3 (MIP-3)	• Neutrophil gelatinase-associated lipocalin (NGAL)
• D- dimer	• Protein C (PC)
• Interleukins: IL-6, IL-1 $\beta$ , IL-8, IL-10	• Tumor necrosis factor (TNF)
• IL-1 receptor antagonist	• Tumor necrosis factor receptor 1a (TNF $\alpha$ -R1a)
• C-reactive protein (CRP)	• Peptidoglycan recognition protein
• C3 and C5 complement proteins	• MR-pro-Adrenomedullin (MR pro-ADM)
• Several miRNA	• Brain natriuretic peptide (BNP)

One option is the checking the levels of different pro-inflammatory cytokines that mediate the initial response of innate immune system to injury or infection (TNF, IL-1 $\beta$  and IL-6). Within this group, IL-6 is the cytokine that has received major attention because it is easier to measure in plasma than the others.<sup>115,119</sup> Stimulation by IL-6, IL- $\beta$  and IL-8 as a consequence of an infection (bacterial or viral) or any other inflammation process (acute or chronic) produces secretion of C-reactive protein (CRP), an acute phase protein produced by the hepatocytes.

Another interesting candidate as sepsis biomarker is procalcitonin (PCT). It is a prohormone of calcitonin synthesised at the thyroid. During a sepsis process, the main producers of PCT are macrophages and monocytes from

different organs, and mainly from the liver. In healthy people, PCT levels are undetectable because it is processed as soon as it is synthesised. The synthesis of PCT can be identified after 2-3 h after onset of infection what makes PCT a useful biomarker for early sepsis diagnosis. The maximum peak of this biomarker is reached after 8 and 24 h after infection onset and the concentration fluctuates in the range of 10-100 ng/mL. PCT is very stable and possesses a median half-life of  $\approx$ 24 h. It is important to note that PCT does not increase during a viral infection. Currently at patients at the ICU with high levels of CRP and PCT are related with sepsis infection, however, these biomarkers have some limitations as they can be involved in others non-inflammatory processes, for example burns or traumas.<sup>107,110,116</sup>

Currently, the standard gold technique for diagnosis of sepsis is the presence of two of the symptoms listed in **Table 1.1** together with a positive bacterial culture. In general, cultures should be obtained from every source of infection such as blood, urine, sputum, or wounds. However, blood is the one most commonly used, being necessary a large volume (commonly 20 mL) for the analysis. Overall, the actual diagnosis of sepsis have many drawbacks as blood culture requires relatively long periods of time, trained personnel and laboratory facilities.<sup>107,108,110,111</sup>

An additional and more straightforward strategy to confirm sepsis and to provide insight on specific therapy is the confirmation of infection and the identification of the responsible microorganism. As infectious pathogens travel through blood, the most common allocations for the infection are lungs, the bloodstream and the urinary track. Infection can be caused by many different bacteria but the most commonly found are: *Staphylococcus aureus*, *Streptococcus pneumoniae* (in lungs), *Haemophilus influenzae*, *Pseudomonas aeruginosa*, *Klebsiella* spp., and *Escherichia coli*.<sup>120</sup>

Techniques for the detection of the infectious agent rely on sending specimens (e.g., blood, saliva or urine) for microbiological analysis to a centralised laboratory. Techniques as microscopy and cell culture, biochemical immunoassays, immunological tests or genetic analysis are employed. Microscopy is commonly used to observe the morphology and the staining pattern (gram stain) of bacteria to distinguish and classify bacterial species by the chemical and physical properties of their cell walls. This is a fast but not specific method. Bacteria cell culture on selective media under

specific growth conditions remains as the gold standard technique. However, it can take up to several days and not all bacteria can be cultured in the laboratory. For example, in routine blood cultures it can take between 6 hours to 5 days for the organism to grow to detectable levels. Extra time is then additionally needed for identification (24 h) and to perform antibiotic susceptibility tests (around 2 days). Moreover, the patient hemoculture often appears negative in patients with sepsis because not all bacteria can grow on laboratory culture media. Finally, methods based on the use of antibodies that specifically recognize bacterial surface epitopes are also commonly employed, such as ELISA and agglutination assays. These methods are reliable but they require substantial time, skilled personnel, bulky laboratory based equipment and relatively high pathogen loads.<sup>18,121–123</sup>

In the latest years, molecular techniques such as genetic analysis have enabled more rapid profiling of bacterial strains. PCR is a very sensitive technique which allows identification of bacteria based on their genetic material. PCR employs designed genetic probes that pair with the target bacterial sequence. Wrong pairing may result in false-positive results, and genetically mutated strains might escape the correct probe matching. Nevertheless, this procedure is still lengthy and expensive and can take several days. A faster procedure is real-time PCR analysis which can be completed within several hours, but still requires specialist equipment and reagents. Also, sequencing of 16S and 18S subunit of ribosomes has been proposed for bacterial identification through amplification because those sequences are highly conserved. Thus, providing strong and reliable identification of bacterial taxonomy and phylogeny.<sup>115</sup>

In general, all these techniques take time, require sample preparation and distinct reagents and equipment, and can be very costly. As a consequence, there is an urgent demand for more rapid, cost-effective, and sensitive tests which can identify whole bacteria in the field or at the point of-care, bypassing multistep processing and purification.<sup>18</sup> Moreover, due to the high mortality of sepsis the prompt start of accurate antibiotic therapies will depend on the ability to diagnose the specific species or strains of the pathogens causing the infection. In the absence of a precise diagnosis, first action taken by physicians is treating with broad-spectrum antibiotics, which contributes to the development of antibiotic resistant bacteria.<sup>124,125</sup>

Moreover, as the mortality rate is very high, antibiotic treatments are started early as prevention. Patients under antibiotic treatment present negative blood cultures. This is counterproductive as the correct initial choice of antibiotic therapy has been shown to save more lives than any other medical intervention.<sup>126-129</sup> In addition a study suggests that there is a 1 to 3 hours diagnosis window from symptom-based sepsis identification to beginning of antimicrobial treatment before the mortality increases.<sup>130</sup> Another study reported a 5-fold decrease in survival as a consequence of inappropriate antibiotic treatment in the first 6 h after sepsis is diagnosed.<sup>131</sup>

In addition, the biomarkers on the list above (**Table 1.2**) and the symptoms in **Table 1.1** are commonly used to diagnose other syndromes or diseases. Therefore, the corroboration of sepsis would be ideally done by detecting more than one of the biomarkers on the list (**Table 1.2**) by laboratory analysis. This way, detection of several biomarkers compatible with sepsis diagnosis puts the doctors closer to an accurate diagnostic. However, this commonly also requires many tests at the working laboratory and high volumes of blood, urine, or sputum samples. In view of that no single biomarker can solely effectively triage septic patients, many researchers have reported attempts to use several biomarkers in order to better identify the condition and the degree of severity. Comparison of novel and routinely used biomarkers of sepsis alone and in combination was done by Kofoed *et al.* in 2007.<sup>132</sup> They concluded that combining information from different biomarkers (three to six) gives more accurate diagnosis for detection of bacterial *versus* non-bacterial systemic inflammation than any biomarker alone. A few years later a study of combined score of pro- and anti-inflammatory interleukins improved the prediction of severe sepsis.<sup>133</sup> They used a commercial multiplexed immunoassay that determined that IL-6, IL-8, IL-10 and monocyte chemoattractant protein-1 (MCP-1) levels in plasma were higher in the death patients. They found that IL-10 was especially higher than the rest.



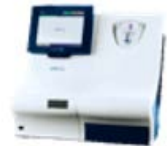


As a conclusion, we can foresee that multiplex traceability of certain biomarkers is very suitable for achieving a correct diagnosis of patients suffering from sepsis. Also, there is an important need of not only diagnosing the presence of sepsis but also to prompt and precisely identify the etiological agents that cause the infection.

### 1.5.2 Commercially available systems for Sepsis diagnosis

As regards to all the above mentioned, the development of a compact device which could monitor the most specific sepsis biomarkers and ideally identify the infectious agent would be very useful in the clinical settings. Especially, a POC platform which can move the diagnosis out of the classical analytical laboratory would be very valuable. This device may easily triage patients with an inflammatory process or with sepsis and also would be able to monitor septic patients along the disease process until their recovery. It might be used by medical professionals in hospitals and clinics like emergency rooms and Critical/Intensive care units, and in ambulatory care (out-patient and doctor's offices). For example, in emergency rooms it could rapidly and accurately diagnose sepsis and, therefore, reduce the patient length of stay. In ICU units it would enable an improved patient monitoring and its response to treatments. Finally, in ambulatory care units, it would enable a more efficient screening.

This opportunity has been seen by some companies which have invested in the development of diagnostic platforms focused on sepsis (or not specifically but might be applied to, see **Table 1.3**).

**Table 1.3:** List of some current commercial technologies that can compete with a new POC device for sepsis diagnosis.

Name of the technology and relevant features	
<p><b>Alere TRIAGE</b></p> <ul style="list-style-type: none"> <li>• 18 immunoassays (cardiac biomarkers, certain microorganism, drug screening) in one platform</li> <li>• Results in 20 min</li> <li>• Possible to use with blood, plasma or urine</li> </ul>	
<p><b>Abbott - i-Stat</b></p> <ul style="list-style-type: none"> <li>• 3 steps required for measurements</li> <li>• Measurement of metabolites, blood gases, <math>\beta</math>-hCG and other coagulation and cardiac markers</li> <li>• Requires 100 <math>\mu</math>L of blood, plasma or serum</li> <li>• Supports electronic medical records (EMR) connectivity and can store up to 5000 profiles</li> </ul>	
<p><b>Radiometer AQT90 Flex</b></p> <ul style="list-style-type: none"> <li>• Quantitative results in 11-21 min</li> <li>• CRP, PCT, troponin and D-dimer tests</li> <li>• Up to 30 samples/hour</li> </ul>	
<p><b>Samsung LABGEO IB-10</b></p> <ul style="list-style-type: none"> <li>• Portable and battery-powered</li> <li>• Results in 20 min in an automatic device</li> <li>• Up to three tests like troponin, D-dimer, TSH or <math>\beta</math>-hCG.</li> </ul>	
<p><b>Biocartis Idylla</b></p> <ul style="list-style-type: none"> <li>• real-time PCR based molecular diagnosis system</li> <li>• RNA and DNA analysis</li> <li>• 2-150 min hands-in results</li> </ul>	
<p><b>Magicplex™ Sepsis Real-time Test - Seegene</b></p> <ul style="list-style-type: none"> <li>• Screening for 90 pathogens</li> <li>• Gram +/- bacteria and fungi and Drug resistance</li> <li>• 3 hours analysis</li> </ul>	



### 1.5.3 Sepsis diagnosis in the frame of RAIS H2020 project

The diagnosis and management of Sepsis is a critical area where fast and accurate results can translate into life changing health outcomes for individuals. In view of this the development of a POC platform to diagnose sepsis was proposed within the frame of the RAIS H2020 European project (RAIS: Scalable, point-of-care and label-free microarray platform for rapid detection of Sepsis, Reference: 644956).

The overall aim of RAIS was to develop a new fully integrated point-of-care label-free microarray platform and validate it for quantifying levels of specific Sepsis' biomarkers. The approach uses a novel interferometric technique ultimately capable of providing very large arrays of tests. The specific objectives and activities included:

- Development of an optical POC microarray reader based on a novel design that combines interferometric lens-free microscopy and a complementary metal-oxide-semiconductor (CMOS) sensor for image sensing and analysis in high-throughput, label-free, rapid and sensitive conditions. The POC platform is reviewed more in detail in Chapter 3.
- A microarray plate, integrated in a proper microfluidic cartridge, consisting of a transparent slide with a novel nanostructured surface geometry to increase the detection sensitivity and covered by specific receptors to capture biomarkers;
- their integration in a portable and battery powered label-free microarray platform potentially capable of measuring more than 1 million of targets simultaneously.

The overall objective was the development of a technology to be capable to detect micro-ribonucleic acids (microRNAs), bacteria, and specific protein biomarkers associated to Sepsis using a few microliters of serum or plasma samples, in a concentration as low as pg/mL, within 30 minutes (sample to result) and at a cost per patient of less than 50€. Achieving such goal would put patients on the right treatment more rapidly, potentially reducing the Sepsis mortality rate of more than 70%, with estimated cost savings of more

than €10 billion per year as a consequence of shorter hospital stays, reduced use of unnecessary drugs and lower associated insurance bills. **Figure 1.10** shows a self-explicative scheme of the project and the partners involved in it.

The **Nanobiosensors and Bioanalytical Applications** research group at the Catalan Institute of Nanoscience and Nanotechnology (ICN2) has expertise in the field of biofunctionalization of surfaces and biosensors development. Therefore, the main tasks assigned within the project were:

- Optimization of the biofunctionalization protocol for each biomarker proposed in the project for its evaluation directly in human samples.
- Full analytical evaluation of the new microarray device for each selected biomarker using spiked analytes in plasma.
- Establishing calibration curves, calibration standards and complete assay for the new microarray device.
- Evaluation of the diagnostic performance of the microarray device for each biomarker in patients' samples.

In this Doctoral thesis we have included the main results achieved for protein and bacterial biomarkers.

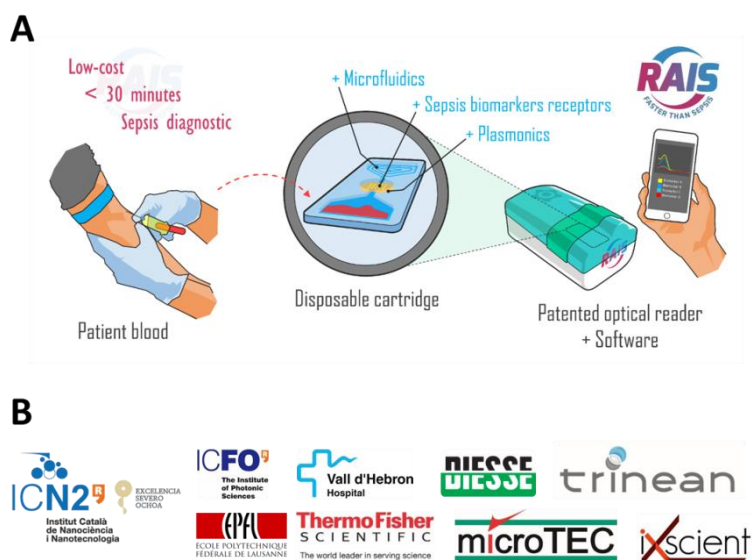


**Figure 1.10:** A: Scheme of the RAIS project. B: Logo of the partners involved in the project.



# Chapter 2

## Materials and Methods

In this chapter the materials and methodology used along this thesis are explained. First, a detailed explanation of the components of the optical POC device is provided, followed by the fabrication protocol of the nanoplasmonic substrates employed. After, a list of all the chemical reagents, buffer and biological compounds is included. In addition, we include all the biofunctionalization protocols tested in this thesis and, finally, a description of the assays developed for the detection and quantification of sepsis protein biomarkers and bacteria is also included.



## 2. Materials and Methods

### 2.1 Optical POC device

The optical POC device employed in this thesis is based on a novel interferometric lens-free microscopy design and consists of three main parts: the light source, the optical components and the electronics. The light source is an external LED fiber which spectrally overlaps the transmission peak ( $\lambda=660$  nm) of the custom-designed gold nanoplasmonic chips used as sensing substrate, which are based on gold nanohole arrays (Au-NHA, detailed below). The device can work with glass substrates, in which case, the light source is an LED block containing high-power LEDs coherently coupled into a single multimode fiber. This LED block is from Thorlabs (USA) and contained three LEDs at 455 nm (blue), 530 nm (green) and 625 nm (red), respectively. The optical assembly comprises optical elements that are mounted to facilitate a vertical optical axis. First, the fiber-coupled light is collimated using a parabolic mirror to enable uniform illumination over the field-of-view (FOV) (See **Figure 2.1**). The collimated and coherent light beam passes through the microarray plate mounted on the sample holder, which is sandwiched between two sets of orthogonal polarizers and Savart plate (SP) pairs, and terminates at the CMOS read-out sensor (area =  $4.2 \times 5.7$  mm<sup>2</sup>). Whereas all optical elements are fixed to the optical column, the top SP holder can be tilted in the z-direction. A step motor, whose rotation axis is shared by a leveler with uneven radius, is used to push one side of the SP holder to generate precisely controlled tilt angles of up to  $\pm 2^\circ$ .<sup>134</sup>

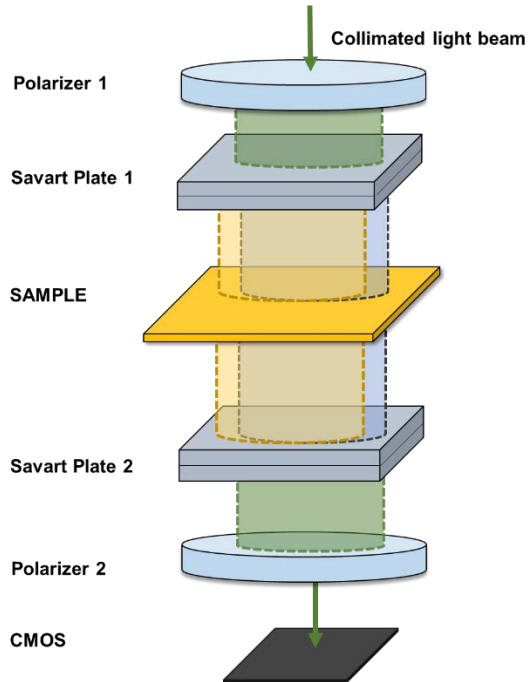


**Figure 2.1:** Schematic representation of the optical components in the POC device. The design includes a LED light source (not shown), a fiber collimator (not shown), a polarizer (1), two SP plates and a second polarizer (2). The sample is placed between the two SP. The output light beam is recorded by a CMOS sensor.

### 2.1.1 Nanoplasmonic sensor chip fabrication

During the project progress, nanoplasmonic chips based on gold nanohole arrays (Au-NHAs) were found to be the optimal configuration as sensing chips. The chips were provided by our collaborators from Ecole Polytechnique Fédérale de Lausanne (EPFL) (Switzerland) responsible for their design and fabrication at their cleanroom facilities. Wafer-scale, high-throughput nanofabrication techniques on a robust transparent substrate (Radio Corporation of America-cleaned 4-inch fused silica wafers of 500  $\mu\text{m}$  of thickness) in a single lithography step were used. Using an e-beam evaporator (Alliance-Concept EVA 760, Cran Gevrier, France), 10 nm titanium and 120 nm gold layers were evaporated. The nanohole arrays (200 nm diameter and 600 nm period) were patterned using a 248 nm deep ultraviolet stepper (ASML PAS 5500/300 DUV, Veldhoven, Netherlands). After resist development, the nanohole arrays are transferred into the Ti/Au layer using an ion beam etching tool (Oxford Instruments PlasmaLab 300

IBE, Abingdon, UK). The resist on the surface is removed using oxygen plasma cleaning. Finally, after coating with a layer of photoresist to protect the sensor surface, the 4-inch wafer is diced into 1 cm<sup>2</sup> chips. The resist layer on the chips is removed by a remover solvent followed by an oxygen plasma exposure to ensure a uniformly clean sensor surface. For more details see Yesilkoy *et al.* 2018.<sup>134</sup>

### 2.1.2 Signal processing and Data analysis

The OPD (optical path difference) signal over the whole FOV was measured with custom-made software written in Python by our collaborators at ICFO (Barcelona, Spain), which rendered intensity mapping images of the arrayed surfaces. This software also controls the POC. Then, the accurate OPD signal quantification and data statistics extraction of routine microarray analysis was calculated with a custom-made acquisition software developed in LabVIEW 2011 (National Instruments, USA) by Trinean NV (Ghent, Belgium). OPD<sub>total</sub> values for bacteria determination were calculated with a software written in Python by our research group. Data analysis was carried out using GraphPad Prism 7 software (San Diego, CA, US).

In the “Preliminary considerations” (section 4.2) OPD values were estimated from the recorded images using the software ImageJ (NIH Image) whereas in the other sections of the chapter the OPD was estimated with the custom-made measuring software.

### 2.1.3 Characterization of the POC for sensor measurements

#### *SiO<sub>2</sub> calibrating plate*

Transparent fused silica chips and Au-NHA chips were patterned to create microarrays of SiO<sub>2</sub> layers. These chips were prepared and provided by our collaborators at EPFL (Switzerland). More detailed information can be found in Yesilkoy *et al.* 2018.<sup>134</sup> Briefly, a single-step lithography was performed. After resist development, various thin SiO<sub>2</sub> layers (1.5, 2.5, 5 and 10 nm) were evaporated on both Au-NHA chips and the corresponding transparent control substrates using an e-beam evaporator (Alliance-Concept EVA 760). Finally, a lift-off process in resist remover solvent was applied,



leaving a microarray of circular SiO<sub>2</sub> thin-film patterns. Chips with each SiO<sub>2</sub> thickness were prepared twice for both glass and Au-NHA substrates. OPD signal produced by SiO<sub>2</sub> spots was measured with the POC system.

#### *Sensitivity on different refractive indexes media*

An Au-NHA chip with a high OPD signal intensity microarray was assembled in a microfluidic cartridge designed and fabricated in Poly(methyl methacrylate) (PMMA) by MicroTEC (Germany). The microfluidic cartridge was custom designed for fitting a 1cm<sup>2</sup> Au-NHA chips. It contained an inlet and outlet apertures were tubes were connected to flow different solutions. A LED light source with emission at 880 nm was coupled in the POC for analysis in aqueous solutions. MilliQ water and PBS buffer were flown through the assembled microfluidics and the OPD signal was measured.

## **2.2 Fabrication of Microarrays with Dip-pen Nanolithography**

The Dip-pen Nanolithography spotter Nano eNabler™ from BioForce Nanosciences (Utah, USA) was used for the generation of microarrays. Two different surface patterning tools (SPT), 30R and 60R from BioForce Nanosciences (Utah, USA) were used to generate spots of different sizes. SPTs were always treated in O<sub>2</sub> plasma chamber for 2 min (0.5 mbar, 99% power, 120 s) before use. Different protein or buffer solutions were spotted on the surface at high humidity conditions (75-80% Relative Humidity). Upon optimized conditions creating an 8x8 microarray takes around 3 min.

## **2.3 Chemical and Biological Reagents**

### **2.3.1 Chemical Reagents and Buffers Composition**

Most of the salts and chemical reagents for preparation of buffers and biofunctionalization protocols were purchased at Sigma-Aldrich (Germany): alkanethiols for SAM formation (16-mercaptohexadecanoic acid (MHDA), reagents for carboxylic group activation (1-ethyl-3-(3-dimethylaminopropyl)carbodiimide hydrochloride (EDC) and N-hydroxysulfosuccinimide (sulfo-NHS)), Tween 20, bovine serum albumin (BSA), glycerol.

Several buffers were used either for functionalization or target analysis: PBS 10 mM (10 mM phosphate, 137 mM NaCl and 2.7 mM KCl, pH 7.4), PBST (PBS buffer + 0.5% Tween 20, MES buffer (0.1 M, pH 5.4) and MilliQ water from Millipore (USA) was always employed to prepare them.

Ethanol and acetone were purchased to Panreac (Spain). EZ-Link™ HPDP-Biotin (HPDP) was purchased to Fisher Scientific (Spain). Antibodies were biotinylated with the commercial kit Lighting Link® Rapid Biotin Type B from Antibody BC (Spain). Skim milk powder from Fluka- Fisher Scientific (Spain). Pooled Normal Human Plasma was purchased to Innovative research (USA).

### 2.3.2 Biological compounds

Streptavidin (SA) and NeutrAvidin (NA) were purchased to Sigma-Aldrich (Germany). Three different anti-CRP monoclonal antibodies were used: C183 and C196 were kindly provided by DIESSE Diagnostica Senese S.p.a. (Italy) whereas C7 was acquired from HyTest Ltd. (Finland). Anti-PCT antibodies (QNO5 and 03-1C2) and PCT were kindly provided by Brahms-ThermoFisher (Germany). Anti-IL-6 monoclonal antibody was acquired to Fisher Scientific (Spain). CRP was provided by BBI solutions (United Kingdom) and IL-6 by Abyntek Biopharma (Spain). Anti *P. aeruginosa* polyclonal antibody ab68538 (anti-Pae) and anti *E. coli* O + *E. coli* K polyclonal antibody ab31499 (anti-Ec) were purchased to Abcam (United Kingdom).

Lyophilized bacterial pellets of *P. aeruginosa* (ATCC 27853) (Pae) and *E. coli* (ATCC 8739) (Ec) were acquired from ieLab (Spain). The bacterial pellets were reconstituted in pure water according to the recommendations of the manufacturer. The concentration of each solution is certified by accredited laboratories conforming to internationally recognize standards. The bacterial solutions were aliquoted and stored at -20°C until needed. Before use, aliquots were centrifuge at 7500 rpm for 10 min at 4°C. The supernatant was discarded and the pellet was suspended in PBST.

## 2.4 Biofunctionalization Strategies

### 2.4.1 Glass surface functionalization by dip-pen nanolithography

The silanized microscope glass slides (Nexterion Slide E for epoxy and 3D Hydrogel Coating Slide H modified with NHS esters) were purchased to SCHOTT (Jena, Germany). Glass surfaces were spotted with 500 µg/mL solution of C7 anti-CRP antibodies in PBS buffer. Incubation at 4° was done in a common fridge while incubation at 37° was carried out in an incubator. Visualization of the microarrays was done using the POC reader with the LED block.

### 2.4.2 Gold surface functionalization by dip-pen nanolithography

Gold chips (1 cm<sup>2</sup>) for control experiments were prepared at our facilities by electron beam deposition (1 Å/s) of 1 nm of titanium and 7 or 120 nm of gold layers with ATC-8E Orion from AJA International Inc (USA). Then, these gold-coated glass chips were cleaned by consecutively immersion in acetone, ethanol, and MilliQ water and sonication for one min. The chips were dried with N<sub>2</sub> and placed in the holder of the Nano eNabler™ for the microarray printing.

Nanoplasmonic chips were cleaned by immersion for 10 s in a 2 min activated piranha solution (H<sub>2</sub>SO<sub>4</sub>:H<sub>2</sub>O<sub>2</sub>, 3:1). Then they were placed in UV Ozone Cleaner-ProCleaner™ for 30 min. After this, the chips were immersed in MilliQ water for 30 min. The dried chips were then biofunctionalized following different strategies, as detailed below.

#### 2.4.2.1 Direct antibody binding through adsorption

*Direct adsorption* of IgGs: an anti-CRP solution at 250 µg/mL dissolved in PBS buffer (with 5% glycerol) was used to generate the microarrays. After spotting, an incubation step for 2 h at room temperature (RT) was done and then, the chips were rinsed with MilliQ water and dried with N<sub>2</sub>.

#### 2.4.2.2 Antibody binding through Protein G orientation

Protein G was attached to the surface via adsorption or through a previously created SAM.

*Protein G adsorption* was done by creating a microarray of Protein G at 500  $\mu\text{g}/\text{mL}$  dissolved in PBS buffer (10 mM, pH 7.4 and 5% glycerol). After deposition, an incubation step of 2 h at RT was done. Then, the chips were rinsed with MilliQ water and dried with  $\text{N}_2$ . BSA (1%) solution was incubated for 1 h to block the sensor surface. An antibody solution (250  $\mu\text{g}/\text{mL}$  in PBS buffer) was added to the whole sensor surface and incubated for 1 h at RT. The chips were rinsed with MilliQ water and dried with  $\text{N}_2$  again.

*Binding of Protein G through a SAM* was done, firstly, by immersing the chips in a 250  $\mu\text{M}$  16-mercaptohexadecanoic acid (MHDA) solution and kept overnight at RT. Then, chips were rinsed with ethanol, MilliQ water and dried with  $\text{N}_2$  to remove excess of MHDA. After this, a solution of EDC (0.2 M) and sulfo-NHS (0.05 M) in MES buffer was added and incubated for 30-40 min. After rinsing with water, a solution of Protein G (50  $\mu\text{g}/\text{mL}$  in PBS) was deposited over the chip and incubated for 1 h. After rinsing, the chip was then placed in the Nano eNabler and arrays of antibody (250  $\mu\text{g}/\text{mL}$  in PBS buffer with 5% glycerol) were spotted.

#### 2.4.2.3 Antibody binding through avidin/biotin interaction

Biotinylation of antibodies was done with the Lightning-Link® Rapid mix according to the supplier. Briefly, every 10  $\mu\text{L}$  of antibody solution (1 mg/mL) was mixed with 1  $\mu\text{L}$  of LL Rapid Modifier reagent. Then the mixture was added directly onto the vial with the lyophilized material. This was gently mixed by withdrawing and redispensing the liquid using a pipette. The vial was incubated for 15 min at RT. Finally, addition of 1  $\mu\text{L}$  of LL Rapid Quencher for every 10  $\mu\text{L}$  of antibody solution was added to the mix. The solution is ready after 5 min.

Biotinylated antibodies were attached to avidin-coated chips. The avidin protein was attached to the surface through different ways: (i) direct *adsorption of SA or NA*, (ii) binding to a *SAM of HPDP-biotin* and binding to a *SAM of SH-PEG-biotin* either (iii) covering the whole surface or (iv)

previously spotted in a microarray design.

*Adsorption of SA or NA* (i) was done by direct spotting of 250 µg/mL solutions in PBS (with 5% glycerol). After deposition, an incubation step of 2 h at RT was followed. Then, the chips were rinsed with MilliQ water and dried with N<sub>2</sub>. Later, biotinylated antibodies (250 µg/mL in PBS buffer) were incubated at RT for 1 h. The chips were rinsed with MilliQ water and dried with N<sub>2</sub> again.

For binding through a *SAM of HPDP-biotin* (ii), first, a layer of HPDP-biotin (1 mM in ethanol incubated overnight) was formed covering the whole surface of the chip. Then, a layer of avidin (SA or NA at 100 µg/mL in PBS buffer) was added and incubated at RT for 1 h. Finally, biotinylated antibodies (250 µg/mL in PBS buffer) were directly spotted in order to achieve the microarray pattern.

A *continuous SAM of SH-PEG-biotin* (iii) was obtained after incubation of a 1 mM solution in ethanol overnight. Then, SA was spotted at 500 µg/mL (in PBS buffer with 5% glycerol). Finally, biotinylated antibodies (250 µg/mL in PBS buffer) with the commercial kit Lightning-Link® Rapid Biotin Conjugation Kit (Type B\*) from Expedeon (San Diego, California, US) were incubated during 1h.

Conversely, SH-PEG-biotin dissolved in PBS (with glycerol 5%) was spotted to generate a microarray-based SAM (iv). After overnight incubation, a solution of BSA (1% in MilliQ water) was added for 1 h to block remaining areas. Then, SA (100 µg/mL) was added and incubated for 1 hour. Finally, biotinylated antibodies (250 µg/mL in PBS buffer and biotinylation reagents) were incubated during 1h.

## 2.5 Immunoassays for protein biomarkers and bacteria (Chapters 5 and 6)

### 2.5.1 Calibration curves

Au-NHA chips were cleaned by immersion for 10 s in 2-minutes-activated piranha solution (H<sub>2</sub>SO<sub>4</sub>:H<sub>2</sub>O<sub>2</sub>, 3:1). After rinsing and drying, they were placed in the UV Ozone Cleaner-ProCleaner™ for 30 min. After this, the chips were immersed in MilliQ water for 30 min. Then, Protein G (500

$\mu\text{g/mL}$  in PBS buffer with 5% glycerol) were spotted on the chips and incubated for 2 h. A BSA solution (1% in MilliQ water) was added to the whole surface and incubated at RT for 1 h to block remaining gold areas. Specific antibodies (250  $\mu\text{g/mL}$  for anti-CRP, anti-IL-6 and anti-PCT and 500  $\mu\text{g/mL}$  for anti-Pae and anti-Ec) were incubated for 1 h also at RT. Finally, several concentrations of CRP, IL-6, PCT or bacteria (10  $\mu\text{L}$  of incubation volume in PBS buffer or in diluted plasma) were analysed in order to generate the calibration curves. Incubation time was fixed at 30 min. Between each step a rinsing with PBS and MilliQ water and drying with  $\text{N}_2$  was performed. OPD signals were recorded with the same custom-made acquisition software as in previous chapter.

## 2.5.2 Hospital samples and clinical validation

The patient's samples used in the validation analysis were previously collected to constitute the Sepsis Bank, a large collection of samples handled by the Biobank Unit at the Vall d'Hebron Barcelona Campus (Vall d'Hebron University Hospital/Vall d'Hebron Research Institute (VHIR)). Informed consent was obtained from all blood donors (healthy donors, SIRS patients as well as sepsis patients) and the protocol had previously been approved by the Clinical Research Ethics Committee of the Hospital with reference number PR(AG)11/2006. The Sepsis Bank was set up in the context of the H2020 RAIS project; accordingly, all data was protected in accordance with the EU Data Protection Directive 95/46/EC "*on the protection of individuals with regard to the processing of personal data and on the free movement of such data*". Specifically, all samples and related clinical data were anonymized, and no personally identifiable data has ever been included in any dataset transmitted outside of VHIR.

Four different microarrays of antibodies (8x8 each one) were printed on 1  $\text{cm}^2$  and marked with hydrophobic pen to be able to study 4 samples simultaneously. Patient plasma samples (200  $\mu\text{L}$ ) were diluted at 25 or 50% in PBS or PBST, respectively. Then, 10  $\mu\text{L}$  of each sample were incubated with the microarrays during 30 min at RT. The chip was then rinsed with PBS buffer and MilliQ water and finally dried with  $\text{N}_2$ . The calculated concentration was achieved by interpolation from the corresponding calibration curve.



# Chapter 3

## Nanophotonic microarray-based biosensor

Given the novelty of the nanophotonic biosensor employed in this thesis, this chapter is dedicated to an in-deep explanation of the optical principles behind this new technology. The optical system used for evaluating in a microarray format with nanoplasmonic chips is described in detail. In addition, experiments performed to test the technology for biosensing applications are also included. Finally, an extended study to find the optimal conditions to create microarrays on the nanoplasmonics sensor surface is also described.





## 3. Nanophotonic microarray-based biosensor

### 3.1 POC nanophotonic biosensor

Light microscopes are devices used to enlarge images by using visible light and lenses. When a sample is illuminated by a light beam it introduces changes in the final illumination. These changes can be associated to optical effects such as absorption, reflection, scattering or their combination. Interaction of light waves with other media different than vacuum produces changes in the wave amplitude and phase. This depends on the properties of the medium where the light travels through. Modifications in amplitude (brightness) are due to scattering and absorption of light. Human eye is only sensitive to amplitude variations, thus, phase changes are often invisible. Samples containing small objects such as cells or biomolecules often do not produce enough changes in the light to be detected, appearing therefore as invisible. Microscopes that measure phase-shifts (or optical path differences, OPD) arose as a solution for allowing transparent objects (to human eye) to be visible.

Current microscopes that exploit phase shifts are phase-contrast,<sup>135,136</sup> holographic<sup>137–139</sup> and differential-interference contrast (DIC)<sup>140</sup> microscopes (see **Figure 3.1**). They offer high sensitivity and resolution to transparent samples but with a limited field-of-view (FOV) (typically less than 0.2 mm<sup>2</sup>) and depth-of-field (DOF) as the light beam is focused on the sample.<sup>141</sup>

During last years, many efforts have been made towards the development of lens-free microscopes (LFMs) in order to reduce the size of the microscope and to enlarge the FOV and DOF. This is done by using unfocused light beams and a photosensitive detector such as a CMOS or a charge-coupled (CCD) camera.<sup>141–147</sup>

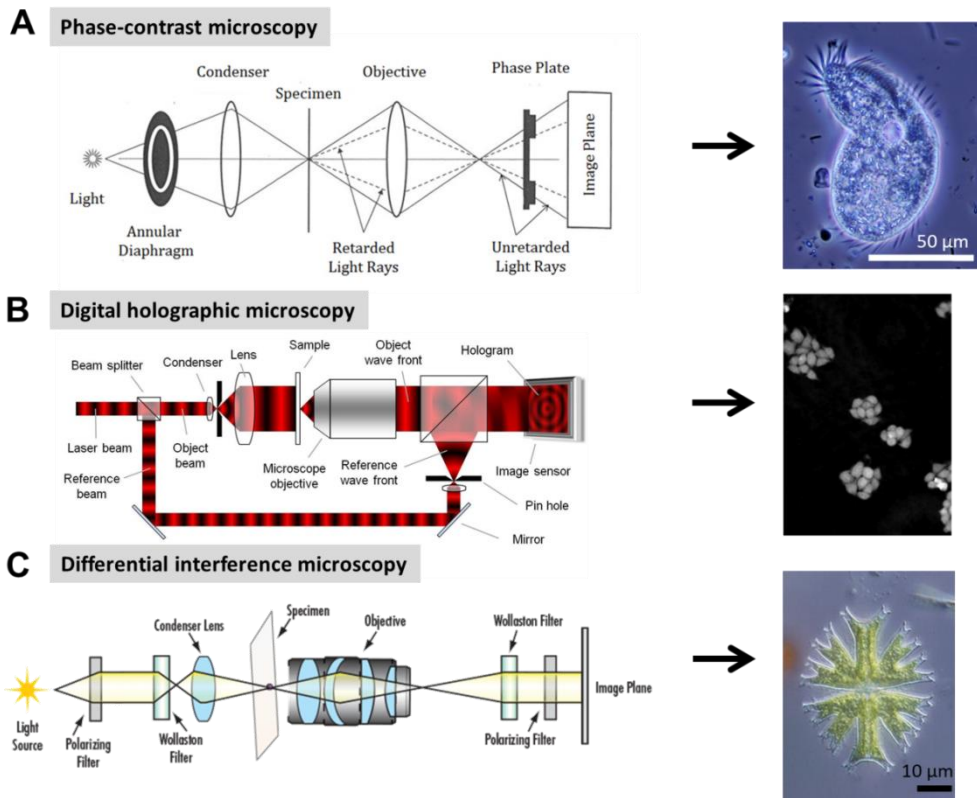


**Figure 3.1:** Scheme of the optical components of microscopes that exploit phase shifts to build the image. Examples of images achieved with these microscopes are included too.<sup>148–150</sup> A: Phase-contrast microscopy. B: Digital holographic microscopy. C: Differential-interference contrast (DIC) microscopy.

Recently, a new large-FOV interferometric microscope (LIM) which measures phase-shifts was presented.<sup>151</sup> It has a novel design that combines DIC, LFM and phase-shifting interferometry (PSI) in a unique manner that makes possible to achieve 20 mm<sup>2</sup> as FOV, 30 mm as DOF, axial sensitivity of OPD < 1 nm and 35 μm as lateral resolution. The design includes a light emitting diode (LED) as light source, a fiber collimator, two polarizers, two SP and a CMOS sensor (**Figure 3.2A**). SP are composed of two birefringent crystals, which act differently on a light beam depending on its polarization.<sup>152</sup> The two SP are located between crossed polarizers to create a balanced Mach-Zehnder interferometer of partially overlapping and sheared beams with orthogonal polarizations. No lenses are required for refocusing the sheared beams with orthogonal polarization as it happens in conventional

DIC microscopes. This is what allows high axial sensitivity and large FOV.

If a sample is located between the SP and introduces any RI change that affects the sheared beams it will lead to a detectable OPD by transforming the phase-shift into intensity (**Figure 3.2B**). The interferometric pattern created over the full FOV of the camera is recorded by the CMOS camera. This information is sent to a connected computer which creates an “image or a picture” that contains the OPD pattern over the the FOV. A holographic image of the surface of the sample is achieved by using a surface reconstruction program which uses deconvolution algorithms. Thus, local deviations in the thickness (i.e. in the RI), such as biomolecules attached to the sensor surface, can be tracked by a camera and then processed by an algorithm to extract the OPD. The algorithm isolates each spot and its surroundings and calculates the difference between the maximum and the minimum phase-shift values found in that area, rendering the final OPD value for each spot. With this approach the topography of the analysed surface, with thickness variations in the nanometre range, can be measured and quantified.

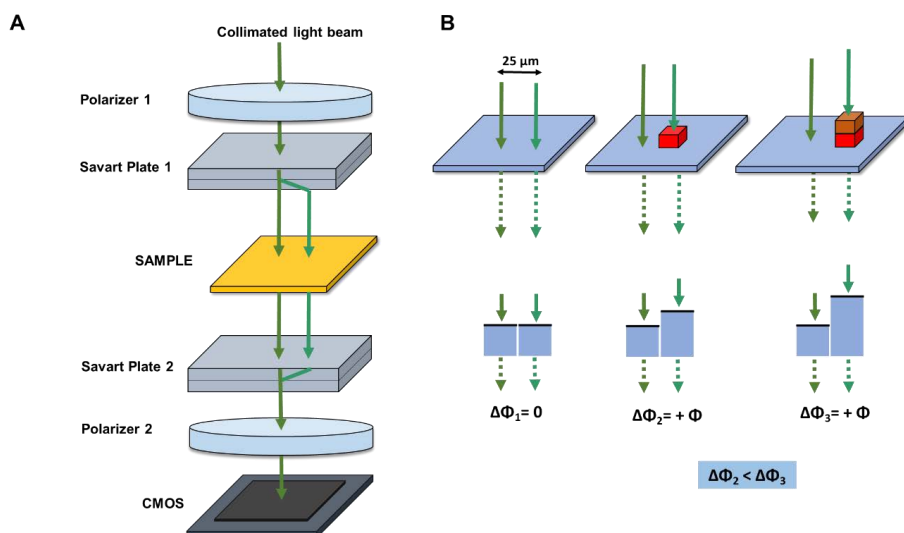


**Figure 3.2: A: Scheme of the optical device.** The design includes a LED light source (not shown), a fiber collimator (not shown), a polarizer (1), two Savart plates and a second polarizer (2). The sample is placed between the two Savart plates. The outcome light beam is recorded by a CMOS sensor. **B: Principle of detection of the OPDs in transparent samples using the phase-sensitive microscope.** In the LIM, two polarized beams are symmetrically sheared by a distance of 25 μm. Depending on the RI on the surface, the resulting phase-shifts (OPDs) will be larger or smaller, resulting in more or less intense signals.  $\Phi$ = Phase-shift.

As detailed in the **Materials and Methods**, all the optical elements are fixed to the optical column; however, the top SP holder can be tilted in the  $z$ -direction to generate precisely controlled tilt angles. During the measurement (which takes around 1 min) the SP is being tilted creating different angles of incidence (screening of  $\theta$ ) of the input beam incident which leads to a larger difference in OPD, therefore, there is a higher sensitivity to OPD changes and a lower threshold for detection. The relative change in OPD measured by the LIM is calculated with the following equation (**Equation 3.1**):

$$\Delta_{OPD} \propto t \left[ \left( \frac{n_o^2 - n_e^2}{n_o^2 + n_e^2} \right) \theta \right] \quad (3.1)$$

where  $t$  is the thickness of the SP, and  $n_o$  and  $n_e$  are the refractive indexes that go through each split light beam formed by the SP.<sup>151</sup>

The potential of the LIM for the detection of changes in the RI was previously assessed with three different kind of experiments performed on transparent substrates.<sup>151</sup> First a ribbon made of transparent indium tin oxide (10 nm thick, 0.5 mm wide and 7 mm long) was deposited on a glass substrate. Upon current injection in the ribbon a clear signal was detected due to thermooptics effect (increase in the local refractive index and the glass beneath) (see **Figure 3.3A**). The more current applied, the larger the local refractive index change, thus, a larger signal is recorded. Secondly, a set of silica substrates were patterned with ultrathin silica (SiO<sub>2</sub> layers of 2 and 5 nm). The pattern was visible with the LIM (**Figure 3.3B**) and the heights matched with the ones evaluated by AFM for comparison. Finally, a glass substrate was patterned with two samples: one with a BSA solution and the other with BSA incubated with anti-BSA antibodies. Both monolayer (only BSA) and bilayer (BSA + IgG) were covalently attached to the glass surface and clearly detected by the LIM (**Figure 3.3C**). Moreover, the OPD signal for the bilayer was larger than for the monolayer, which exemplifies the potential of the developed LIM to perform analysis in a label-free scheme.

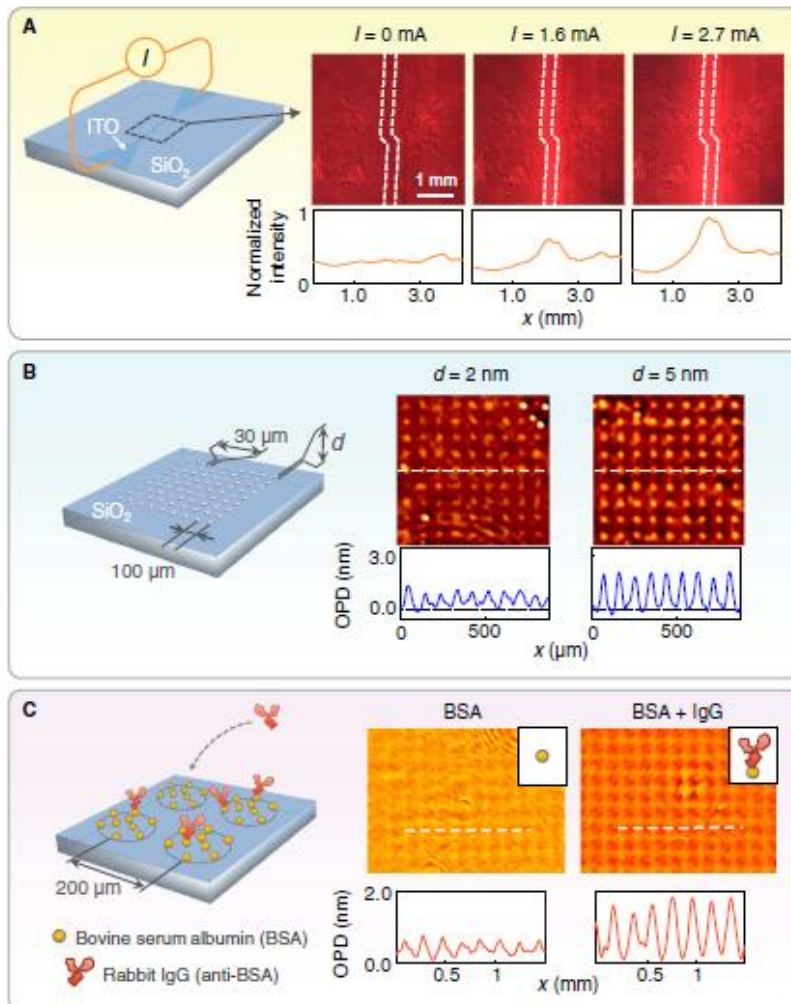


**Figure 3.3:** Detection of transparent patterns with the LIM. A: transparent indium tin oxide (ITO) ribbon. B:  $\text{SiO}_2$  silica patterns. C: mono and bilayer of biomolecules. Figure extracted from <sup>151</sup>.

To improve the usability and feasibility as user-friendly analytical device, miniaturization of the novel LIM and its integration with cheaper components was done within the European RAIS project. A smaller and more compact device (20 x 14 x 23 cm, **Figure 3.4A**) was achieved, thus, making possible its use as a truly point-of-care platform. The improved LIM contains an external LED (**Figure 3.4B**) and a holder to introduce the samples (**Figure 3.4C**).

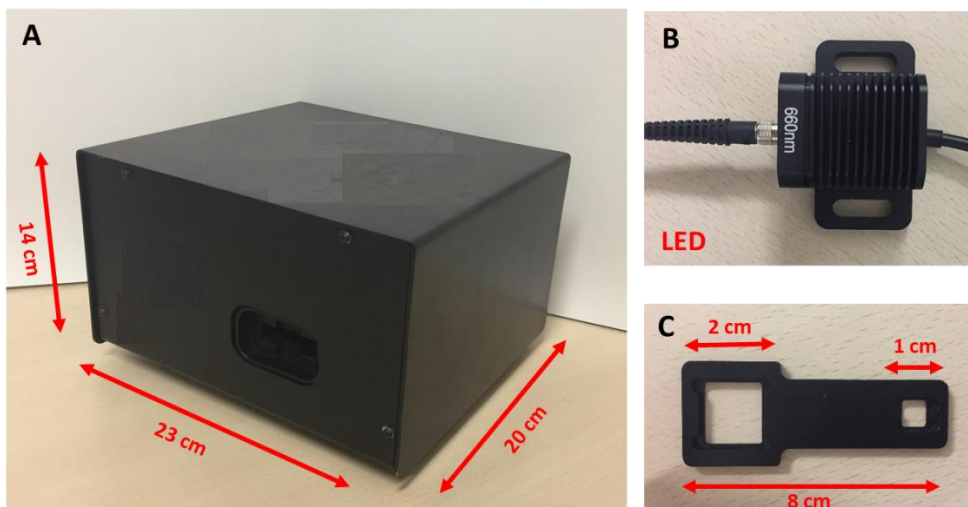


**Figure 3.4:** Pictures of the POC biosensor (and its external components. A: The POC device is a black box with a robust armour; B: external LED light source (660 nm); C: Holder that can carry 1 cm<sup>2</sup> and 2 cm<sup>2</sup> chips.

The optical principle of the LIM/POC device (i.e. each point of one of the sheared beams interferes with the corresponding other sheared beam point) makes it the ideal candidate for the measurement of periodic patterns with dimensions equal or larger than the shear distance (25  $\mu\text{m}$ ). Due to this, the POC biosensor was proposed to be used as a label-free microarray reader for biomarker detection.

### 3.2 Custom-designed nanoplasmonic structures for signal enhancement

The POC biosensor can operate with substrates that transmit light at the specific wavelength of the LED light source coupled. Initial tests<sup>151</sup> showed the feasibility of label-free measurements with the POC device using conventional glass substrates. However, also within the RAIS European project, a metal nanoplasmonic plate was specifically designed by the collaborators in EPFL to enhance the phase shifts (i.e. the sensitivity) of the device.<sup>134</sup>

The nanoplasmonic plate was designed and fabricated to operate in transmission mode under normal incidence of light to amplify the

interference of the detection and reference signals. Periodically-ordered sub-wavelength nanohole arrays (NHAs) were chosen due to their high transmission efficiency at narrow wavelength range (EOT effect), their tuneable optical properties, and the possibility to be fabricated using large-area, low-cost, high-throughput nanofabrication methods. Under normal circumstances a light beam would not cross a subwavelength aperture, however, due to the coupling of light with plasmons and the presence of constructive interferences on the surface of the periodically patterned metallic film, light is transmitted through the substrate.<sup>67,153</sup>

In these plasmonic nanostructures, geometrical parameters (i.e. symmetry and periodicity of the nanohole, nanohole diameter and metal film thickness) are crucial parameters to be tuned in order to maximize the transmission and enhancement of OPD. After numerical simulations and experimental trials, arrays with 200 nm diameter nanoholes with a 600 nm period (**Figure 3.5C**) were selected. These parameters fit to a maximum transmission around 660 nm in air, and therefore, an LED light source at that wavelength was coupled to the POC device. The sensitivity of the POC device with these nanostructures was numerically estimated as  $5 \cdot 10^{-4}$  nm per Refractive Index Unit (RIU).<sup>134</sup> When comparing this sensitivity with other photonic devices (see **Table 3.1**) we observe that although not being the most sensitive sensor, it could be useful for some biosensing applications as other sensor systems like grating couplers or photonic crystals based devices, which work within the same sensitivity range. In addition, the main advantage of the LIM technology over the others ones is the high-throughput capabilities that can be easily implemented (up to thousands of interaction spots).

An important feature of the nanoplasmonic chips is the geometrical lattice arrangement of the nanoholes. Two lattices, hexagonal and squared, were tested. Both have similar sensitivities for similar resonance wavelengths.<sup>153</sup> Squared gold-NHAs are produced by a Deep Ultra-Violet lithography (DUVL)<sup>154</sup> technique while the hexagonal gold-NHAs are done by Talbot lithography.<sup>155,156</sup> Initially, sensor chips produced by Talbot lithography did not reach a hole size below 200 nm, so there was a strong direct transmission through the holes widening the resonance peak (**Figure 3.5D**). On the contrary, as the resolution of the DUVL was improved, it was possible to fabricate smaller holes and the resonance was more uniform, shrinking the



transmission peak. Further optimization of the Talbot process allowed the production of square lattices and smaller holes, resulting in sharper resonances. Although hexagonal lattice seems to be more sensitive (i.e. they generate larger phase-shifts<sup>153</sup>), due to fabrication process optimization, it was decided to continue working with sensor chips fabricated with the squared lattice by the DUVL technique.

**Figure 3.5A,B,C** shows AFM pictures of the nanoplasmonic chips with both geometrical arrangements. As can be seen in **Figure 3.5D**, the transmission spectrum of squared lattice is sharper than the hexagonal one at 660 nm.

**Table 3.1:** Sensitivity of the most common photonic biosensors.

TRANSDUCER	LIMIT OF DETECTION (PG/MM <sup>2</sup> )	BULK SENSITIVITY (RIU)	REFERENCE
Surface Plasmon Resonance (SPR&LSPR)	01-5	$10^{-5} - 10^{-7}$	157
SPR imaging	1	$10^{-6}$	74
Grating couplers	0.3-5	$10^{-4} - 10^{-6}$	158
Mach-Zehnder Interferometer	0.01-0.06	$10^{-7} - 10^{-8}$	159,160
Bimodal Waveguide Interferometer	0.01	$10^{-7} - 10^{-8}$	161
Young Interferometer	0.013-0.75	$10^{-8} - 10^{-9}$	162,163
Microring resonators	1-3	$10^{-5} - 10^{-7}$	164-167
Photonic Crystals	0.4-7.5	$10^{-4} - 10^{-5}$	17

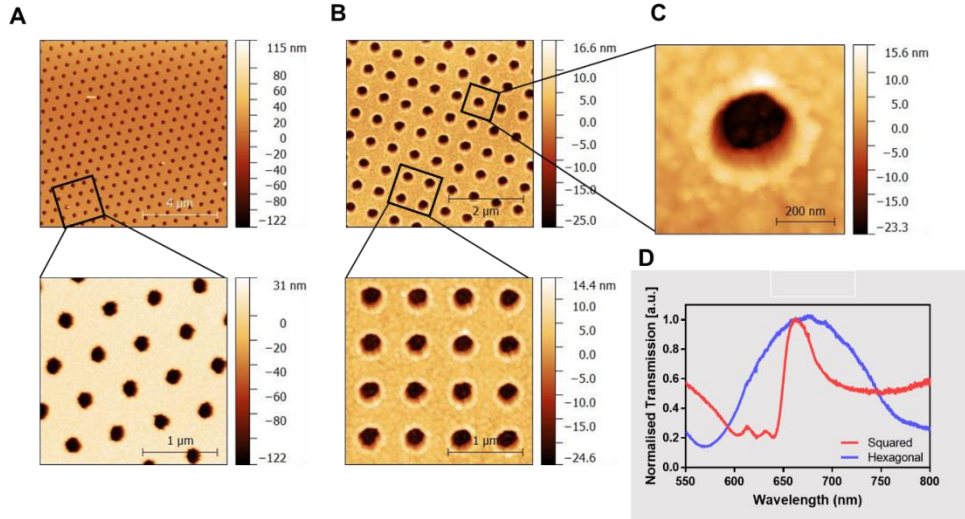


**Figure 3.5:** AFM pictures of the two types of nanoholes pattern arrangement. A: Hexagonal lattice. B: Squared lattice. C: Nanohole detail. D: Transmission spectra of hexagonal and squared lattice nanohole plasmonic plates.

As mentioned in the introduction, nanoholes are highly sensitive to surface conditions due to their highly confined local electromagnetic fields, which strongly interact with the surrounding medium. As pointed in **equation [3.1]**, OPD depends on the RI of the medium where the light is being transmitted. The transmission maximum peak appears at 660 nm when the light goes through air (RI=1), that is, dry conditions. If the plasmonic plate is placed in a medium with a higher RI, the transmission peak will be displaced to higher wavelengths. We can observe in **Figure 3.6** how the transmission peak appears around 880 nm when measuring in aqueous media (RI  $\approx$  1.33). Therefore, measurements in aqueous media require a change in the employed LED to meet this wavelength maximum.

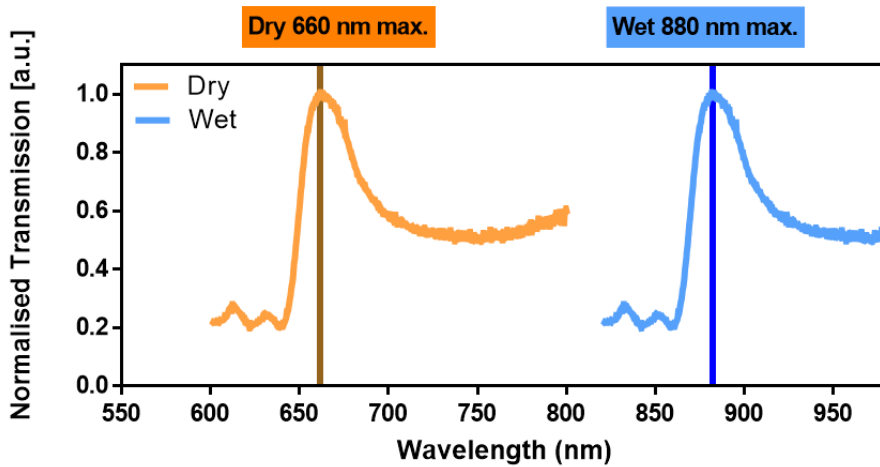


**Figure 3.6:** Transmission spectrum of the squared-lattice NHA chips in air/dry (orange, RI=1) and in water/wet (blue, RI=1.33).

Finally, some examples of the OPD intensity pattern images generated with the LIM are showed in **Figure 3.7**. Orange/black scaled images correspond to the first software developed for the initial design of LIM, while full colour scale was displayed with the software generated for the optimized LIM (POC-based design). Preliminary studies were done with the first software and the first version of LIM until the final POC version was delivered during the execution of the European project. All the images contain the same type of information, being the colour scales the only difference.

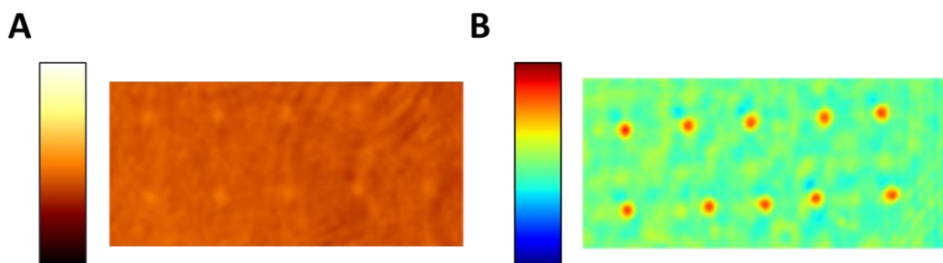


**Figure 3.7:** OPD intensity pattern images generated with:  
A: First version of the LIM and B: POC version of the LIM.

### 3.3 Characterization of the POC for biosensing applications

In the following section, those preliminary experiments done to test and characterize the POC technology and its sensing application are described.

#### 3.3.1 Signal enhancement due to the Nanoplasmonic chip

In order to evaluate the real enhancement produced by the nanoplasmonic nanostructures, the wafer was diced in  $1\text{ cm}^2$  chips (Au-NHA) and different thicknesses (1.5, 2.5, 5 and 10 nm) of  $\text{SiO}_2$  were evaporated in a microarray-based design (i.e. mimicking the spotting of few  $\mu\text{m}$  area). Also,  $1\text{ cm}^2$  glass chips were also coated with  $\text{SiO}_2$  with the same pattern and thickness layers.

Two examples of the OPD colour code maps generated by 5 and 10 nm thickness layer, respectively, are shown in **Figure 3.8A**. Visually the  $\text{SiO}_2$  spots evaporated over the Au-NHA chip are more intense than the ones generated only on the glass surface. The OPD in air (dry) was recorded in both substrates and the results were plotted (See **Figure 3.8B**). The OPD signal recorded for the same thickness of  $\text{SiO}_2$  was ten times larger for the Au-NHA chip than for the bare glass substrate. Therefore, the Au-NHA chips were enhancing the OPD by one order of magnitude.

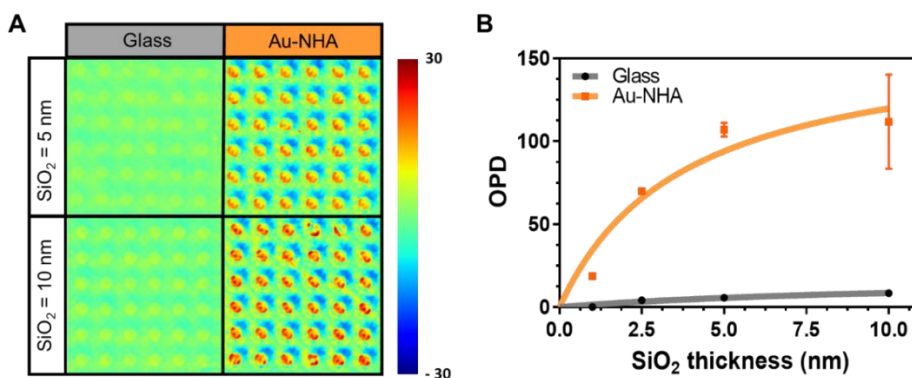


**Figure 3.8:** Comparison of OPD signals on bare glass and on nanohole-patterned surfaces. A: Colour code OPD maps for 6x6 microarrays of 5 and 10 nm  $\text{SiO}_2$  layers on bare glass and Au-NHA surfaces, respectively. B: Plot containing the OPD values for the different thickness of  $\text{SiO}_2$  over bare glass and Au-NHA surfaces, respectively .

### 3.3.2 Influence of the evaluation medium

As the transmission spectrum of the Au-NHAs depends on the refractive index of the surrounding media, evaluations in water and buffer were performed in order to assess the feasibility of performing analysis without drying the chip and, eventually, directly in complex media such as human serum or plasma. An already spotted Au-NHA chip with a microarray with high intensity OPD spots was assembled in the microfluidic cartridge specifically designed (**Figure 3.9C**) which fits in a holder that contains an inlet to inject the sample. The transmission spectrum shows experimentally that when the RI is around  $\approx 1.33$ , the maximum transmission peak is shifted to 880 nm (**Figure 3.6**), thus an LED light source with the appropriate wavelength was assembled in the POC device. MilliQ water and PBS buffer were flown through the assembled microfluidics and the OPD signals were recorded. **Figure 3.9A** shows images of the same set of spots measured in air, water and PBS buffer using the appropriate LED light. The average OPD of these spots is summarized in **Figure 3.9B**. When the Au-NHA chips is in air (RI=1.0) we can observe that the OPD signal intensity of the microarray spots is larger ( $89.1 \pm 9.51$ ) than when the spots are in aqueous media,  $61.76 \pm 10.01$  for MilliQ water (RI=1.33299) and  $54.78 \pm 6.31$  in PBS buffer (RI=1.33451).

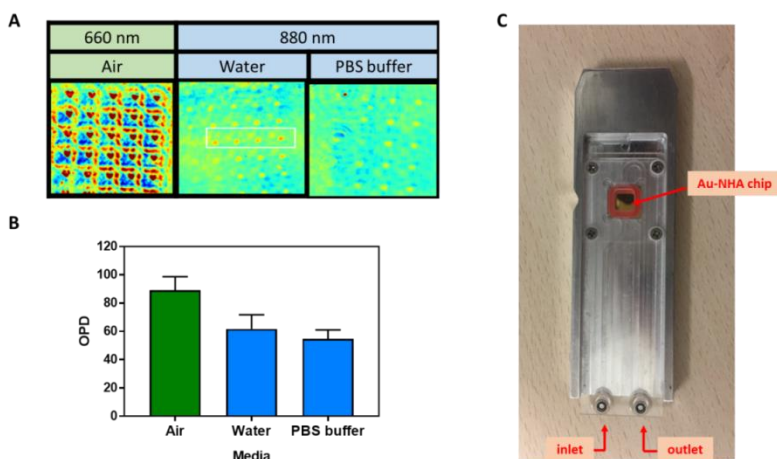


**Figure 3.9:** A: Colour code OPD maps obtained for the same microarray measured in air (dry), MilliQ water and PBS buffer. Dry measurement was done with a LED light source with emission at 660 nm while wet measurements were done with a LED emission at 880 nm. B: Numerical OPD values obtained in the different media. C: Picture of the designed microfluidic cartridge.

The decrease in the OPD signal in aqueous media can be understood by **equation [3.1]** and with the scheme in **Figure 3.10**. The OPD depends on the contrast/difference on the RI of the surface respect the surrounding media. The sheared beam 1 crosses a protein layer (protein spot) whose refractive index is commonly between 1.42 and 1.57.<sup>168–170</sup> In water (or PBS) the surrounding media where the sheared beam 2 passes through, has a RI around 1.33, closer to the values of proteins than in air (RI=1.0) Therefore, the difference is going to be always significantly lower (i.e. lower signal intensity and thus, lower sensitivity). This is however an inherent consequence of refractive index-based sensing because the difference in RI is going to be higher in air than in aqueous media, thus, more sensitive. Due to this, it was preferred to test the performance of the POC device in air (dry conditions).

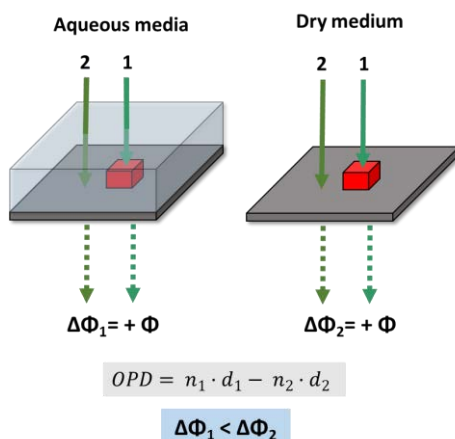


**Figure 3.10:** Scheme explaining how the refractive index of the media where the reference sheared beam 2 goes through affects the final OPD value and sensitivity of the measurement. We consider that sheared beam 1 corresponds to the protein layer (spot).

### 3.3.3 POC device applied to biosensing

As described in the introduction, the developed POC was intended to be used for clinical diagnosis, and, in particular, for the diagnosis of sepsis. Having in mind all the aforementioned considerations and experimental singularities, a biosensing procedure was designed (see **Figure 3.11**). First, nanoplasmonic chips (Au-NHA fabricated in square lattice) were biofunctionalized in a microarray designed (by means of a dip-pen nanolithography printer), with specific antibodies that act as bioreceptors for

sepsis biomarkers (**Figure 3.11A**). Then, the chip was inserted inside the POC device which, after data processing, generates an OPD intensity image pattern of the sensor surface (**Figure 3.11B**). The OPD value for each spot containing the antibody alone is the  $OPD_{t_0}$ . After incubation with the sample containing the analyte, change in the OPD ( $OPD_{t_t}$ ) will occur as a result of the specific biointeraction (**Figure 3.11C**). Finally, the difference ( $\Delta OPD$ ) between  $OPD_{t_0}$  and  $OPD_{t_t}$  is calculated, and then, related with the biomarker concentration (**Figure 3.11D**). Theoretically, each spot can be constituted by different receptors, in such a way that many biomarkers can be analysed simultaneously. Also, the same receptor can be used for several spots, in such a way, the resultant signals can be averaged. This latter approach was followed as the first step to assess the performance of the device during the assay development (i.e. selection of the biofunctionalization strategy, study of the reproducibility of the microarray generation, target detection and also for the evaluation of the signal processing and the final sensitivity).

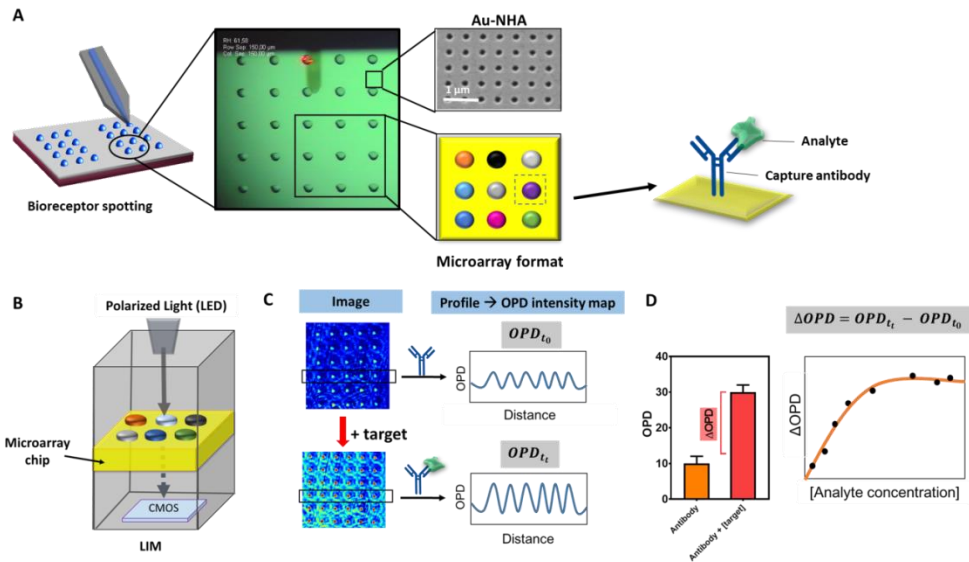


**Figure 3.11:** Scheme showing the sequential steps involving the use of the POC for biosensing. **A:** Biofunctionalization of the Au-NHA chips using a dip-pen nanolithography molecular printer. A microarray image with different drops with a diameter of 55  $\mu\text{m}$  and a SEM image of the nanoplasmonic chip are shown. **B:** Scheme of the POC with an Au-NHA chip. **C:** Colour code OPD maps of the arrays generated after software processing. **D:** Differences in the OPD ( $\Delta OPD = OPD_{t_t} - OPD_{t_0}$ ) in each spot with and without the target can be related with the analyte (biomarker) concentration.

### 3.4 Conclusions

In this chapter we have evaluated the novel POC device for its application as a biosensor. The phase-shift signal enhancement produced by the custom-designed nanoplasmonic plate has been evaluated. Upon testing SiO<sub>2</sub> patterns over glass and the novel nanoplasmonic plate it was confirmed that the OPD signal was increased by one order of magnitude. This improves the final sensitivity of the device and makes it suitable for biosensing applications.

One important feature of the new nanoplasmonic plate is that the maximum transmission peaks depends on the RI of the measuring media. We observed that upon a RI of 1.0 (air, dry conditions) the maximum peak is around 660 nm while when the RI is around 1.33 the peak is located at 880 nm. As protein layers have a RI of 1.42-1.57 we explored how the sensitivity performs upon different media (air, MilliQ water and PBS buffer). As expected from the optical configuration of the novel POC biosensor, a loss in sensitivity is produced upon measuring in water due to the smaller contrast/difference between the protein layer and the surrounding media. As a consequence, and taking into account the reported  $5 \cdot 10^{-4}$  RIU sensitivity of the POC device, we firstly decided to evaluate its performance as a biosensor. Dry conditions would be tested in the following chapters as the contrast would be higher, thus, better sensitivity will be achieved.

Finally, based on these findings, a protocol was established to use the POC device as a biosensor for measuring biological samples. The procedure that we will follow consists on creating microarrays with the specific antibodies that act as bioreceptors for the selected biomarkers. The difference in the OPD intensity image pattern between the antibody alone and after incubation with the sample containing the analyte will be related with the biomarker concentration.





# Chapter 4

## Optimization of antibody immobilization for biomarker detection

In this Chapter, the best strategy to immobilize the bioreceptors that will further recognise the selected biomarkers for fast Sepsis detection is sought. Firstly, a preliminary study was done with different working surfaces compatible with the optical configuration of the POC. Later, a wide range of biofunctionalization strategies for antibody immobilization over the Au-NHA sensor chips were explored. The best antibody biofunctionalization protocol in terms of sensitivity and selectivity was chosen for the next step of sepsis biomarkers analysis.



## 4. Optimization of antibody immobilization

### 4.1 Biofunctionalization strategies for gold and glass surfaces

As the detection principle of the POC device is based on the transmission of the light through the sensor surface (where the biomolecules are attached), a transparent media to the wavelength of the LED source is required. As previously mentioned, besides glass substrates, gold-based structures as NHAs were selected as optimal substrates. Therefore, the optimal biofunctionalization of both types of materials were studied. Thus, we started the optimization with transparent glass, ultrathin-layer gold chips (as are still a transparent substrate) and finally with the Au-NHA chips custom-made for the POC instrument of the European project. For this optimisation studied we decided to focus on CRP detection, as this protein is one of the most common biomarkers used for sepsis diagnosis and other inflammatory processes.

The main challenge in the manufacturing of a reliable protein microarray chip is selecting the most appropriate surface chemistry. Protein attachment on solid surfaces should be done in a controlled manner to guarantee its integrity, native conformation and biological function. In addition, the overall performance of the biofunctionalised surfaces depends on the chemical and physical properties of the solid surface due to its influence on specific binding of the target analyte while avoiding non-specific interactions. The orientations of the antibodies and their density over the surface have a strong effect on the binding efficiency thus affecting the final sensitivity of the sensor device. In addition, for label-free optical sensors where the sensitivity is highly dependent with the proximity of the interaction event to the sensor surface, the net distance between the surface and the immobilized bioreceptor is also relevant.

Optimal recognition can be achieved when immobilization of the bioreceptor fulfils these parameters: good orientation and adequate packing density over the surface, good stability and activity of the bioreceptor in the assay conditions and avoidance of non-specific binding of other molecules present in the sample that can hinder the analyte recognition. Thus, choosing the best immobilization strategy is paramount to achieve a good overall

performance. Accordingly, many biofunctionalization strategies to control the attachment of biomolecules have been developed. In proteins, there are several mechanisms of immobilization:

#### *Physical adsorption*

**Physical adsorption** is the direct deposition of the biomolecules (See **Figure 4.1A**). This immobilization is triggered by ionic bond formation, polar, electrostatic and hydrophobic interactions.<sup>171</sup> The chemical nature of the protein and the surface involved in the interaction are the ones rolling the dominative intermolecular forces. The newly formed protein layer will be heterogeneous and biomolecules will be randomly oriented because proteins tend to place themselves minimizing repulsive interactions with the surface or previously adsorbed proteins. We may take into account that a passivation step will be needed after immobilization to block the remaining areas.<sup>172</sup> This strategy can lead to improper folding or unfolding of the proteins (denaturation), thus, the protein may lose its function. For the particular case of antibodies, we must take into account their non-symmetrical structure (**Figure 1.9A**), (i.e. the recognition part (Fab) is located at one end, which should therefore be exposed). Hence, employing this strategy will result in a random **non-oriented attachment** and it may face some loss of functionality.<sup>17</sup>

#### *Physical entrapment*

A strategy that has been used to avoid the direct contact of the biorecognition element and the surface to prevent its denaturation and to keep its conformation is the **physical entrapment (Figure 4.1B)**. This is done by creating a uniform matrix of polymer that allows the insertion of the bioreceptor without modifications. This ensures the biological activity and provides a better environment for storage. Nevertheless, it can be difficult for the analyte to access the receptor due to diffusion and mass transport problems related to the polymer entrapment.<sup>173</sup>

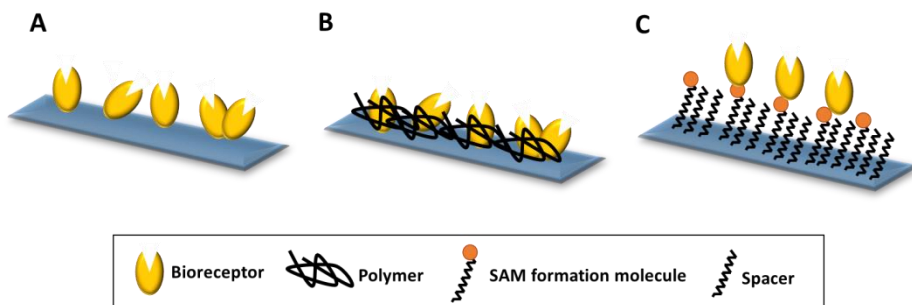


**Figure 4.1: Methods to immobilize a bioreceptor to a solid surface.** A: Direct physical adsorption. B: Physical entrapment by a polymer. C: Covalent or non-covalent binding to a self-assembled monolayer.

### *Covalent immobilization*

In this case, the attachment of the proteins is based on the formation of covalent bonds between active groups placed on the surface and accessible reactive groups in the amino acid chains of the protein. The most commonly used reactions are through amine and thiol coupling. Some examples of amine-reacting surface functional groups are: N-hydroxysuccinimide-ester (NHS-ester), aldehyde, isothiocyanate and epoxide groups.<sup>174,175</sup>

Often, protein chips are prepared by immobilizing proteins on chemically activated planar glass microscope slide. Glass slides have been widely used as microarray supports because their low auto-fluorescence, easy availability, flatness, rigidity, transparency, amenability of the surface to chemical modifications, non-porosity and cheap price. Although they also have limitations such as low capacity for analyte binding, non-uniform spot size which ends in complications for the reading with microarray software scanners.<sup>172,176</sup>

Usually, the functionalization of glass slides starts with the activation of the glass surface to generate enough silanol groups (Si-OH) by pretreatment of the surface with oxygen plasma or piranha solution ( $\text{H}_2\text{O}_2/\text{H}_2\text{SO}_4$ ). After this, silanization protocols are employed to introduce reactive groups such as aldehyde, epoxy isothiocyanate, amino, carboxyl or mercapto.

In this thesis, two of the most common ones, epoxy and carboxyl groups activated as NHS-ester groups were explored over **glass surfaces**. Both can react with primary amines forming an amide bond in the case of NHS and amine bond with epoxy groups as can be seen in the scheme of **Figure 4.2**.

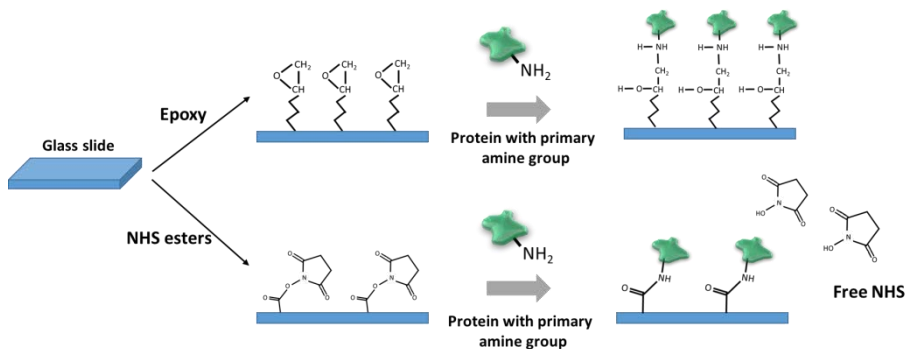


**Figure 4.2:** Scheme of the two glass functionalizations tested. Glass surface modified with epoxy and NHS esters groups are used. Epoxy reaction creates an amine bond whereas NHS ester creates an amide bond, both will link covalently the proteins to the glass surface.

Epoxy chemistry is simple and very suitable for performing fast protocols that require neutral pH values, wet conditions and minimal modification of the protein. Proteins, peptides or amino acids with a primary amine behave as a nucleophile, attacking the epoxy groups and binding through covalent bond. Although covalent reactions between proteins and the epoxy groups are slow, it is seen that adsorbed proteins reacts faster, thus, a two-step mechanism has been proposed: first, fast adsorption of molecules to the glass, followed by chemical attachment triggered by the higher concentration of epoxy groups on the surface.

NHS is commonly used as an activating agent of carboxylic acids to form amide bonds with primary amines. NHS ester groups present on the surface of the glass slide react with the nucleophilic groups of the proteins when they are dissolved in low ionic-strength buffer. The efficiency of the immobilization relies on several parameters like pH, concentration, ionic strength and reaction time.

**Gold surfaces**, on the other hand, can exploit their strong affinity to thiol (-SH) groups in order to be covalently biofunctionalised with biomolecules. Thiol-containing molecules such as proteins with exposed cysteine (Cys) residues can directly create a strong bond in gold surfaces, although this is rarely used as the number of accessible Cys is usually very low. However, this strong affinity is commonly exploited through the formation of self-assembled monolayers (SAM) using thiol-modified molecules. SAM are self-organized monolayers made of amphiphilic molecules formed by carbon

alkyl chains that spontaneously create a compact layer upon interaction of a surface-active head group (in solution) with an appropriate substrate (**Figure 4.1C**). The side exposed outwards can have a functional group that is used for covalent or non-covalent attachment of the molecules.<sup>177</sup> By tuning the concentration of the amphiphilic molecules and the composition, we can control the bioreceptor packing density.<sup>178</sup>

The exposed outwards functional groups can be a carboxyl group too in which case the NHS-ester chemistry can be exploited too with the use of -ethyl-3-(3-dimethylaminopropyl)carbodiimide hydrochloride (EDC). The carboxylic acid reacts with the EDC to form an active ester intermediate that is displaced by the NHS that is again later displaced by the primary amine (**Figure 4.3**). EDC can also be used alone but it is less efficient due to the instability of the intermediate. Often, deactivation of the remaining active carboxy groups and removal of residual NHS-esters on the surface is done with ethanolamine.<sup>179</sup>

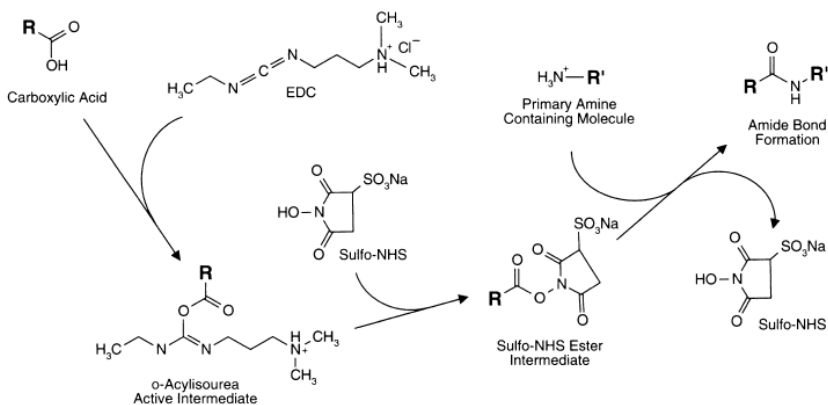


**Figure 4.3:** EDC/NHS mechanism of reaction: EDC reacts with carboxylic acids to create an active-ester intermediate. In the presence of an amine nucleophile, an amide bond is formed with release of an isourea by-product. The reaction of EDC can be more efficient by the formation of a sulfo-NHS ester intermediate because this intermediate is more effective at reacting with amine-containing molecules. From <sup>179</sup>.

As commented before, the main advantage of the covalent attachment is the generation of a permanent bond ensuring a stable binding of the bioreceptor to the sensor surface. However, one drawback is the need of having reactive groups on the outer part of the bioreceptor molecule. Another



disadvantage is that reactive groups can be present in the binding/interacting site of interest in the bioreceptor (for example the antigen binding site of an antibody), thus, depriving its functionality.

### *Bioaffinity immobilization*

Finally, another strategy exploited for immobilization is the use of affinity interactions. One of the most well-known methods used for noncovalent conjugation is the natural strong affinity of the pair **avidin/biotin**. Biotin is the common name for the water-soluble B<sub>7</sub> vitamin. Avidin is a tetrameric biotin-binding protein that can be found in the eggs of birds, reptiles or amphibians. One variety of avidin protein is SA, which is a similar biotin-binding protein but of bacterial origin (originated in *Streptomyces avidinii*). As avidin, it comprises four identical subunits and each one can bind to a single biotin molecule (i.e.: it possesses four biotin binding sites). The binding affinity of these molecules is one of the strongest found in nature ( $K = 10^{13} - 10^{15} M^{-1}$ ) especially in the first pocket to be occupied, then the affinity decreases gradually upon binding of more molecules. It is commonly accepted as an irreversible interaction and of comparable strength than covalent bonds. The binding occurs rapidly and it is not highly affected by pH or temperature.

To use this strategy, the bioreceptors need to incorporate a biotin group in order to be attached (**Figure 4.4A**). There are many commercial reagents to add functional biotin groups to proteins, nucleic acids or to other molecules. For instance, antibodies can be attached to a layer of SA by conjugating them to biotin molecules. Placement of this biotin within the antibody implies chemical modification of the antibody, which can lead to alterations in the Fab fragment. It is generally preferred to create a stack composition of biotin/SA/biotin layer (**Figure 4.4B**) rather than direct immobilization of SA because it yields a lower degree of organization.<sup>172</sup> This can be controlled by tuning the density of the initial layer of biotin by using two different heterobifunctional cross-linkers (one compound is biotinylated and the other one not).

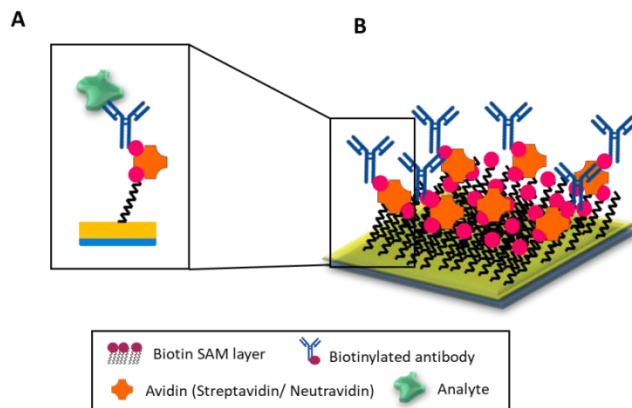


**Figure 4.4:** A: Scheme of a biotin SAM layer and how the avidin binds through one of its 4 binding sites. Only antibodies with a biotin tag can attach to the free remaining binding sites. B: a stack composition of biotin/SA/biotin layer. SAM forming molecules without biotin tags may be added to the SAM solution for spacing the location of avidins over the surface.

Another example of affinity site-directed immobilization of antibodies is by using **Protein G, Protein A or recombinant protein A/G**, which specifically binds to the Fc region of the immunoglobulins (see **Figure 1.9A**). Protein G and A are bacterial proteins that appear in certain species of pathogenic staphylococcal and streptococcal bacteria. Group C and G *Streptococci* express Protein G while Protein A is expressed in *Staphylococcus aureus*. These proteins are highly used in the field of affinity chromatography and especially for antibody purification. They capture immunoglobulins on the surface by binding the Fc region and directing outwards the antigen-binding region, in such a way that the antibodies can interact more efficiently with the antigen. Native Protein G also binds to albumin but in the recombinant protein G expressed in *Escherichia coli* (the most commonly used in laboratories) the amino acid sequence that creates the BSA-affinity has been removed. One minor disadvantage of this affinity binding type is the dissociation of the Fc from the Protein G when they are in a low pH solution (2.0 to 3.0). One important feature to take into account when using this strategy is the host animal where the antibodies were produced because they have different affinity to the different IgG types.<sup>175</sup>

Many other strategies for affinity binding have been reported, as metal ion affinity (nickel and nitrilotriacetic acid), histidine tags, calixarene derivatives, among others; the choice of the most suitable strategy will

depend on the nature of the ligand-analyte interaction.<sup>180</sup>

In this Thesis, first, a preliminary study of different biofunctionalization strategies for immobilization of antibodies over different surfaces compatible with the optical principle of the POC device was explored. Glass slides coated with epoxy or NHS ester groups were tested. Also, gold surfaces were explored with direct adsorption of antibodies or through their attachment *via* SAM formation. Specifically, we have employed three different types of SAM forming molecules: MHDA, HPDP and SH-PEG-biotin.

MHDA molecules contains one thiol group in one end (which interacts with the gold surface creating a covalent bond) and a carboxyl group in the opposite which can be activated for forming covalent amide bonds (**Figure 4.5A**). HPDP (**Figure 4.5B**) is a molecule that contains two sulphur groups which can trigger strong attachment to the gold surface and expose biotin groups, as previously reported in the literature.<sup>179</sup> The ends containing a biotin group can act as anchoring point for SA or NA and later bind to biotinylated molecules. SH-PEG-biotin is a SAM forming molecule that included a thiol group for gold anchoring, a polyethylene glycol (PEG) chain which is a molecule that includes a long chain which provides low non-specific binding and a biotin group (see **Figure 4.5C**).

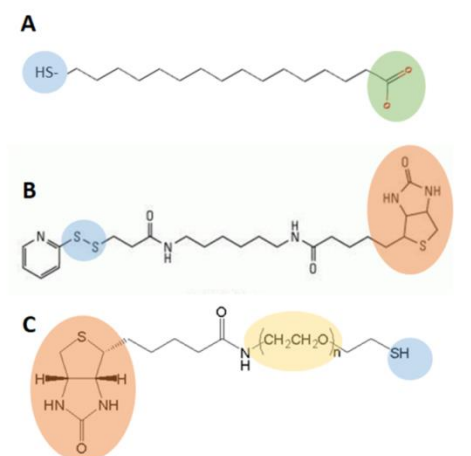


**Figure 4.5:** Chemical structure of the three different compounds employed to create a SAM. A: 16-Mercaptohexadecanoic acid (MHDA). In green the carboxylic group and in blue the thiol group that will bind to the gold surface. B: HPDP. Blue circles show the sulphide bond that interacts with gold. Orange circle shows the biotin group at the end of the molecule. C: SH-PEG-biotin. Yellow circle shows the PEG groups which can be tuned to different lengths.

## 4.2 Initial study of the attachment of antibodies over different surfaces compatible with the POC biosensor




As commented in **Chapter 3**, the detection of 2 nm thickness protein layers covalently attached over epoxy-coated glass slides was possible with the LIM technology.<sup>151</sup> In this section we explain the preliminary studies performed over glass, ultrathin gold layers and the initial version of the custom-designed nanoplasmonic plate. This was done to anticipate the best biofunctionalization strategy upon receiving the final version of the nanoplasmonic plate designed within the European project.

### 4.2.1 Functionalized glass surfaces

#### *Epoxy functionalized glass slides*

Several glass epoxy surfaces were biofunctionalized with anti-CRP (500 µg/mL in 10 mM PBS buffer with 5% glycerol), generating microarrays with several spot sizes and different period. After the microarray deposition, several incubation times (and temperatures) were tested to evaluate the optimal conditions for the coupling of the antibody.

**Table 4.1:** Summary of conditions tested for epoxy functionalised glass surface. o.n.: overnight; RT: Room temperature.

Time	Temperature	POC image	Mean OPD
<b>o.n.</b>	RT		≈ 15
<b>o.n.</b>	37°		≈ 12
<b>3h</b>	RT	not visible	-
<b>3h</b>	37°		≈ 15

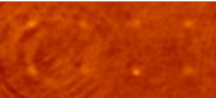
As we can observed in the **Table 4.1**, when incubating the sensor chips overnight at both temperatures, RT and 37°C, the spots were visible. By incubating at 37°C but for shorter times (3h) was also enough to see the microarray. The OPD values were between 12-15 units ( a more precise value

could not be provided at this stage as the dedicated software able to extract this value was not available yet). For comparison purposes, this approximate value was extracted using ImageJ software, which allowed determining intensity values in a relative manner. A separation of 250  $\mu\text{m}$  was employed because this gap provided very well defined spots from the surrounding area.

#### *N-Hydroxysuccinimide (NHS) esters functionalized glass slides*

In **Table 4.2** a summary of the results for this surface chemistry is shown. After creating the microarray with anti-CRP (500  $\mu\text{g}/\text{mL}$ , in 10 mM PBS buffer with 5% glycerol), incubation for 3h at RT and at 37°C was tested. Only the microarray incubated at 37°C was visible. In this case the OPD value was slightly lower than with the attachment *via* epoxy chemistry.

**Table 4.2.:** Summary of conditions tested for NHS esters functionalized glass surface.

Time	Temperature	POC image	Mean OPD
3h	RT	Not visible	-
3h	37°		8

#### 4.2.2 Gold surfaces

##### *Ultrathin gold (1 nm Ti + 7 nm Au)*

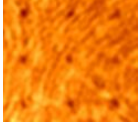


Before testing the nanoplasmonic chips, a preliminary study was done with chips with thin layers of continuous evaporated gold. We prepared glass slides with a 1 nm of titanium that function as an adhesion layer and 7 nm of gold. This ultrathin metal layer (8 nm in total) allows transparency to the LED light so the chip can operate in the POC device.

First, direct physical adsorption was studied. Direct adsorption of antibodies to a surface is simple and easy. However, physisorption is not strong and the antibodies can be displaced with successive washing steps. Clear microarrays were observed when antibody was directly deposited and after an incubation step of 3 h (see **Table 4.3**). Two different types of SAMs were generated to attach the antibody: one based on MHDA, resulting in a carboxyl monolayer, and another one made of HPDP-biotin, which rendered

a monolayer of biotin molecules facing outwards (see **Figure 4.5** for chemical structure). The carboxyl group of the MHDA was activated with EDC to enable the binding of antibodies or protein G. First, we tried spotting a solution that mixed EDC and antibodies at high concentration (500  $\mu\text{g}/\text{mL}$ ), however, we did not observe the microarray afterwards. This can be attributed to a less efficient reaction (since the sulfo-NHS was not present) or that the spotting time was too long. Time is important when using EDC because these molecule tends to hydrolyse gradually and relatively fast (i.e. approximately in less than 1 h), which can be too short if the spotting process requires more time. Therefore, this can eventually affects the uniformity of the microarray generation (i.e. first spots may have fresh EDC ready to interact with the carboxyl group, whereas at the end of the spotting process, the reactive EDC might have decreased significantly, affecting the coupling of the antibody). Accordingly, we decided to incubate the whole surface with a solution of EDC and sulfo-NHS for 30 min and then spotting the antibody, as the active ester intermediate is more stable against hydrolysis than with only EDC. Although the spotting time could still have an influence in this case, we were able to see arrays, with an intensity similar to the one obtained by direct adsorption. In addition, a bioaffinity approach with the addition of a Protein G layer before spotting the antibody was explored. The signal obtained after antibody binding with this strategy was similar to the covalent attachment with EDC, however when using Protein G, the antibodies are oriented, which is better than random orientation (**Table 4.3**).

HPDP is a sulphhydryl-reactive biotinylation reagent that conjugates *via* a disulphide bond to enable its use in a variety of purification methods or protein labelling..<sup>181</sup> After forming the SAM of HPDP two different types of avidins were tested: SA and NA. The former one is the avidin from bacterial origin ( $\text{pI} \approx 5$ ) while the latter one is a deglycosilated recombinant avidin which  $\text{pI}$  is 6.3 (near neutral pH) that minimized non-specific interactions especially with negatively charged molecules. After incubation of the chips with each avidin, we proceeded to deposit the biotinylated antibodies (250  $\mu\text{g}/\text{mL}$ ) to generate the microarray. Surprisingly, we only observed microarrays on the chips that were incubated with SA, although even in this case, the signals were apparently faint. A summary of the main results with representative images of the microarrays are included in **Table 4.3**.

**Table 4.3:** Summary of the surface chemistries assayed with 7 nm gold-coated chips.

Surface chemistry			POC OPD map	Mean OPD
1- SAM layer	2-Intermediate steps	3- Spotted solution		
-	-	Antibody (adsorption)		≈ 5
MHDA (250 μM)		Antibody + EDC	-	-
MHDA (250 μM)	EDC/Sulfo-NHS	Antibody		≈ 5
MHDA (250 μM)	EDC/Sulfo-NHS Protein G	Antibody		≈ 4
HPDP (1 mM)	SA	Biotinylated antibodies		≈ 6
HPDP (1 mM)	NA	Biotinylated antibodies	-	-

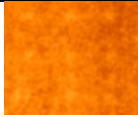
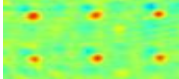
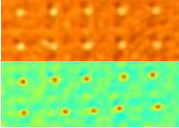
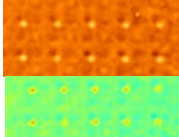
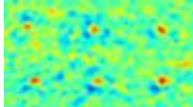

#### *Nanoplasmonic chips: Talbot and DUVL chips*

Previous experiments with ultrathin gold layer chips suggested that the proposed strategies could be suitable for the immobilization of the antibodies, although, as expected, the signal intensity signal was quite low (i.e. these substrates are neither completely transparent nor possess the enhanced performance that nanoplasmonics can provide). Therefore, these strategies were all tested with Au-NHA chips. It should be mentioned, that for these experiments, we employed nanoplasmonic chips whose fabrication process (either Talbot lithography or DUVL) was not optimised yet. All the biofunctionalization strategies are summarised in **Table 4.4** with representative pictures of the resulting microarrays.

In the case of direct antibody adsorption on Talbot chips, again the spots could be observed although they were very faded. Similar result was observed for the strategy based on the covalent binding using only EDC (i.e. the protocol resulted in non-observable arrays for both types of AuNHAs), therefore this approach was discarded. Affinity based approaches (i.e. Protein

G and SA/NA) were the most successful and the microarrays showed higher OPDs with more intense spots.

**Table 4.4:** Summary of the surface chemistries assayed over Au-NHA nanoplasmonic chips.

Au-NHA chips <i>via</i> TALBOT – Surface chemistry			POC OPD map	Mean OPD
1- SAM layer	2-Intermediate steps	3- Spotted solution		
-	-	Antibody (adsorption)		≈ 8
MHDA (250 μM)		Antibody + EDC	-	-
MHDA (250 μM)	EDC/Sulfo-NHS Protein G	Antibody		≈ 29
HPDP	SA	Biotinylated antibodies		≈ 26
HPDP	NA	Biotinylated antibodies		≈ 18
AU-NHAs chips <i>via</i> DUVL – Surface Chemistry				
MHDA (250 μM)		Antibody + EDC	-	-
MHDA (250 μM)	EDC/Sulfo-NHS Protein G	Antibody		≈ 37
HPDP	SA	Biotinylated antibodies		≈ 28

**Figure 4.6** compares OPD values obtained with regular thin layer gold chips and those obtained with AU-NHAs for those strategies with better results: (i) with a MHDA SAM modified with a Protein G layer and oriented antibody (**Figure 4.6A**) and a HPDP SAM, modified with a SA or NA layer and biotinylated antibodies over nanoplasmonic chips (DUVL and Talbot)



and non-nanoplasmonic (thin gold) surfaces. As we can observe from the images and from the graph, the OPD signal is larger in the nanoplasmonic chips (around 25-37) compared to regular thin gold chips (less than 10) which demonstrate the enhancement, confirming somehow that both strategies are similarly efficient in capturing the specific antibody and generating the microarrays.

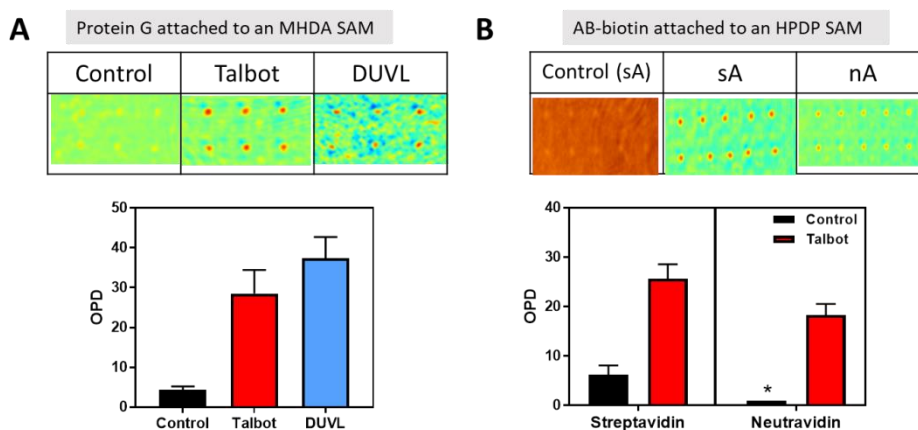


**Figure 4.6:** Colour code OPD maps and values of microarrays created following two different biofunctionalization strategies. A: Functionalization with Protein G attached to an MHDA SAM. B: Functionalization with biotinylated antibodies over a gold surface modified with a SAM layer of HPDP. NA and SA were tried as an intermediate layer. Thin layer gold (used as control), Talbot-based Au-NHAs and DULV-based Au-NHAs are compared in both cases. \*: microarray not seen.

### 4.3 Optimization of antibody immobilization on Au-NHAs chips

Based on the previous results, the strategies that led to more promising results were further more in-depth studied on the final version of the nanoplasmonic plate to evaluate their performance for biomarker detection. At this stage of the project we already had been provided with the especial software custom-designed to calculate the real values of the spots at the Colour code OPD maps. The selected strategies were based on direct antibody binding, anchoring of antibody through Protein G and anchoring via affinity interaction with the pair avidin/biotin.

#### 4.3.1 Direct antibody binding

##### *Direct adsorption*

As mentioned above, physisorption or adsorption of antibodies over a surface is easy and simple (**Figure 4.7**). As it was seen in preliminary tests (**Table 4.3** and **4.4**) direct adsorption seems to be successful.



**Figure 4.7:** Schematic representation of the direct antibody adsorption protocol.

Antibodies were spotted in a microarray format over the nanoplasmonic chips. After deposition, the antibodies were incubated for 2 h at RT. Then, we observed the microarrays with the POC device and we saw that adsorption was successful (see **Figure 4.8A**, **left images** for some representative images). The mean OPD signal achieved (**Figure 4.8B**) for antibody adsorption was  $17.38 \pm 2.91$ . The SD value (obtained after averaging all the spots of an 8x8 array) may be attributed to the homogeneity of the adsorption. Commonly this SD increases with successive steps. Another parameter to study the reproducibility and robustness of the protocol is the Coefficient of Variance (CV %):

$$CV (\%) = \frac{SD}{Mean} \cdot 100 \quad (4.1)$$

In this case, the CV is 16.74%. This is an acceptable value as it is within the acceptable range according to reported data related to protein microarray formation and the probe dispensing method.<sup>182–184</sup>

After incubation with the biomarker CRP (100 µg/mL in PBS buffer, 30 min) the arrays were not visible anymore (see arrays 1, 3 and 4 in **Figure 4.8A**). The most plausible explanation for this is that weak interactions trigger desorption between the gold and the antibodies after the incubation or washing processes. The remaining antibodies produce a low OPD, which cannot be detected by the POC device or the software.

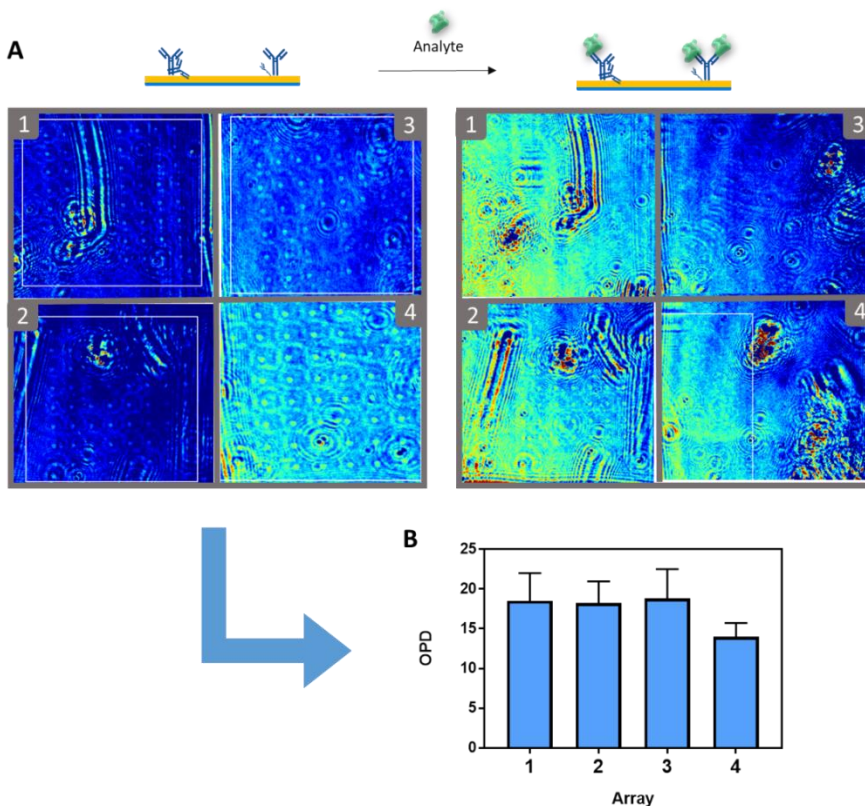


**Figure 4.8:** A: Colour code OPD maps of four 8x8 antibody-spotted microarrays. Right images show the antibodies after the adsorption protocol; left images show the microarrays after incubation with CRP (100 µg/mL). B: OPD signals of the four antibody microarrays after immobilization.

### 4.3.2 Antibody binding through Protein G orientation

Two different approaches were tested to immobilize the Protein G: direct adsorption and covalent attachment *via* SAM. A scheme of both strategies is shown in **Figure 4.9**.

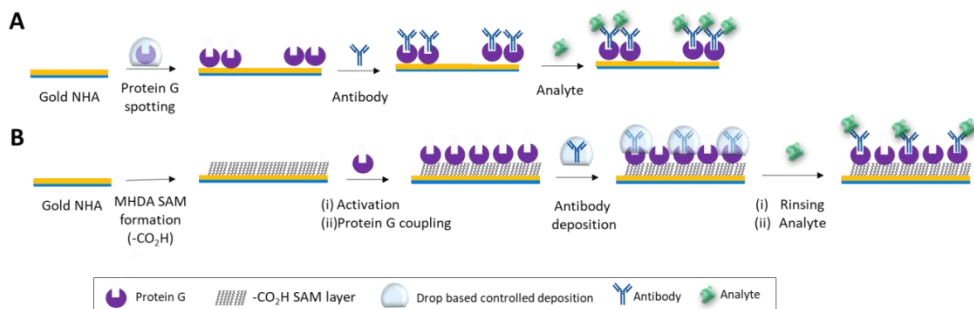


**Figure 4.9:** A: Adsorption of spotted Protein G and subsequent incubation of antibodies. B: Attachment of Protein G over an active EDC/Sulfo-NHS surface and subsequent oriented capture of spotted antibodies.

#### *Adsorption of Protein G*

Deposition of Protein G for its adsorption creates a microarray of anchoring points for antibodies. After adsorption of Protein G, a layer of BSA was added. This was done to prevent the non-specific adsorptions of antibodies because, as seen in previous section, antibodies can directly adsorb on the surface. Protein G has been found to bind BSA; however, we use recombinant Protein G where the BSA binding domain is removed.<sup>175</sup> Four representative images of the protocol shown in **Figure 4.9A** are shown in **Figure 4.10A**. The mean OPD values achieved are shown in the plot of **Figure 4.10B**.

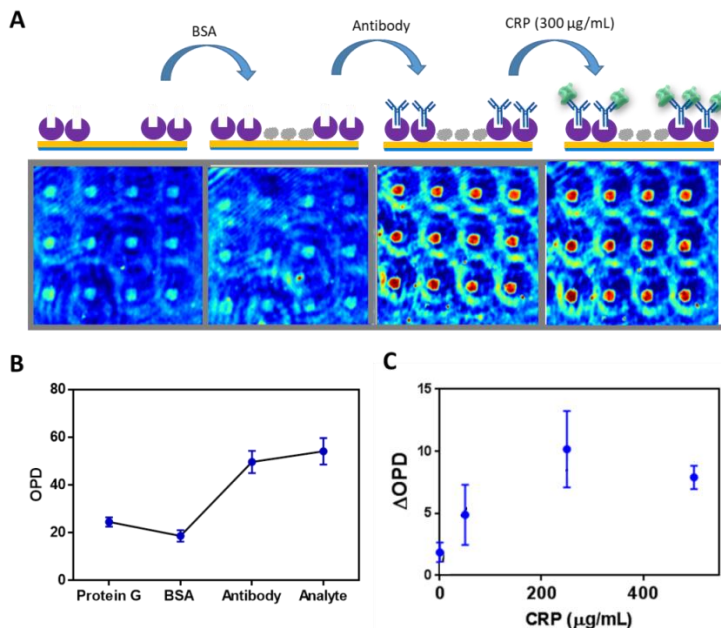


**Figure 4.10:** A: Colour code OPD maps of a microarray of Protein G and successive steps: Blocking with BSA, antibody binding, analyte measurement. B: OPD signals along the complete protocol. c) Preliminary calibration curve of CRP detection (data with SD correspond to the average of four replicates for each concentration).

Protein G average OPD value is  $24.52 \pm 1.98$  for 4 chips (i.e. 16 microarrays). This low SD indicates that the adsorption is quite uniform. In addition, the CV is 8% which is a very low value that shows the high reproducibility of the protocol at the initial steps. After the blocking step with BSA, we observed that OPD was reduced to  $18.6 \pm 2.46$  (CV=13.2%) (see **Figure 4.10B**). This suggests that a monolayer of BSA was created over the surface. We made a rough estimation on how many BSA molecules can be fitted in a surface of  $1 \text{ cm}^2$  (dimensions of the gold nanohole chips). Accurate net free surface was calculated after subtracting the area covered by Protein G spotted arrays. We found that 0.01% (w/v) of BSA was enough to cover the entire chip surface. So, in this case, we have added a significant excess (1%). As seen in **Chapter 3**, the nanophotonic POC records differences between two light beams crossing the sample and changes of the refractive index (i.e. mass) directly affect these values. The formation of a monolayer of BSA changes the surface reference (**Figure 4.11**), thus, reducing the difference in OPD between the antibody and the surrounding area.

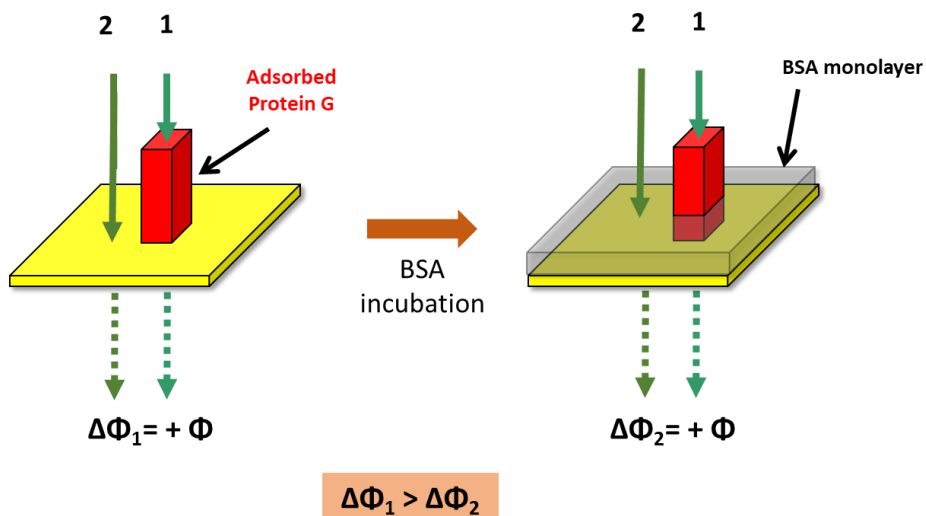


**Figure 4.11:** Change in the surface reference due to the addition of a monolayer of BSA.

Antibody incubation resulted in an increase of the OPD signal around 30 units ( $49.6 \pm 4.6$ ,  $CV=9.3\%$ ), which clearly illustrates a high binding efficiency of antibodies to the immobilized Protein G. Finally, when evaluating different concentrations of CRP, we observed a proportional signal increase which is a promising result (**Figure 4.11C**).

#### *SAM of Protein G*

Alternatively, we tried to anchor Protein G with a covalent bond, aiming at a more robust immobilization in terms of stability. **Figure 4.12** shows four microarrays obtained following this method. The average OPD values for antibody immobilization is  $22.9 \pm 3$  ( $CV=13.1\%$ ). If we compare these results with the ones obtained with the spotting of antibody for direct adsorption using the same experimental conditions, a similar signal was obtained ( $OPD \sim 17.38$ ). Based on this, we can infer that similar amounts of antibodies are attached although with this strategy the antibody is oriented.

Incubation with CRP at different concentrations resulted in a not always visible signal increase in the OPD and, when it was observed, it was not consistent with a linear quantification (see **Figure 4.12B**, where different CRP concentrations are evaluated).

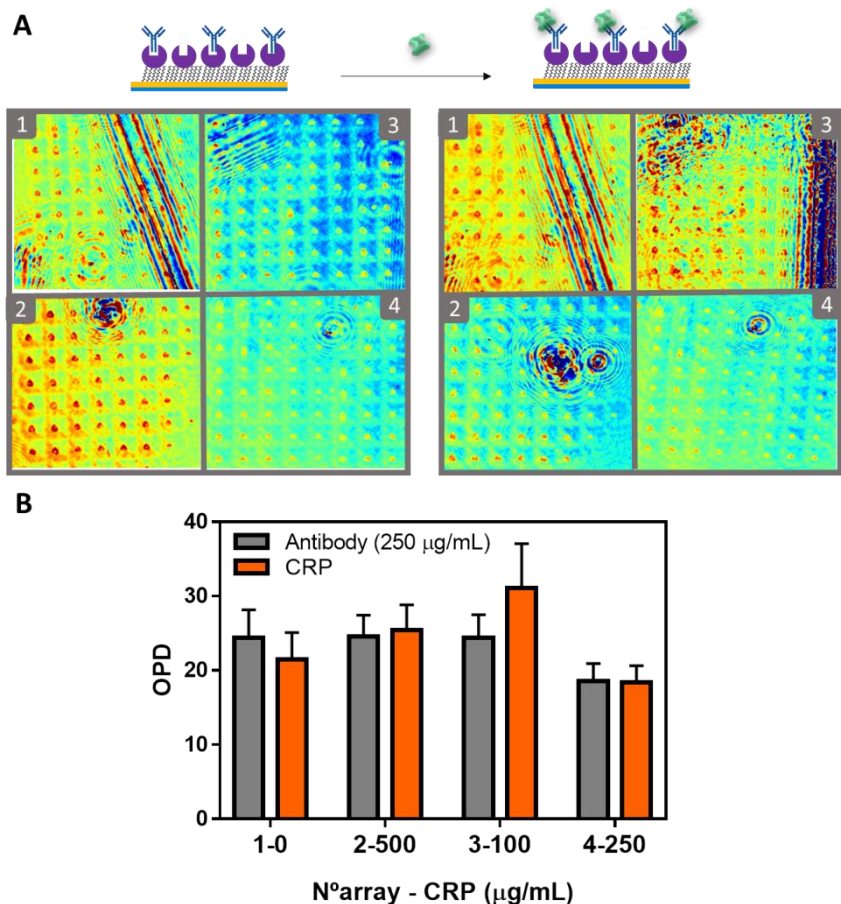


**Figure 4.12:** A: Representative colour code OPD maps of four microarrays obtained after spotting of the antibody (250 µg/ml) over a layer of covalently bound Protein G. B: OPD values of the antibody signal and the signal after incubation with four different CRP concentrations: 0 (negative control), 100, 250 and 500 µg/mL.

As this strategy seemed to result in antibody arrays with significant yield, additional conditions were studied in order to obtain more consistent read-out results. Thus, two different concentrations of antibody (250 and 500 µg/mL) and two different concentrations of CRP (250 and 500 µg/mL) were tested on the same chip (**Figure 4.13A**). The average OPD value was twice as much for antibody at 500 µg/mL than for 250 µg/mL (**Figure 4.13B**), which is consistent with a linear increase on antibody concentration. However, when incubating with CRP (250 µg/mL), we observed similar OPD increase regardless of the antibody concentration. Moreover, in this example the  $\Delta$ OPD produced with 500 µg/mL of CRP was lower. Several attempts (i.e.

more than 30 chips) to build a preliminary curve for CRP were done, however, the target detection was erratic and with low reproducibility.

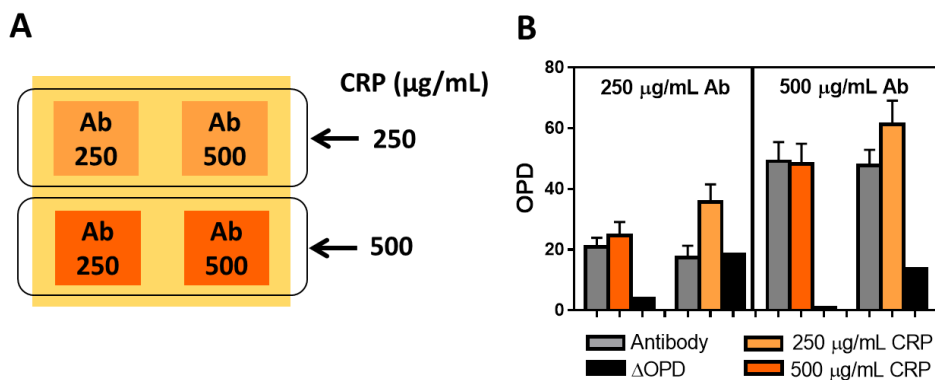


**Figure 4.13:** A: Schematic representation of the design of a chip with four different antibody microarrays: two with a concentration of 250  $\mu\text{g/mL}$  and two of 500  $\mu\text{g/mL}$ . After antibody immobilization the arrays were incubated with CRP at 250 and 500  $\mu\text{g/mL}$  of CRP. B: OPD signals for antibody capture and CRP detection.

As a summary, using Protein G is an interesting option as antibodies recognise better the analyte thanks to the orientation. Moreover, we have compared the addition of antibodies in two different ways: spotted (over a layer of Protein G) and incubated (over a Protein G-spotted array). The results showed that despite both biofunctionalizations are robust (and resulted in similar amount of antibody), the detectability was significantly better when incubating the antibodies rather than spotting them. This may indicate that the spotting process perhaps is damaging the antibodies and/or affecting its recognition function.

### 4.3.3 Antibody binding through avidin/biotin interaction

The strong pair avidin/biotin was explored following four different procedures which involved the formation of a layer of avidin-related proteins (SA and/or NA) and the subsequent capture of biotinylated antibodies (see **Figure 4.14**): (A) through *adsorption of SA or NA (via direct spotting)*, (B) through their binding to a *SAM of HPDP-biotin*, and through their binding to a (C) whole-surface SAM of *SH-PEG-biotin* or to a (D) spotted SAM pattern.



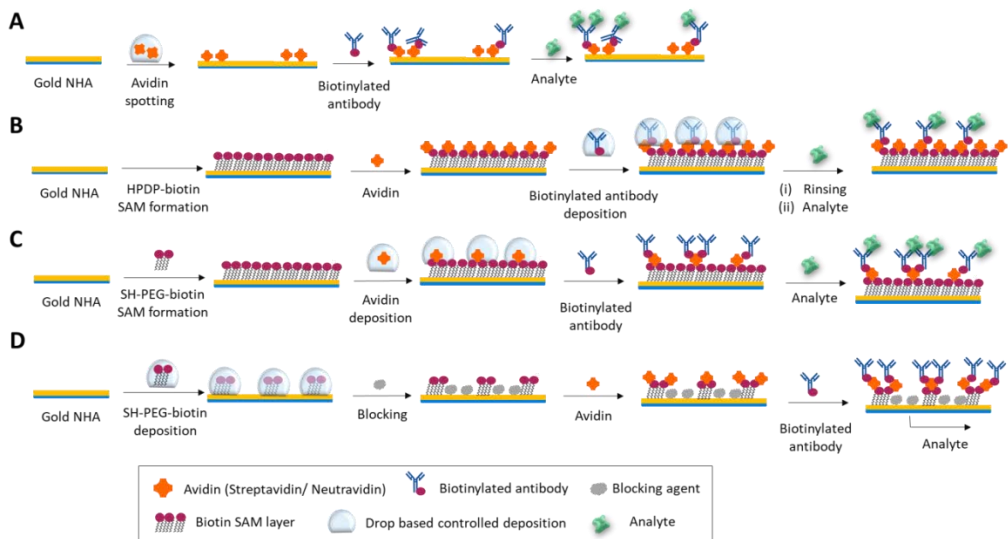


**Figure 4.14:** Schematic representation of the four strategies based on avidin/biotin. A: Spotting of avidin molecules and incubation of the whole surface with biotinylated antibodies. B: SAM layer of HPDP-biotin, followed by the formation of a whole surface of avidin, then spotting of biotinylated antibodies to create the microarray. C: SH-PEG-biotin layer where avidin is spotted followed by incubation of biotinylated antibodies. D: Spotting of SH-PEG-Biotin, blocking of the remaining surface with BSA, avidin incubation and final biotinylated antibodies incubation.

#### (A) Adsorption of SA or NA

The direct spotting of both SA and NA resulted in visible arrays as we can see in **Figure 4.15A**. The OPD signals measured for 250  $\mu\text{g/mL}$  of SA and NA (see **Figure 4.15B**) were similar ( $18.7 \pm 2.6$  and  $18.0 \pm 2.6$ , respectively). However, similarly to what was observed with adsorption of antibodies, upon incubation of the biotinylated antibodies for 30 min and after rinsing and drying, the microarrays were undetectable (**Figure 4.15A, right**). This could be the result of desorption of the avidin from the chip due to weak interactions. Three different strategies based on adsorption have been tried: adsorption of antibodies, protein G and both avidins. Only Protein G adsorption has resulted in a stable physisorption, this may be due to the fact that the amino acid sequence of the protein and the protein surface trigger stronger intermolecular forces with the gold surface.

In view of that neither SA nor NA can establish strong interactions to prevent their desorption in the successive steps of the biofunctionalization protocol, this option was discarded and those strategies based on the

attachment of the avidin to a biotin layer previously formed over the gold surface were attempted.

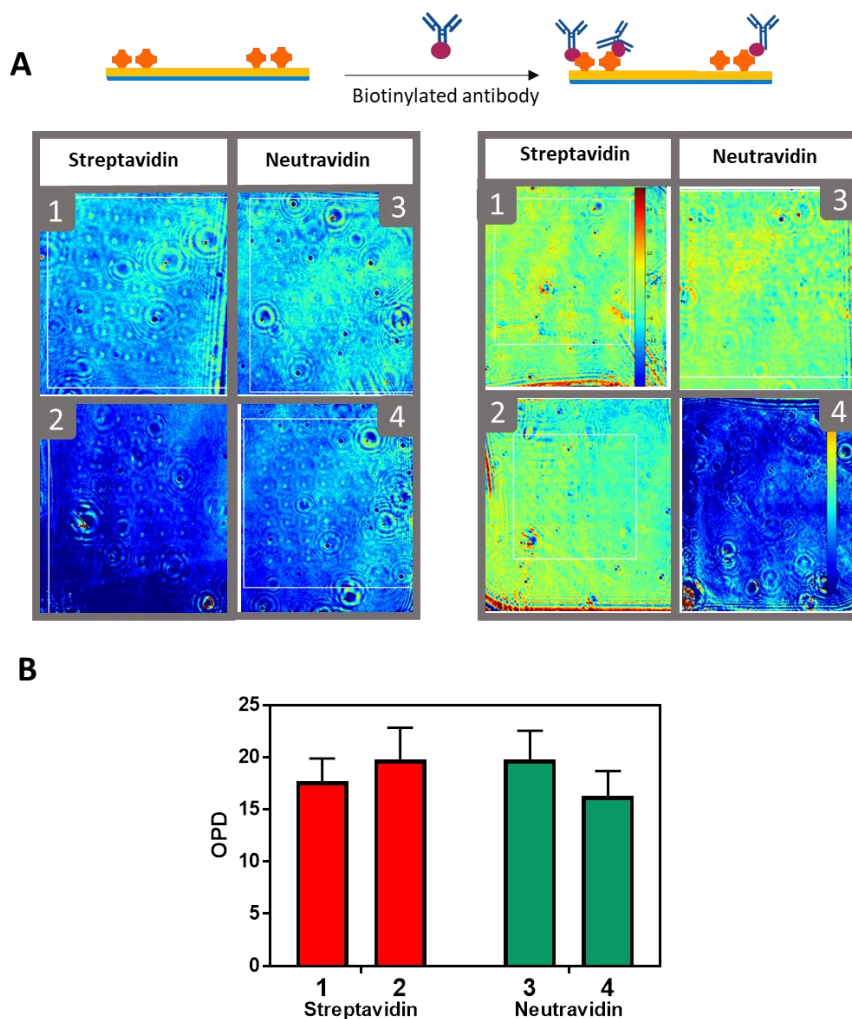


**Figure 4.15:** A: Colour code OPD maps of four 8x8 microarrays obtained after spotting SA at 250  $\mu\text{g}/\text{mL}$  (arrays 1,2) and NA at 250  $\mu\text{g}/\text{mL}$  (arrays 3, 4). Left images show the microarrays after adsorption; right images show the microarrays after incubation with biotinylated antibodies. B: OPD signals for adsorbed avidin microarrays.

*(B) SAM of HPDP-biotin*

A first attempt was based on the use of HPDP-biotin as thiolated-modified compound. First, a layer of HPDP was formed covering the whole surface of the chip. Then, a layer of avidin was added and, finally, the biotinylated antibodies were directly spotted in order to achieve the microarray based

pattern. **Figure 4.16** compares the OPD change between the antibody attachment and the final incubation with different concentrations of CRP. Microarrays were very clear and easy to visualize, with more intense spots and OPD values ( $29.2 \pm 5.13$ ,  $CV=17.6\%$ ) higher than the ones obtained following the previous strategies. However, the variability with this strategy was slightly worse, with higher SD and CV close to or around 20%.

Addition of CRP showed non-significant detection (an example of one chip incubated with CRP can be seen in **Figure 4.16B**) even at concentrations relatively high (i.e.  $500 \mu\text{g/mL}$ ). Due to these results, the use of HPDP-biotin was discarded.

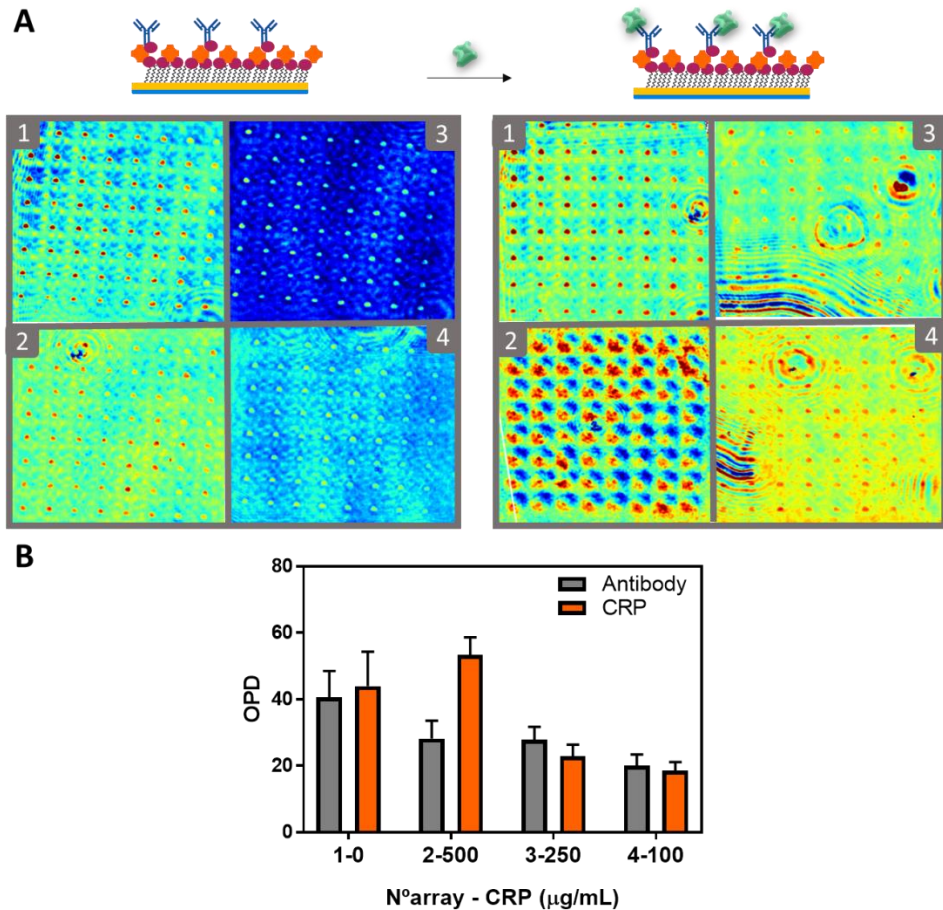


**Figure 4.16:** A: Example of 4 microarrays of biotinylated antibodies over a layer of HPDP-biotin/SA. B: OPD values for the antibody after CRP incubation with four different concentrations: 0 (negative control), 100, 250 and  $500 \mu\text{g/mL}$ .

### (C) SAM of SH-PEG-biotin

*SH-PEG-biotin* is a molecule that contains three main parts: a sulfhydryl group for attachment to gold surfaces, a biotin group to attach avidin and in between a PEG linker which offers better water solubility, flexible linkage structure and major biocompatibility. This molecule was selected because it offers higher stability of binding and, in view of future evaluations of real human samples (as human plasma), PEG can prevent non-specific interactions.<sup>179,185</sup>

After constructing a full layer of *SH-PEG-biotin*, SA or NA were deposited in a microarray format (see **Figure 4.17A**). This allows us to incubate the biotinylated antibodies, thus, avoiding the spotting process which, as seen before, may damage the bioreceptor. Then, biotinylated antibodies were added, generating the following average OPD signals:  $22.3 \pm 6.88$  (CV= 30.92%) for SA and  $20.5 \pm 4.14$  (CV=20.21%) for NA, respectively. Finally, when adding different concentrations of CRP, the increase was not significant or very small even when using high concentrations (see **Figure 4.17B** for representative results of incubating 500  $\mu\text{g/mL}$  of CRP).

In addition, we observed that the morphology of the spots was different from the one previously seen (**Figure 4.17A**). The spots were wider and less defined, and a possible reason might be related to the flexibility of the PEG linker that generated less compact SAMs. In any case, this observation was not further in-depth studied as the target detection was not conclusive as abovementioned (**Figure 4.17B**).

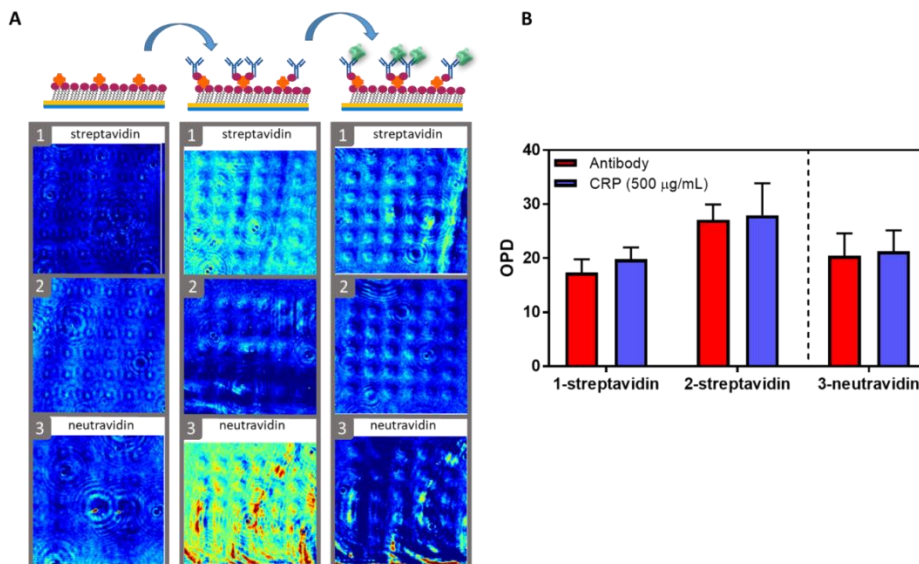


**Figure 4.17:** A: Three microarrays: two of SA and one of NA over a layer of SH-PEG-biotin. Pictures of successive steps of antibody binding and analyte detection are also included. B: OPD values of the antibody signal and the signal after incubation with 500 µg/mL of CRP.

#### (D) Microarray of SH-PEG-biotin

In this case, instead of forming the SAM layer of the SH-PEG-biotin over the whole gold surface, another approach was followed, based on its direct spotting, in such a way, the avidin was incubated over the whole chip and bound only on the biotinylated spots.

The sequential steps are summarized in **Figure 4.18A**. After SH-PEG-biotin spotting, a blocking step with BSA for preventing adsorption over the free remaining surface was done. The mean values for 4 different chips showed that avidin addition increased the OPD signal from  $16.5 \pm 4.60$  (CV=27.8%) to  $19.5 \pm 3.77$  (CV=19.3%) and the antibody binding resulted in 12 OPD units more ( $32.2 \pm 4.42$ , CV=13.7). Detection of CRP was attempted several times and  $\Delta$ OPD signals are represented in **Figure 4.18B**. In general terms, the SD was higher for the mean value and compared to other protocols tested, resulting in also higher CV%. Moreover, the CRP target detection was not very reproducible as can be seen in a preliminary calibration curve (**Figure 4.18C**) preventing a reliable quantification of this biomarker.

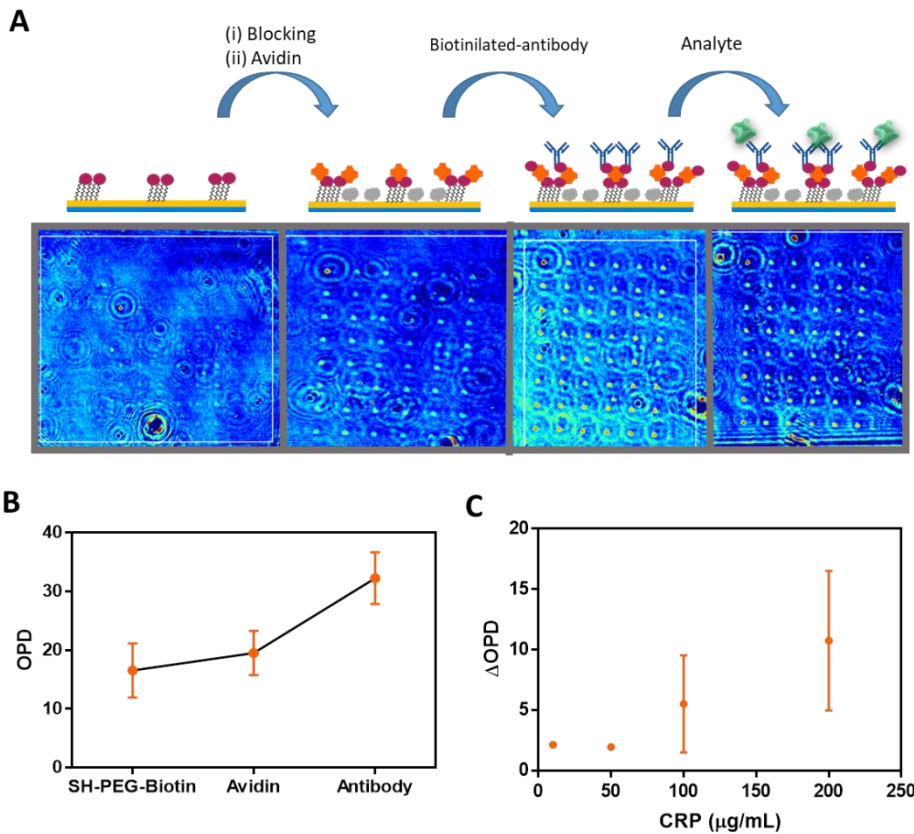


**Figure 4.18:** A: Colour code OPD maps of a microarray of SH-PEG-biotin and successive steps: Blocking with BSA, antibody binding, analyte measurement. B: OPD signals along the protocol (BSA signal not included). C: Preliminary calibration curve with CRP (data with SD corresponds to the mean of 4 replicates).

**Table 4.5** summarizes all the different strategies tested, the main advantages and disadvantages of each of them, and the detection of CRP when it has been possible.

**Table 4.5:** Summary of strategies tested for antibody immobilization on Au-NHA chips

	<b>Biofunctionalization</b>	<b>Advantages</b>	<b>Disadvantages</b>	<b>Detection</b>
<b>Direct antibody binding</b>	Antibody adsorption	<ul style="list-style-type: none"> <li>✓ Direct - Easy</li> <li>✓ No need of Ab modification</li> </ul>	<ul style="list-style-type: none"> <li>▪ Possible denaturation of the Ab structure and activity</li> <li>▪ Ab desorption upon incubation with the analyte</li> </ul>	Not possible
<b>Protein G binding</b>	Deposition of Protein G through spotting and adsorption	<ul style="list-style-type: none"> <li>✓ Direct - Easy</li> <li>✓ No need of Ab modification</li> <li>✓ Oriented Ab</li> <li>✓ Good reproducibility (CV&lt;20%)</li> </ul>	<ul style="list-style-type: none"> <li>▪ Possible denaturation of Protein G</li> </ul>	<b>Reproducible results</b>
	Full layer of Protein G anchored <i>via</i> SAM	<ul style="list-style-type: none"> <li>✓ Orientation of antibodies</li> <li>✓ Controlled distribution</li> <li>✓ Easy to multiplex on the same microarray</li> </ul>		Non-consistent detection Poor reproducibility
<b>Avidin/Biotin binding</b>	SA and NA adsorption	<ul style="list-style-type: none"> <li>✓ Direct</li> <li>✓ Easy</li> </ul>	<ul style="list-style-type: none"> <li>▪ Antibody needs biotin labels</li> <li>▪ Desorption upon incubation with analyte</li> </ul>	Not possible
	HPDP-biotin SAM	<ul style="list-style-type: none"> <li>✓ Good OPD signals (29.15)</li> </ul>		Non-consistent detection
	SH-PEG-biotin SAM	<ul style="list-style-type: none"> <li>✓ Antifouling surface</li> </ul>		Non-consistent detection
	Microarray of SH-PEG-biotin	<ul style="list-style-type: none"> <li>✓ Antifouling surface</li> </ul>	<ul style="list-style-type: none"> <li>▪ High SD (difficult to standardize the protocol)</li> </ul>	Low sensitivity

## 4.4 Conclusions

Selecting the most appropriate surface chemistry is paramount to attach a bioreceptor in a controlled manner to guarantee its integrity, native conformation and biological function. In this Chapter, first, preliminary studies of surface biofunctionalization with bioreceptors were attempted with glass, ultrathin gold layer and a first version of the gold nanoplasmonic chips. All these surfaces were explored as they are compatible with the optical principle of the POC (i.e. light transmission from the coupled LED light source) and because the final version of the gold nanoplasmonic was not ready.

Microarrays of antibodies covalently bound on glass surfaces coated with epoxy and ester-NHS groups were visualized with very low OPD signals (<15). Also, ultrathin gold chips showed similar values (<8). These OPD signals were very low compared to the signal produced for the same biomolecules but on the nanoplasmonic chips ( $\approx$  15-40). These larger signals are obtained thanks to the extraordinary transmission effect of the nanoplasmonics chips which ends up in better assay sensitivity. Most of the immobilizations tried on gold were successful, especially the ones involving physical adsorption and the use of SAMs.

Once having the final version of the nanoplasmonic plate a more comprehensive exploration was done for antibody immobilization and analyte detection. Direct binding of antibodies was tested, as well as their anchoring *via* orientation with Protein G and *via* the affinity tags avidin/biotin. Strategies that required spotting of antibodies seemed to work worse than the ones that required antibody incubation. Also, adsorption strategies (antibodies or avidin) created unstable interactions which ended in desorption upon incubation, except for Protein G. Finally, the optimal methodology tested and the one that offered the more reproducible results in terms of immobilization of antibodies and analyte detection was adsorption of Protein G. This is a direct and label-free assay and it is very advantageous because the analyte does not need any pre-treatment of tag-addition that can affect its chemical or structural properties.





# Chapter 5

## Evaluation of Protein Biomarkers for Sepsis diagnosis

In this chapter we describe the application of the optimal immobilization protocol selected in the previous Chapter to the detection and quantification of three protein biomarkers related to sepsis: CRP, IL-6 and PCT. The assays were first developed in buffer in both an individual and a multiplexed configuration. Then, the effect of human plasma on the assay performance was assessed and the detection in this biofluid was attempted, before using the POC device for analysing real clinical samples.



## 5. Evaluation of Protein Biomarkers for Sepsis

### 5.1 Introduction

Many efforts are being done in clinical research in order to establish a reliable panel of biomarkers for the detection of sepsis. Within the European project, the clinical partner proposed the quantification of CRP, IL-6 and PCT. We have tried to perform this analysis in an individual and in a multiplexed manner with the novel POC biosensor. These three biomarkers were chosen because of their demonstrated diagnostic value in sepsis, as they are routinely analysed, and also because of their structural properties (i.e. MW), which can have an important effect on the performance of the assays. Thus, they cover high MW (CRP, with 120 kDa), relatively medium size (IL-6, with 24 kDa) and relatively small size (PCT peptide, with 13 kDa). As mentioned in the POC device description, the molecular weight (i.e. size and therefore amount of mass immobilized or captured) has a direct effect on refractive index changes. Therefore, this range of MW could be useful for assessing the experimental sensitivity of the novel POC.

CRP is an acute phase protein produced by the hepatocytes after the stimulation by IL-6, IL- $\beta$  and IL-8 as a consequence of an infection (bacterial or viral) or any other inflammation process (acute or chronic). CRP binds to bacteria (opsonisation) promoting its aggregation and phagocytosis by leukocytes (**Figure 5.1**).

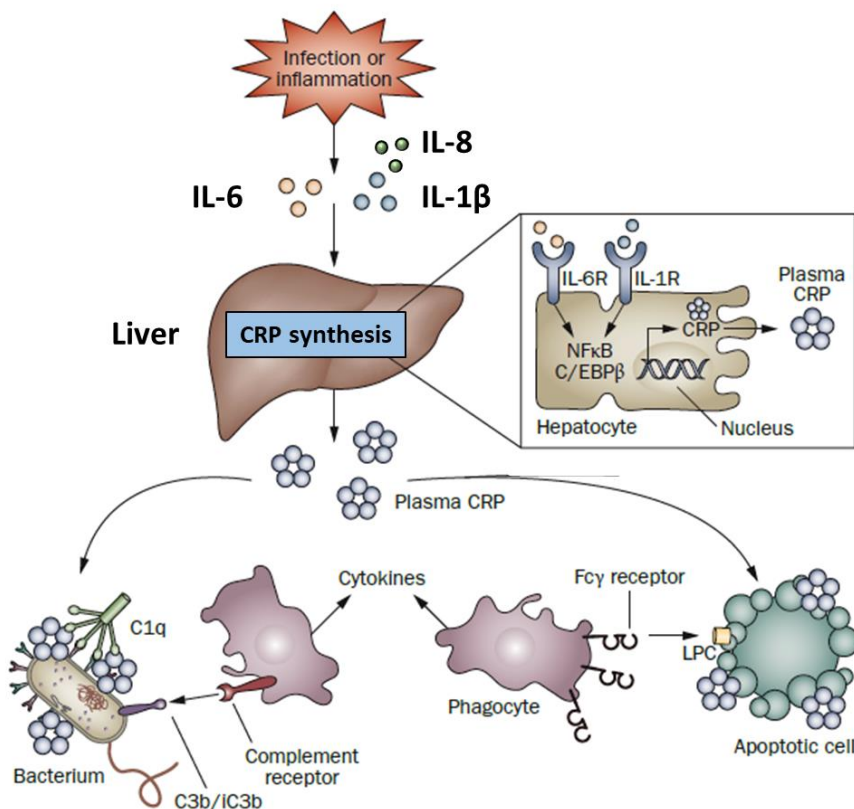


**Figure 5.1:** Schematic representation of the role of IL-6 and CRP in inflammatory processes. Upon infection or inflammation interleukins like IL-6, IL-8 and IL-1 $\beta$  go to the liver and activate production of CRP that will travel through blood searching for pathogenic patterns and opsonizing bacterium. Adapted from <sup>186</sup>.

Secretion of CRP by hepatocytes starts within 4 to 6 h after detection of the pathogen and peaks after 36-50 h. CRP concentrations in healthy subjects is  $<5 \mu\text{g/mL}$  and can reach levels higher than  $500 \mu\text{g/mL}$  during inflammation. Despite the fact that CRP concentration can increase by other non-infectious conditions, several studies have reported higher levels of this biomarker in septic patients as compared to critically ill patients with non-infectious SIRS. **Table 5.1** summarises the cut-off values for CRP and the status of the patient.

In the clinical setting, CRP detection is commonly done with ELISA, as well as, immunophelometric and immunoturbidimetric assays.

**Table 5.1:** Normal range level of CRP, IL-6 and PCT for healthy and non-healthy individuals.<sup>120,187–190</sup>

	CRP (120 KDA)	IL-6 (24 KDA)	PCT (13 KDA)
TYPE OF PATIENT	Concentration		
HEALTHY SUBJECTS	< 5 µg/mL	< 5 pg/mL	< 0.1 ng/mL
NON-INFECTIOUS (SIRS)	5 - 40 µg/mL	40-80 pg/mL	0.1-0.25 ng/mL
SEPSIS	40 - 200 µg/mL	>120 pg/mL	10-100 ng/mL
SEVERE SEPSIS	>200 µg/mL	> 300 pg/mL	> 1 µg/mL

IL-6 is produced by different types of cells including monocytes, fibroblasts, endothelial cells, keratinocytes, T-lymphocytes and tumour cells. Together with TNF- $\alpha$  and IL-1 $\beta$ , it mediates the initial response of the innate immunity to injury or infection, enhancing the liver's production of the acute phase reactants, including CRP (see **Figure 5.1**). These three cytokines are essentially responsible for the features of SIRS. However, like TNF- $\alpha$  and IL-1 $\beta$ , IL-6 is not specific for sepsis and levels are also increased in other inflammatory processes, such as arthritis and myocardial infarction.

IL-6 responds very rapidly to infection and is released into the bloodstream during the first 4–6 h of infection. Blood levels subsequently decrease over the next 24–48 h. IL-6 has been used as an ideal biomarker in early diagnosis of neonatal sepsis or as a predictive marker of bacteremia in febrile children.<sup>191,192</sup> **Table 5.1** summarizes which are the cut-off values reported for each sort of patient.

On the other hand, PCT is the precursor of a hormone called calcitonin. It is a protein of 116 amino acid sequence that is secreted by the cells of the thyroid gland. When sepsis occurs the main producers of PCT are macrophages and monocytes cells of different organs, especially liver. Procalcitonin works as a chemokine, modulating the induction of anti-inflammatory cytokines. In healthy people, PCT levels are undetectable because it is processed as soon as is synthesised. The synthesis of PCT can be identified after 2-3 h after the onset of an infection what makes PCT a useful biomarker for early sepsis diagnosis. The maximum peak of this biomarker is reached after 8 and 24 h after infection onset and the concentration fluctuates in the range of 10-100 ng/mL. PCT is very stable and possesses a median

half-life of  $\approx 24$  h. It is important to note that PCT does not increase during a viral infection. In addition, several studies have reported that higher PCT levels could differentiate Gram-negative sepsis from Gram-positive and fungal sepsis.<sup>193,194</sup>

High levels of CRP and PCT are nowadays related with sepsis infection, however, they have some limitations as they can be also involved in others non-inflammatory processes, for example, burns or traumas.<sup>107,110,116</sup>

## 5.2 Design, optimization and analytical evaluation of the protein biomarkers in buffer

According to the results obtained in the Chapter 4, the strategy based on Protein G adsorption was the one offering the best performance for (i) capture of antibodies and (ii) target detection. This one was therefore selected to develop all the assays for the protein biomarkers detection C-reactive protein.

Taking the conditions described in the Chapter 4 for this strategy as a starting point, some parameters of the surface biofunctionalization were optimized in order to improve the performance of the assay. First, different concentrations of Protein G (from 100 to 500  $\mu\text{g}/\text{mL}$ ) were tested. We found that below 250  $\mu\text{g}/\text{mL}$  the spots were hardly visualized, resulting in no OPD signal was (see **Figure 5.2A**). Also, different incubation times (2, 3 and 24 h, **Figure 5.2B**) were assayed and we observed that the amount adsorbed was similar (i.e. similar OPD values). Thus, the incubation time of the spotted Protein G was set at 2 h.

Several antibodies specific for CRP and commercially available were tested in order to select the best one in terms of sensitivity. The analysis was done over 8x8 microarrays. Preliminary assays were done with C7 monoclonal antibody, as it has been successfully used with other biosensor label free platforms like Surface Plasmon Resonance (SPR).<sup>185</sup> The results were compared with those obtained with another two monoclonal antibodies (C183 and C196).

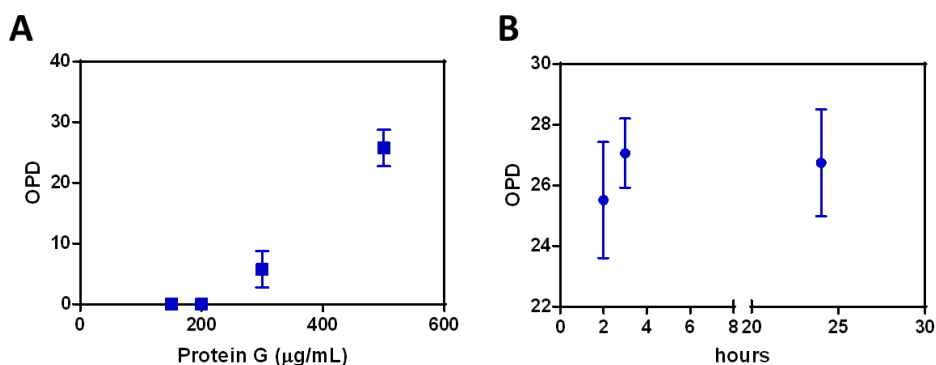


**Figure 5.2:** A: Protein G adsorption at different concentrations (incubation for 3h). B: Protein G at 500µg/mL incubation at different times. The data show the mean and SD of at least 4 microarrays (3 chips).

**Figure 5.3A** shows the OPD signals for the 3 immobilization steps (Protein G, BSA blocking and antibody binding) while **Figure 5.3B** shows the  $\Delta$ OPD achieved by the three antibodies after incubating them with 250 µg/mL of CRP. Similar  $\Delta$ OPD signals were observed in the antibody immobilization steps ( $\Delta$ OPD $\approx$ 32 units). It is important to highlight that between the three antibodies tested, C183 shows the largest binding efficiency to CRP although it also shows the lowest antibody immobilization signal. According to these results, further experiments were performed with C183 (named as anti-CRP).

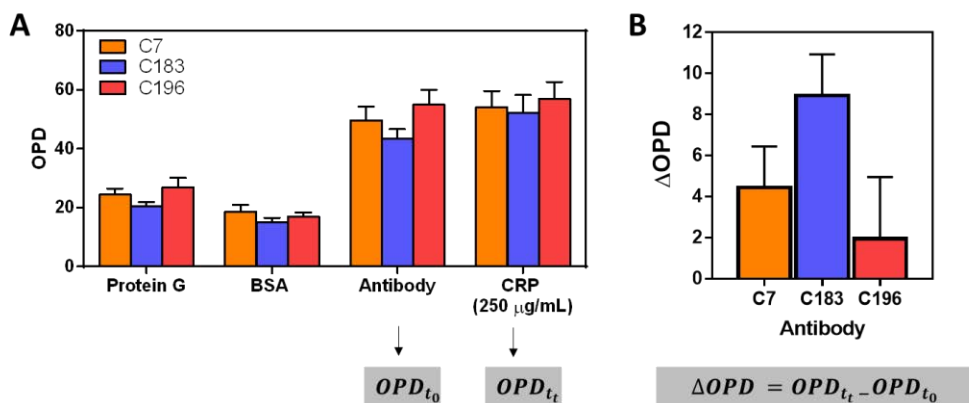


**Figure 5.3:** A: OPD values obtained for the immobilization of three different anti-CRP antibodies: C7, C183 and C196, and the detection of CRP (250 µg/mL). B:  $\Delta$ OPD achieved after incubation with [CRP]= 250 µg/mL. The results correspond to one sensor chip for each antibody (4 microarrays).



After this, different sensor chips (n= 30) were prepared to test the reproducibility and to standardise the OPD signal for each step of the immobilization procedure (Protein G, BSA and antibody ( $OPD_{t_0}$ )). The same OPD pattern was observed in all cases with very similar overall signals and excellent reproducibility according to the SD obtained. **Table 5.2** contains the average values obtained intra and inter-chip variability.

**Table 5.2:** Intrachip and interchip variability in the three-step Protein G based biofunctionalization protocol for CRP

Interchip variability <sup>a</sup>						
	CRP					
	Mean±SD			%CV		
<b>Protein G</b>	25.76 ± 2.9			11.5		
<b>BSA blocking</b>	24.37 ± 3.5			14.3		
<b>Antibody capture</b>	43.96 ± 4.7			10.9		
Intrachip variability <sup>b</sup>						
	Chip 1		Chip 2		Chip 3	
	Mean±SD	%CV	Mean±SD	%CV	Mean±SD	%CV
<b>Protein G</b>	11.5 ± 1.4	11.9	10.5 ± 1.2	11.4	14.8 ± 2.3	15.3
<b>BSA blocking</b>	8.7 ± 1.3	14.6	8.0 ± 1.2	14.6	17.9 ± 2.5	13.9
<b>Antibody capture</b>	21.9 ± 1.7	7.7	19.9 ± 1.6	8.3	24.2 ± 5.3	21.9

<sup>a</sup>: Interchip variability observed with 30 chips biofunctionalized following the same protocol

<sup>b</sup>: Intrachip variability observed in 4 arrays prepared in a single chip. 3 different chips are shown as representative examples.

Graphical representation of the averaged values achieved for 30 sensor chips for each step of the biofunctionalization protocol is shown in **Figure 5.4A**. Protein G average OPD value is  $25.7 \pm 2.96$  (CV=11.50%), for BSA the average is  $24.4 \pm 3.5$  (CV=14.36%) and for the antibody is  $43.9 \pm 4.7$  (CV=10.7%). After BSA blocking, the OPD is reduced, which suggests that the layer of BSA is successfully created over the free remaining gold areas (this is illustrated in **Figure 4.11**). We also included some representative images of three different sensor chips and the arrays in each step of the biofunctionalization protocol (**Figure 5.4B**). We can see that the intensity of the spots increases when the antibody is captured by the spots of Protein G. The colour bar is not related with the OPD value but with the intensity within the picture.

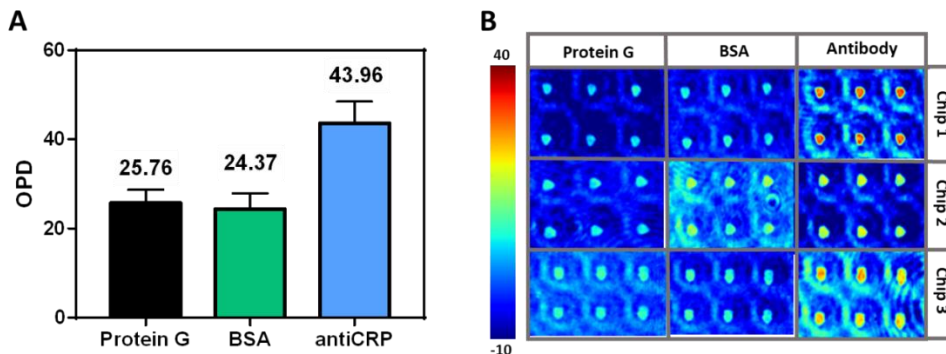


**Figure 5.4:** A: OPD mean values obtained for the three-step anti-CRP immobilization protocol (n=30 chips). B: Representative colour code OPD maps of 2x3 microarrays through the different immobilization steps in three different sensor chips.

The specificity of the CRP assay was assessed with different controls as summarized in **Figure 5.5**. The addition of the target protein resulted in a clear signal enhancement ( $\Delta\text{OPD} = 8.83$ , in **Figure 5.5(1)**). However, no OPD increase was observed if the array was incubated with a different protein (in **Figure 5.5(2)**). Similarly, incubation of CRP over a non-specific antibody resulted in negligible increase in the OPD ( $\Delta\text{OPD} = -1.47$ ) (see **Figure 5.5(3)**). Moreover, in the absence of any antibody (i.e. only spotted Protein G arrays and BSA) the CRP did not bind (**Figure 5.5(4)**) corroborating the lack of non-specific binding over the blocked surface. These different tests confirmed that the signal corresponds exclusively to the specific recognition of the protein for its specific antibody (in this case, CRP and anti-CRP, but extendable to any other antigen-antibody pair).

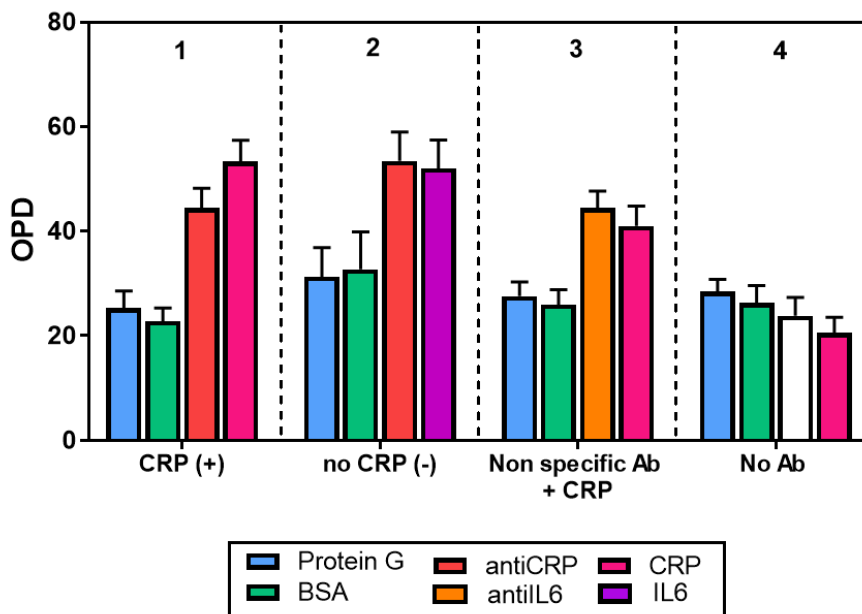


**Figure 5.5:** Specificity study for the CRP assay showing the variation in the OPD in 4 different arrays. Each experiment shows the OPD signal of each step of the assay (immobilization and detection). (1) Positive control ([CRP] = 500  $\mu\text{g}/\text{mL}$ ) incubated on an anti-CRP functionalized array; (2) Control protein ([IL-6] = 200  $\mu\text{g}/\text{mL}$ ) incubated on an anti-CRP functionalized array; (3) [CRP]=500  $\mu\text{g}/\text{mL}$  incubated on array functionalized with a non-specific antibody; (4) [CRP]= 500  $\mu\text{g}/\text{mL}$  incubated on unmodified array (i.e. only Protein G spots on a BSA blocked surface). White column represents the incubation of the array with only PBS, (i.e. no antibody), prior to the addition of the CRP

Once the biofunctionalization protocol was shown to be reproducible and specific for CRP, we proceeded to obtain a calibration curve. To do that, different concentrations of CRP ranging between 0 to 500  $\mu\text{g}/\text{mL}$  were incubated for 30 min over 8x8 microarrays of anti-CRP antibodies. **Figure 5.6A** shows the results obtained for the  $\Delta\text{OPD}$  of at least three different replicates of each concentration. The calibration curve for CRP (**Figure 5.6A**) showed a linear concentration-dependent region before reaching a saturation at 200  $\mu\text{g}/\text{mL}$ . The coefficient of determination ( $R^2$ ) of the curve is 0.892 which is acceptable and a limit of detection (LoD) of 18  $\mu\text{g}/\text{mL}$  was estimated. The curve fitted to a one-site binding curve (**Equation 5.1**):

$$y = \frac{B_{max} \cdot X}{K_d + X} \quad (5.1)$$

Where  $X$  is the concentration,  $y$  is the  $\Delta$ OPD signal,  $K_d$  is the equilibrium binding constant and  $B_{max}$  is the maximum number of binding sites. The limit of detection (LoD) was calculated as three times the average of the standard deviation of four blank samples.<sup>195</sup> Since CRP levels in blood plasma of healthy individuals are commonly found below 10  $\mu\text{g/mL}$ , and can drastically increase to around 300  $\mu\text{g/mL}$  in patients with severe infection,<sup>196</sup> our approach can comfortably allow the detection of this protein in any infection and particularly in sepsis.

In order to establish the accuracy of the method, spiked samples within the linear range of the curve (between 0 and approximately 100  $\mu\text{g/mL}$ ) were tested. **Figure 5.6B** shows the correlation of the values. The slope of the curve is 0.8592, which indicates a slight underestimation (i.e. slopes higher than 1 implies a certain overestimation while below 1 is indicative of underestimation).

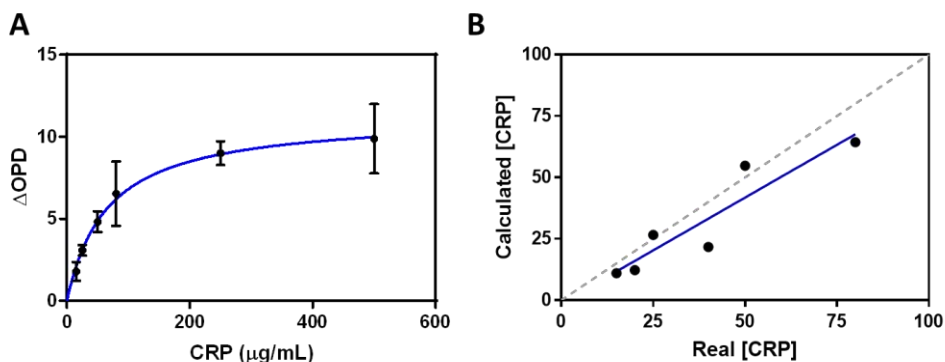


**Figure 5.6:** A: CRP calibration curve in PBS buffer. B: Correlation plot of spiked samples. Dashed line corresponds to a slope=1.

For a potential commercialization in the long-term, the nanoplasmonic chips functionalized with the antibodies will need to be stored for long time (i.e. 6, 12 or even 24 months) before being used. As a short-foreseen stability study, we assessed the conditions that allowed the biofunctionalised chips to remain intact for several days. This was done by preparing a set of sensor chips and storing them in dry conditions at 4°C during different times up to one week. Ideally the results achieved after a week of preparation should be similar to the results achieved with a freshly prepared chip. **Figure 5.7A** summarizes the OPD signals of antibody functionalized chips ( $OPD_{t_0}$ ) and

those obtained after storage of the sensor chips for 24, 48, 72 h and seven days. A slight decrease in the OPD was observed over time. Upon incubation with CRP (500  $\mu\text{g}/\text{mL}$ ) we could observe recognition (i.e. increase in the OPD) but the  $\Delta\text{OPD}$  was gradually lower over time compared with freshly prepared antibody coated sensor chips (**Figure 5.7B**). A possible explanation for this is that the antibodies are losing recognition function upon storing as a consequence of their partial denaturation in dry conditions.

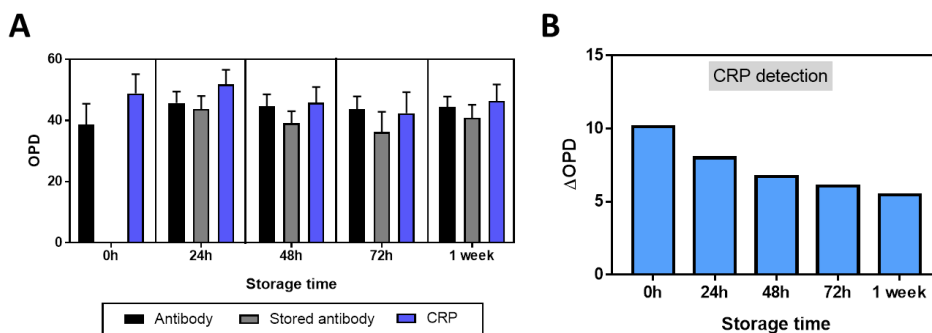


**Figure 5.7:** A: OPD signals measured of 5 different microarrays of antibodies stored at 5 different times: 0 (non-stored, fresh measurement), 24, 48, 72 h and 1 week. The last bar is the OPD after incubation with 500  $\mu\text{g}/\text{mL}$  CRP. B:  $\Delta\text{OPD}$  calculated after incubating CRP at 500  $\mu\text{g}/\text{mL}$  on the stored sensor chips.

Finally, as explained in **Chapter 1, section 1.3**, several technologies are commercially available to perform the deposition of small volumes and create microarrays of spots. Thus, to evaluate if the spot size or the spotting technique had an effect on the final performance of the assay, we compared these results with those obtained using a different spotter whose deposition working principle is different. The dip-pen nanolithography-based spotter Nano eNabler™, from Bioforce Nanosciences, routinely used in this Thesis, renders spots with more or less the same diameter ( $\approx 55 \mu\text{m}$ ) because it employs a tip that has a width of  $60 \mu\text{m}$ . Conversely, sciFlexArrayer from Scienion AG (Berlin, Germany), tested as comparative technique, employs ink-jet printing to produce larger spots (around  $100 \mu\text{m}$ ). Both types of spots can be seen in **Figure 5.8A**. The effect of the deposition on the different steps of the immobilization protocol (Protein G, BSA and antibody) was then compared with both techniques.

We observed that, although the OPD signals obtained after Protein G

spotting was slightly smaller when using the ink-jet printing (**Figure 5.8B**), this difference was minimal in the last step of antibody immobilization, so, overall no significant difference was found. The subsequent target incubation and detection resulted also in similar OPDs for the concentrations tested (i.e. CRP, 50 and 250  $\mu\text{g/mL}$ ) (**Figure 5.8C**). Overall, although the immobilization signals were slightly different in the deposition itself, then the subsequent steps until antibody capture resulted in similar amounts of receptor, which eventually translated in similar target detection signals. Thus, we can conclude that there is no apparent effect from the spot diameter that could affect the detection principle of the POC biosensor.

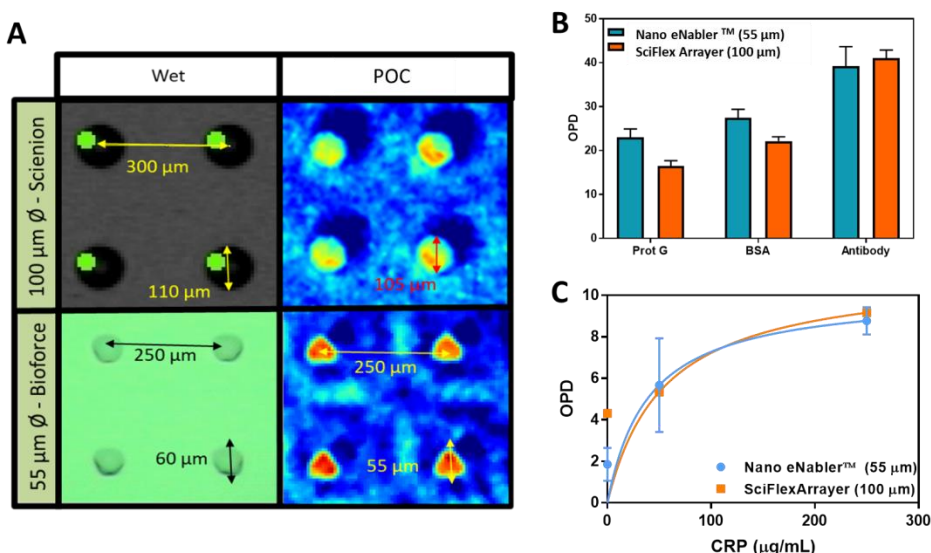


**Figure 5.8:** Summary of the main results for the effect of the deposition method and spot diameter in the detection performance. **A:** Images of the spots produced with each spotter. Top: left picture of the spots obtained with the SciFlexArrayer (Sciension) instrument; right picture corresponds to the colour code OPD map obtained with the POC device. Bottom: left picture of the spots obtained with the Nano eNabler™ (Bioforce) instrument; right one picture corresponds to the colour code OPD map obtained with the POC device. **B:** OPD values obtained for each step of the immobilization protocol. **C:** Calibration curves obtained with arrays prepared with both printers.

### 5.2.1 Interleukin-6

For the detection of IL-6, we started from the same protocol conditions (i.e. same Protein G spotting and BSA incubation) with the aim to further pursue multiplexed analysis. We evaluated two different antibody concentrations (250 and 500  $\mu\text{g}/\text{mL}$ ), as in the case of the CRP assay. The first two columns in **Figure 5.9A** show the OPD values obtained after incubation with both concentrations which resulted in  $44.2 \pm 1.04$  (CV=2.35%) and  $38.1 \pm 2.73$  (CV=7.16%) for 250 and 500  $\mu\text{g}/\text{mL}$ , respectively. The OPD signal for 500  $\mu\text{g}/\text{mL}$  was lower than at 250  $\mu\text{g}/\text{mL}$ , which may suggest that a saturation of the Protein G sites has been reached. After incubation with IL-6 at two different concentrations (40 and 200  $\mu\text{g}/\text{mL}$ ) we observed that  $\Delta\text{OPD}$  was higher precisely for 250  $\mu\text{g}/\text{mL}$  of antibody (see **Figure 5.9A,B**), thus this concentration was selected for further experiments.

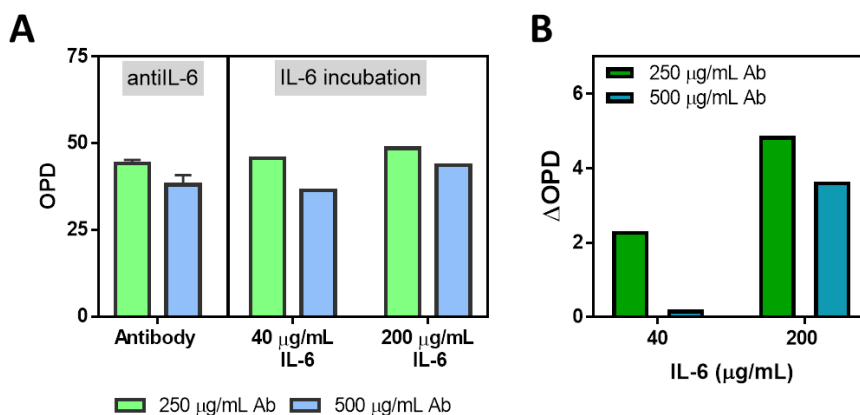


**Figure 5.9:** A: OPD signals for antibody immobilization at 250 and 500  $\mu\text{g}/\text{mL}$  (left) and upon incubation with IL-6 at 40  $\mu\text{g}/\text{mL}$  and 200  $\mu\text{g}/\text{mL}$  (right). B:  $\Delta\text{OPD}$  achieved upon IL-6 incubation.

The reproducibility of the antibody signal was assessed as in the case of CRP assay, by repeating the biofunctionalization with a significant number of sensor chips (n=10). See **Table 5.3** for more details.

**Table 5.3:** Interchip variability in the three-step Protein G based biofunctionalization protocol for IL-6

Interchip variability <sup>a</sup>		
IL-6		
	Mean±SD	%CV
<b>Protein G</b>	27.4 ± 5.98	21.8
<b>BSA blocking</b>	24.7 ± 3.4	13.8
<b>Antibody capture</b>	44.88 ± 4.51	10.1

<sup>a</sup>: Interchip variability observed with 10 chips biofunctionalized with the same protocol

<sup>b</sup>: Intrachip variability observed in 4 arrays prepared in a single chip. 3 different chips are shown as representative examples.

**Figure 5.10A, B** shows the average OPD value achieved in the three steps of the immobilization protocol of the anti-IL-6. Protein G OPD averaged value ( $27.4 \pm 5.98$ , CV=21.80%) was similar to the average in CRP sensor chips but the SD found was higher. BSA values were also similar ( $24.7 \pm 3.38$ , CV=13.8%), as well as the antibody binding ( $44.8 \pm 4.51$ , CV=10.1%). With exception of the Protein G adsorption step the whole protocol behave with a CV lower than 20%: some pictures of microarrays at the different steps of the protocol are showed as example (**Figure 5.10B**). The immobilization values are overall very similar to those obtained with the CRP assay, which confirms the reproducibility of the assay regardless of the monoclonal antibody used.

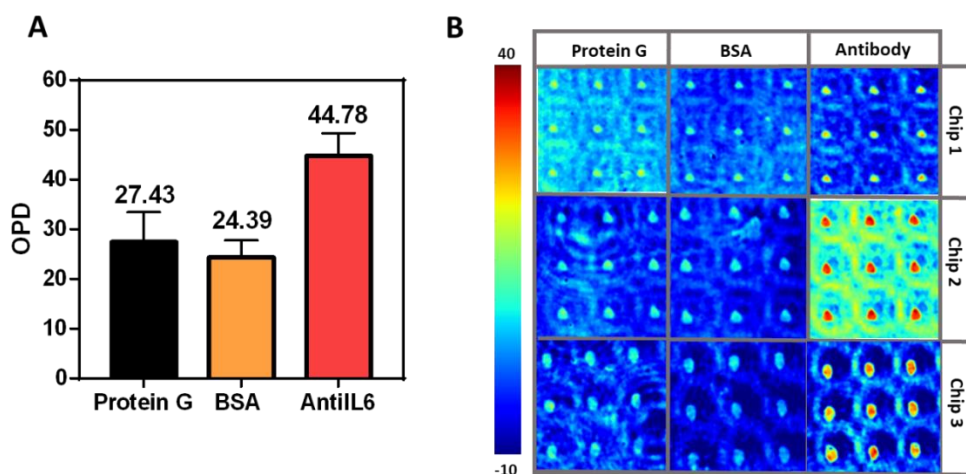


**Figure 5.10:** A: OPD mean values obtained for the three-step anti-IL-6 immobilization protocol (n=10 chips). B: Representative colour code OPD maps of 3x3 microarrays through the different immobilization steps in three different sensor chips.



A calibration curve in buffer PBS was also generated by analysing several IL-6 concentrations (**Figure 5.11A**). We did not observe a saturation of the signal for this interval of concentrations. We believe that the main difference among IL-6 and CRP assays, relies on their different MW or on the antibody affinity. The affinity of the antibody might have an influence in this lower level of detectability compared with CRP. According to the graphs it may be possible that the anti-CRP shows higher affinity for its target than anti-IL-6. However, it might be also possible that some restrictions of accessibility to the antibody binding sites for a larger molecule like CRP occur, which might be translated to a lower number of effective available receptors, resulting in a premature saturation. However, this can be also associated to the much lower MW of IL-6 (120 kDa for CRP *versus* 24 kDa for IL-6), since the working principle of the POC is related to the refractive index changes on the surface, which in turn is related to the mass.

Although the fitting was slightly better ( $R^2 = 0.9647$ ) compared with the one for the CRP curve, the LoD was 88  $\mu\text{g/mL}$ , which is much higher. This may also be related to the lower MW of this biomarker compared to CRP. In this case, the assay is far from reaching the common clinical values found for IL-6 in sepsis patients ( $>120 \text{ pg/mL}$ ) that are summarised in **Table 5.1**. The sensitivity of the assay could be improved by adding an amplification step, provided for instance by a second antibody in a sandwich-type assay or by changing the approach for a competitive assay where the analyte concentration is indirectly quantified by the signal generated by the antibody in solution.

The accuracy of the assay was also assessed with spiked samples (**Figure 5.11B**). In this case the slope obtained in the correlation plot was 0.996 which is almost equal to 1. Hence, the IL-6 curve shows an excellent accuracy. Overall, these results are very promising because, although the sensitivity achieved is not enough for sepsis diagnosis, they demonstrate the sensing capacity of the POC for proteins with medium molecular weight (24 kDa).

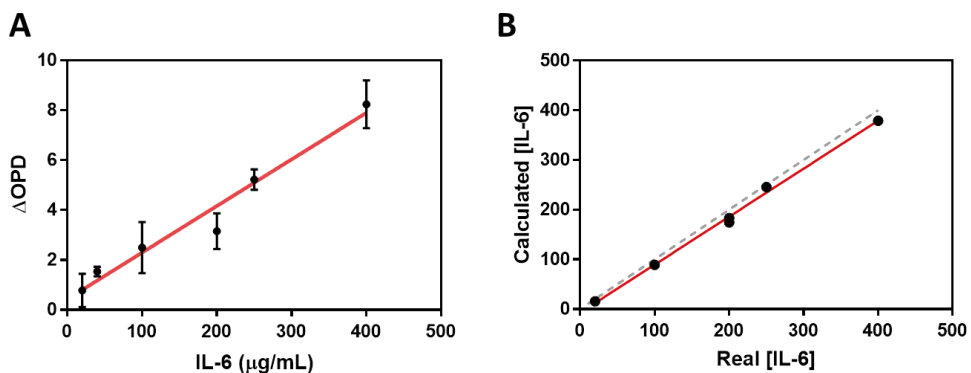


**Figure 5.11:** A: IL-6 calibration curve in PBS buffer. B: Correlation between calculated and real concentration of IL-6. Dashed line corresponds to a slope=1.

## 5.2.2 Procalcitonin

For the detection of PCT two different monoclonal antibodies: QNO5 and 03-1C2 were tested. These high-quality antibodies are employed in the Kryptor Gold Analyzer, a well-established technology developed by Brahms-ThermoFisher (partner in the RAIS project). Hence, they have proven their good performance previously, in particular in a sandwich assay for PCT detection. The OPD signals for the immobilization of these antibodies (at a concentration of 250 µg/mL) was higher for 03-1C2 antibody ( $63.6 \pm 7.54$  (CV=11.8%)) compared with  $48.1 \pm 3.5$  (CV=7.3%) for QNO5. However, the detection of PCT (250 µg/mL) was only observed with QNO5 antibody ( $\Delta\text{OPD} = 8.65$ ) (see **Figure 5.12**).

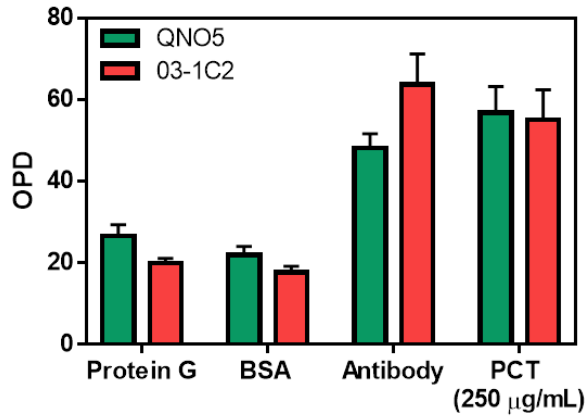


**Figure 5.12:** OPD values obtained for the immobilization of two different anti-PCT antibodies: QNO5 and 03-1C2, and the detection of PCT (250 µg/mL).

According to this preliminary results, QNO5 antibody was selected as capture immobilized antibody. The reproducibility of the immobilization was studied (**Figure 5.13**). In **Figure 5.13A** we have included the average values of 6 sensor chips and pictures of some arrays are included in **Figure 5.13B**. The pattern of lower OPD after incubation with BSA was observed again, Protein G signal was  $32.1 \pm 5.39$  (CV= 16.7%) and BSA was  $23.2 \pm 3.5$  (CV=15.1%). Anti-PCT binding gives a high signal:  $47.6 \pm 4.35$  (CV=9.14%).

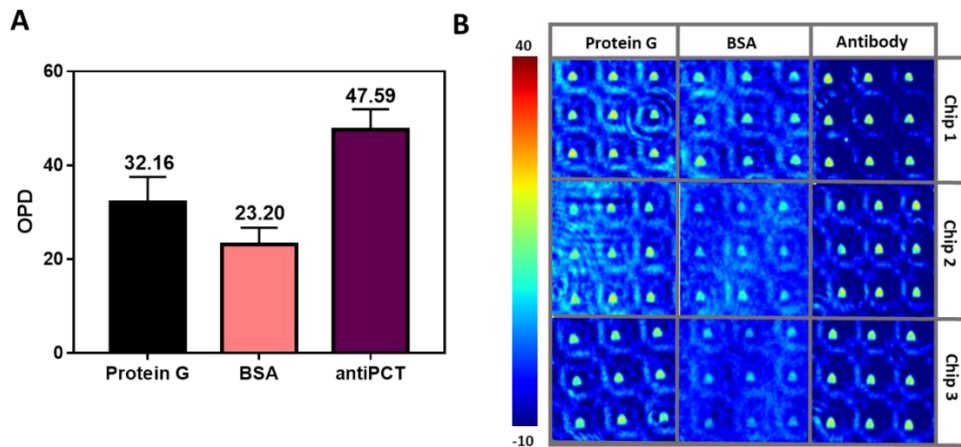


**Figure 5.13:** A: OPD mean values obtained for the three-step anti-PCT immobilization protocol (n=6 chips). B: Representative colour code OPD maps of 3x3 microarrays through the different immobilization steps in three different sensor chips.

Although these initial results showed: (i) similar immobilization patterns and efficiency for anti-PCT and (ii) promising detection of PCT, we observed that when repeating target measurements with different PCT concentrations, the  $\Delta\text{OPD}$  values obtained for several PCT concentrations were not reproducible and the results were not reliable. A high variability was regularly found, being the  $\Delta\text{OPD} \sim 0$  even for high PCT concentrations (**Figure 5.14B,C**, blue spots). As the quality of the antibody was not the problem, a reasonable cause for this might be related with the low molecular weight of PCT, which, as seen in previous section, has a significant effect on the RI change. Low RI changes difficult the detection and shows the sensitivity limits of the POC technology developed in this project. As introduced in the description of the device (Chapter 3), the detection limit of our current optical configuration using these nanostructures is around  $5 \cdot 10^{-4}$  RIU,<sup>134</sup> which is between one and two orders of magnitude higher compared with other imaging label-free optical devices (which can be around  $10^{-5}$ - $10^{-6}$ , see **Table 3.1**). This inevitably has a remarkable effect on the sensitivity achieved with the protein assays, with LODs in the  $\mu\text{g/mL}$  range.

In order to enhance the signal (by increasing the RI change on the surface), a sandwich assay with the other antibody previously tested (03-1C2) was explored. Sandwich assays consist of the addition of a second antibody that recognizes another epitope of the analyte, already captured by the primary antibody (**Figure 5.14A**). This way the signal can be amplified. However, also in this case, the signal obtained for the second antibody was also erratic, being sometimes not significant or not proportional to the incubated concentration or even lower than the signal with only the PCT (see **Figure 5.14B,C**, red spots).

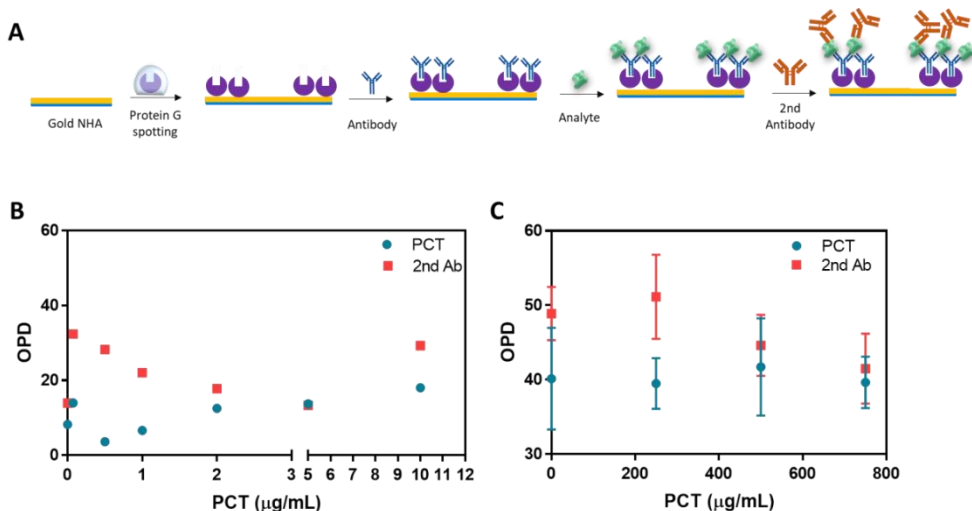


**Figure 5.14:** A: Scheme of the biofunctionalization protocol in a sandwich format. OPD signals achieved when (B) low and (C) high PCT concentrations were incubated (blue spots) and after addition of the second antibody (red spots).

As a final conclusion, it was not possible to quantify PCT in a reliable way with the POC instrument. As future alternatives to achieve this, we propose the use of larger tags such as nanoparticles which may be useful for amplifying the signal but in detriment of adding extra steps to the immunoassay. However this option would end up in a more complex POC device and a labelled assay (which should be avoided for the sake of analysis simplicity).

Finally, PCT is a very small protein which requires high sensitivity to be detected and, at the moment, this POC biosensor is not yet able to reach that sensitivity limits.

### 5.3 Multiplex measurement of CRP and IL-6

The results seen in Chapter 4 points out that immobilized antibodies work better when they are incubated instead of spotting. This is a limitation to our POC device as fitting several antibodies within a small surface for multiplexing becomes a challenge. In an ideal scenario, antibodies should be spotted while fully keeping their biorecognition capabilities; hence, tens of antibodies for different biomarkers could be analysed on a single microarray with the POC biosensor.

With the aim of studying the multiplexed capabilities of the POC, we divided the gold nanoplasmonic chips in four sections and in each of them, we spotted 8x8 microarrays of protein G and we later incubated: two microarrays with anti-CRP and the other two with anti-IL-6. The sections were physically divided with a hydrophobic pen that created a hydrophobic barrier among them, thus, permitting incubation of different solutions.

Both targets were incubated either individually or together in one solution (see **Figure 5.15A** and **5.16A**). Two different target concentrations were evaluated individually (100 and 200  $\mu\text{g/mL}$ ). The results are summarized in **Figure 5.15B**. When tested individually, only in the microarrays where the protein was incubated with its specific antibody, an increase in the OPD was observed, which confirms the specificity of both assays. The  $\Delta\text{OPD}$  signals achieved are: for CRP, 3.45 (200  $\mu\text{g/mL}$ ) and 5.49 (100  $\mu\text{g/mL}$ ), while for IL-6 3.48 (200  $\mu\text{g/mL}$ ) and 2.24 (100  $\mu\text{g/mL}$ ). When analysed together as a single solution containing both CRP and IL-6 at the same concentration (200  $\mu\text{g/mL}$ ), we observed similar  $\Delta\text{OPDs}$  (see **Figure 5.16B**), although slightly higher for CRP compared with the same concentration in a solution only containing this protein (9.7 units for incubation over anti-CRP and 2.69 units for incubation over anti-IL-6). A possible reason for this behaviour could be related to the overall higher concentration of reagents in the solution (i.e. 200  $\mu\text{g/mL}$  of CRP plus 200  $\mu\text{g/mL}$  of IL-6 in 10  $\mu\text{L}$ ) which might have caused a slight material accumulation and sedimentation at the dry film edges of the 10  $\mu\text{L}$  incubation droplet, resulting in an altered OPD readout in those spots close to the film boundary. These material accumulation and sedimentation are found to affect the real OPD value as they increase the amount of mass over the spots, thus, increasing the final  $\Delta\text{OPD}$ . Most of the times these marks can be seen with bare eye, however, sometimes it is not possible.

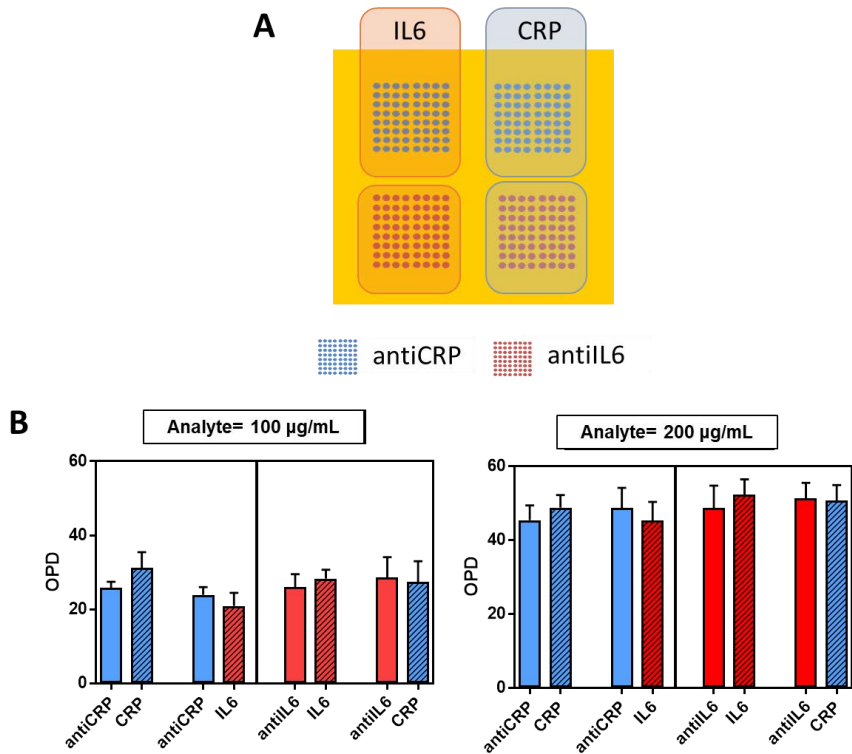


**Figure 5.15:** A: Schematic representation of the single analyte multiplex test. B: OPD signals obtained for the antibody immobilization (solid columns being blue: anti-CRP and red: anti-IL-6 and after protein incubation (dashed columns being blue: CRP and red: IL-6). Protein concentrations were 100  $\mu\text{g/mL}$  (left) and 200  $\mu\text{g/mL}$  (right).

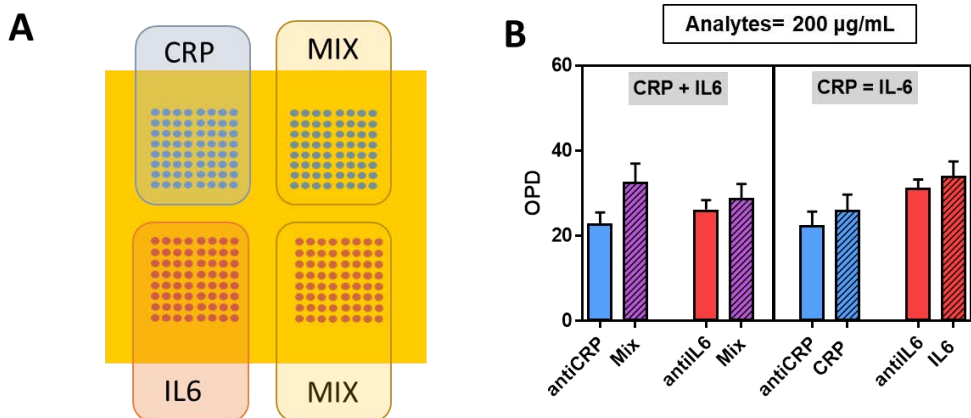


**Figure 5.16:** A: Schematic representation of the single vs mixed analyte multiplex test. B: OPD signals obtained for the antibody immobilization (solid columns being blue: anti-CRP and red: anti-IL-6) and after protein incubation (dashed columns being blue: anti-CRP, red: anti-IL-6 and purple: CRP+IL-6). Protein concentrations were 200  $\mu\text{g/mL}$  each one.

These latest results show the capability of the POC device to evaluate two biomarkers at the same time. Nevertheless, as 4 microarrays (8x8) can be fitted on a single chip, the potential multiplexing capabilities of the POC biosensor can reach up to 4 different biomarkers analysis. In addition, in terms of specificity, the antibodies for CRP and IL-6 do not show any type of cross-reactivity, confirming the specificity of the assay. The  $\Delta$ OPD was interpolated on the calibration curves and the recovery was calculated to evaluate the accuracy with the equation:

$$Accuracy (\%) = \frac{\text{Calculated concentration}}{\text{Real concentration}} \cdot 100 \quad (5.2)$$

Main results are summarised in **Table 5.4**.

**Table 5.4:** Accuracy experiments obtained in the multiplexed detection of CRP and IL-6<sup>a</sup>

Individual incubation		Mix incubation	
Test	Accuracy (%)	Test	Accuracy (%)
CRP 100	72,95	CRP 200	18,355
CRP 200	17,265	(Ab) CRP 200 + IL-6	195,5
IL-6 100	97,06	IL-6 200	61,385
IL-6 200	81,735	(Ab) IL-6 200 + CRP	60,58

<sup>a</sup>: data extracted from Figure 5.15B and 5.16B.

These results show a better accuracy for IL-6 detection (i.e. accuracy between 60-90%) than for CRP, which showed more irregular recoveries. CRP at 200  $\mu$ g/mL (both times in both chips), showed a very small signal for what was expected. This may be related with the proximity to the plateau area in the calibration curve. Mixed incubation of CRP and IL-6 over anti-CRP showed overestimation, probably due to the high protein concentration on the sample. Nevertheless, these results correspond to a single experiment, not an average, thus, increasing the number of tests might be necessary to improve the reliability of the multiplexed analysis. Besides, increasing the number of multiplexed tests to more concentrations should be tested.



These proof-of-concept experiments, although with a limited degree of multiplexing (i.e. eventually four biomarkers in a 4-array design like the one shown in **Figure 5.15A**), exemplify the potential of the biofunctionalization strategy and the POC biosensor for the simultaneous analysis of different proteins in a single chip.

## 5.4 Design, optimization and analytical evaluation of proteins in plasma

Clinical analysis done in blood samples are commonly performed in plasma or serum. Plasma and serum are samples that are routinely collected in hospitals and in an easy way (blood withdrawal). Plasma is the soluble remaining fraction of the blood when cell fraction is removed by addition of anticoagulants and centrifugation. Serum is part of the blood that is left over after the red blood cells, the white blood cells, the blood platelets, and clotting factors have been removed from the blood.

Plasma composition contains mostly water (90%) and proteins (i.e. globulins, fibrinogens, albumins), glucose, clotting factors, electrolytes, hormones, CO<sub>2</sub> and O<sub>2</sub> among other substances. However, the high variability in the composition of blood plasma samples represents an important barrier in laboratory analysis for the reliable detection and quantification of clinical biomarkers. Interferences produced by other compounds different than the target analyte produce what is called matrix effect. This matrix effect is very critical in all analytical devices and, more particularly, in devices that exploit optical changes. In our case, the POC biosensor measures changes on the RI, which may be affected by the interferences (mass change) produced by non-specific binding that affects the optical measured properties.

Non-specific binding occurs when proteins or lipids present in plasma are adsorbed to the surface of a solid sensing support. The interactions between the proteins and the surface are mainly electrostatic or hydrophobic. In our POC this non-specific adsorption may be critical as the addition of an extra layer may change the total refractive index of the surface, and the thickness, affecting the OPD evaluation. As a consequence, it is mandatory to evaluate the effect of such fluids on the assay performance and reduce it as far as

possible. The non-specific binding can be minimized or even removed either by changing the solution conditions (when sample is diluted) or by modifying the sensor surface. Changes in buffer solution can be done by increasing salt concentration, adjusting pH to stabilise proteins; or adding surfactants like sodium dodecyl sulphate (SDS) or polyethylene glycol sorbitan monolaurate (Tween 20) to influence surface wetting.<sup>197,198</sup> Another option is to cover the remaining exposed part of the surface after ligand/bioreceptor immobilization with a biologically inert protein. Commonly, protein blockers such as BSA, casein, fish gelatin, PEG molecules or skim milk are used for this purpose because they block the non-occupied sites on the surface and stabilize biomolecules bound to the surface to reduce steric hindrance.

#### 5.4.1 Effect of the plasma in the CRP assay

The antibody functionalized chips already contain a layer of BSA (1%) covering the remaining free gold areas of the chip after Protein G deposition. This layer was added to precisely prevent antibody adsorption during chip preparation. Therefore, a first evaluation to check if BSA at 1% was efficient enough as blocking agent for plasma or serum analysis was done. Two microarrays were incubated with 100% commercial plasma (see **Figure 5.17A, 1 and 2**) and two microarrays with 100% commercial serum (see **Figure 5.17A, 3 and 4**). Under incubation with both blood derivatives a significant increase in the OPD values was observed (**Figure 5.17B**) together with a visible deterioration of the microarrays, being significantly worse for serum rather than for plasma. Overall, this initial evaluation suggests that 1% BSA is not totally successful in preventing non-specific bindings. Further conditions were pursued although only with plasma, given its less severe effect.

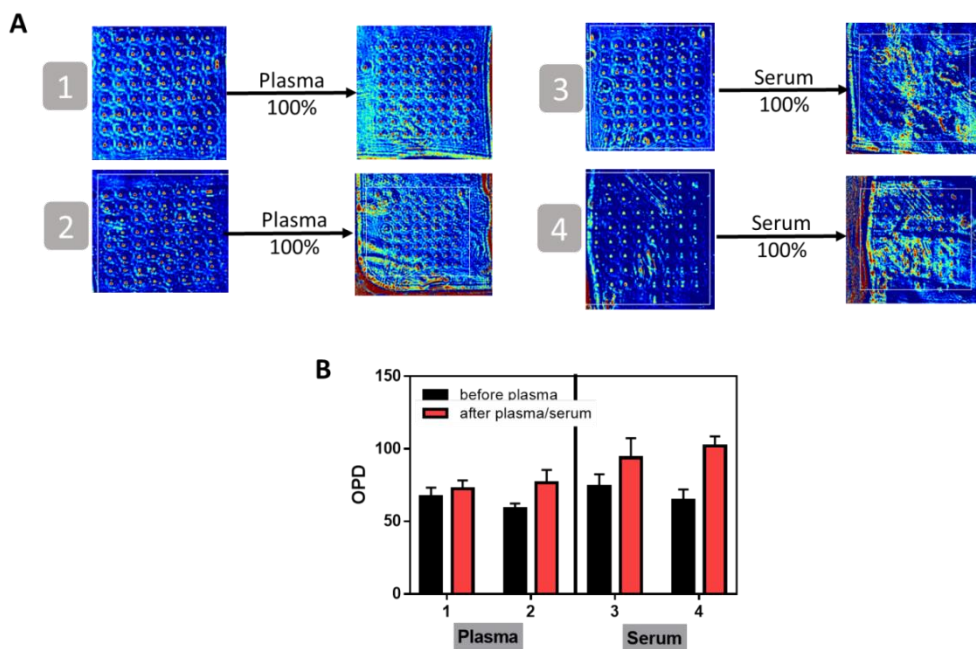


**Figure 5.17:** Colour code OPD maps of two microarrays pictures before and after incubation with plasma 100% (Arrays 1 and 2) and serum 100% (Arrays 3 and 4). C: OPD value of each microarray before and after incubation with plasma/serum.

Plasma was then diluted with PBS (from 100% to 0.1%) and incubated over different arrays (**Figure 5.18A**). An increase in the OPD (i.e. adsorption of mass) was observed in all the cases (**Figure 5.18B**). Although each diluted plasma solution was tested only once, it was observed a general trend, when the higher the plasma dilution, the lower the  $\Delta$ OPD value. The minimum dilution tested was 0.1% and it gave a  $\Delta$ OPD of 2 units, which may be negligible considering the typical SD obtained with this device. However, this dilution is not useful from a practical point of view, as it implies a 1000-fold dilution, worsening the detectability levels in a great extent.

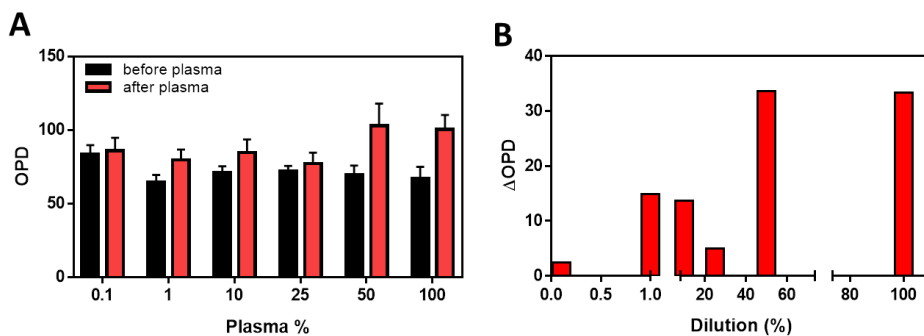


**Figure 5.18:** A: OPD signals achieved upon incubation of an antibody coated microarrays with plasma at different dilutions. B:  $\Delta$ OPD observed for every plasma dilution.

As a BSA layer is not effective enough in preventing non-specific adsorption, the addition of other types of antifouling compounds instead of BSA was tried. Then, the addition of skim milk was tested. This is commonly used blocking agent in western blot and other immunoassays to block non-specific binding of antibodies and to reduce background signal,<sup>172</sup> **Figure 5.19A** shows one microarray and the successive steps of blocking with skim milk at 2%, antibody binding and plasma incubation (1, 10, 25 and 50% diluted). As we can observe from the numerical values in **Figure 5.19B** skim milk also binds to the Protein G spots at some extent as the OPD of the spots increases. When we add BSA we normally observe a decrease in the OPD signal and we attribute this to the albumin covering only the free remaining areas. This can be understood as if the reference signal of the readout mechanism is increased thus the difference between the spot and the surrounding area is reduced. Although it seems that indeed skim milk partially binds to protein G, this does not completely prevent the antibody from interacting with Protein G, as the later step of antibody addition is successful (but with a much lower extent, i.e.  $\Delta$ OPD = 9.4 compared to 19.59 with BSA). Finally, upon addition of different dilutions of plasma: 1, 10, 25 and 50%, we observe an increase of 47, 45, 68 and 80 OPD units, respectively. This shows that skim milk does not work as an effective blocking agent.

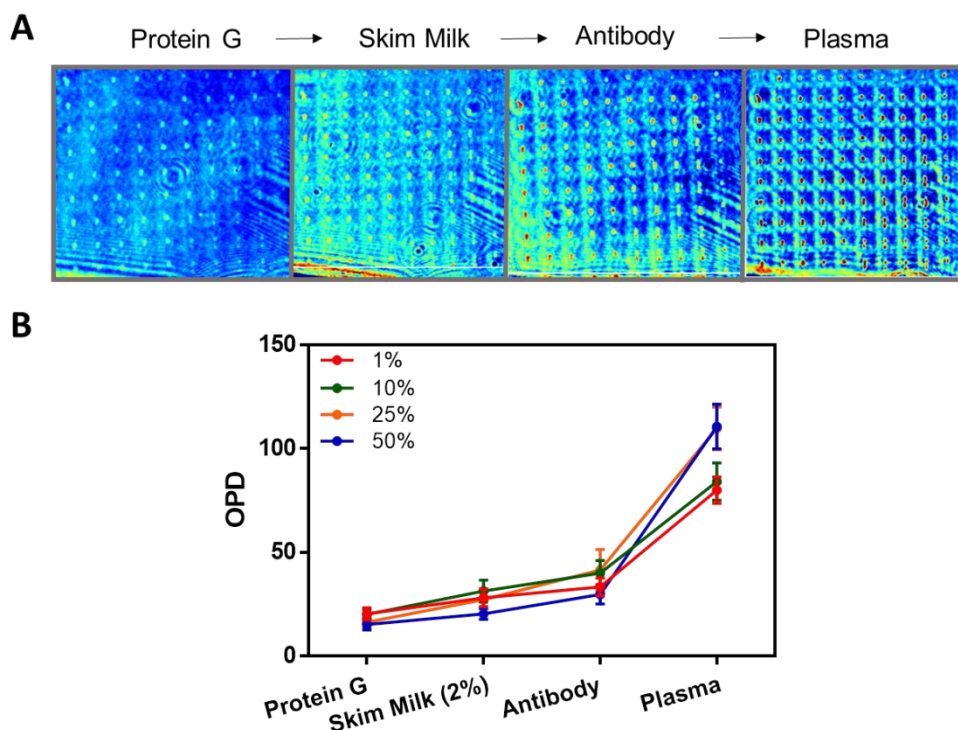


**Figure 5.19:** A: Colour code OPD maps of one microarray along the successive steps of the protocol: Protein G, skim milk addition, antibody binding and incubation with different dilutions of plasma. B: Plot that contains the OPD values achieved in 4 different microarrays incubates first with skim milk at 2% and later with plasma diluted at different concentrations (1, 10, 25 and 50%).

As the complete removal of the non-specific binding turned complicated, we evaluated if the detection of CRP was possible in diluted plasma with the initial BSA layer. In this case, the background signal from the diluted plasma was considered as blank signal, and used as reference for the calculation of the  $\Delta$ OPD after target incubation (i.e. the background signal produced by diluted plasma was subtracted to the signal produced by CRP incubated in plasma at the same dilution). In order to standardize this calculation, this value should be constant regardless of the sensor chip and plasma sample employed, in such way that a constant value could be always subtracted. To test this, we incubated several times the plasma diluted at 5, 10, 25 and 50% with and without 50  $\mu$ g/mL of CRP and we got the following average values showed in Table 5.:

**Table 5.5:** Summary of the OPD average values and SD obtained for diluted plasma with and without CRP

% Plasma	Plasma		Plasma + 50 µg/mL CRP		ΔOPD
	Mean±SD	%CV	Mean±SD	%CV	
5	6.20±4.8	76.6	8.5±5	58.8	2.3
10	24.3±7.7	31.6	34.72±4.2	12.1	10.4
25	32.25±6.4	19.8	37.4±7.2	19.3	5.4
50	34.7±7.6	21.9	37.65±6.5	17.3	2.95

Thus, the overall ΔOPD (i.e. Plasma with CRP without the average plasma signal) are: 2.3, 10.4, 5.4 and 2.95. **Figure 5.20** illustrates these values and shows that the presence of CRP additionally increases more the OPD respect to only the diluted plasma. As we can see there is a high variability in the plasma measurements, as reflected by the high values of CV compared with the ones obtained in PBS buffer. Besides, the signal difference between the plasma incubation with and without CRP shows a large variation as compared to the signal obtained in PBS buffer, 4.35 units of ΔOPD for 50 µg/mL CRP. Taking into account these parameters, we selected a plasma dilution of 25% and 50% to generate the calibration curve of CRP as lower CVs were obtained and the overall ΔOPD signals were closer to the one achieved in PBS buffer.

Calibration curves with 25 and 50% diluted plasma were generated, by removing the average background OPD signal produced in 10 sensor chips, which are 19.80 and 22.18, respectively. These values are slightly lower than the ones observed in **Figure 5.20**, however, it stills fits within the SD observed. CRP at concentrations ranging from 0 to 400 µg/mL in plasma diluted at 25% and 50% were analysed (**Figure 5.21**). The LoD achieved was 6 µg/mL and 8 µg/mL in plasma at 25% and 50%, respectively. Despite these LoD values seem better than the LoD of CRP in PBS buffer (18 µg/mL) the fitting is worse as can be also seen in the **Figure 5.21**. The R<sup>2</sup> are 0.8444 and 0.8261 for 25% and 50% plasma, respectively. Thus, these LoDs, although apparently show better sensitivity than in PBS, cannot be fully trusted.

Besides this, as the CRP curve in plasma is normalised by removing the average background signal (as mentioned above), a strong variability is introduced because the SD in the measurements is very high.

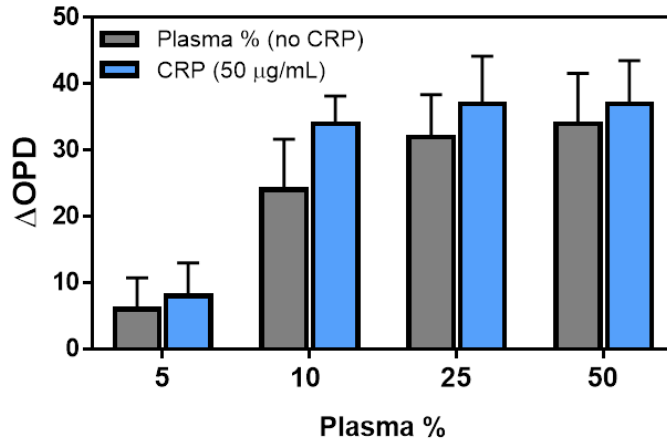


**Figure 5.20:** OPD signals achieved upon incubation with diluted plasma and 50 μg/mL of CRP in the same diluted plasma.

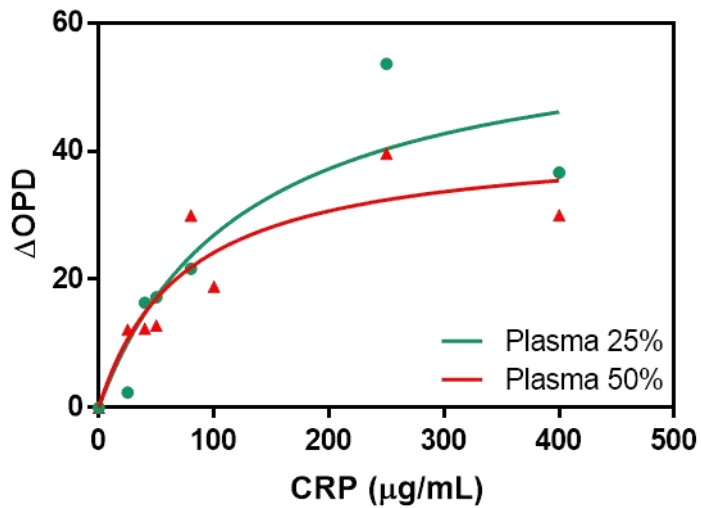


**Figure 5. 21:** Calibration curve of CRP in plasma diluted at 25 and 50% in PBS.

As a summary, a rough determination of CRP concentration on diluted plasma was achieved. The determination of the  $\Delta$ OPD signal based on subtracting an average background signal produced by non-specific adsorption is not the ideal situation. However, due to proper anti-fouling conditions were not found we proposed this strategy as a solution. In the future, more surface blocking agents and additives on the diluting solution may be tested to find a better and more reliable fitting.

#### 5.4.2 Plasma effect in the IL-6 assay

An analogous set of experiments were performed with plasma and the IL-6 assay (i.e. subtracting the OPD background signal of the diluted plasma to the OPD signal obtained after target incubation). First a comparison between the signal obtained for plasma and for plasma with IL-6 was done (see **Figure 5.22**). The average  $\Delta$ OPD signals for the incubation with 5, 10 and 25% diluted plasma with and without 125  $\mu$ g/mL of IL-6 are shown in **Table 5.6**:

**Table 5.6:** Summary of the OPD average values and SD obtained for diluted plasma with and without IL-6.

% Plasma	Plasma		Plasma + 125 $\mu$ g/mL IL-6		$\Delta$ OPD
	Mean $\pm$ SD	%CV	Mean $\pm$ SD	%CV	
5	8.14 $\pm$ 4.50	55.3	10.6 $\pm$ 3.41	32.0	2.46
10	11.7 $\pm$ 5.25	44.8	12.6 $\pm$ 6.70	53.3	0.83
25	23.3 $\pm$ 5.20	22.3	24.8 $\pm$ 7.80	31.4	1.51

Thus, the overall  $\Delta$ OPD (i.e. Plasma with IL-6 without the average plasma signal) are: 2.46, 0.83 and 1.51. These are very low signals for that concentration of IL-6, which in PBS buffer corresponds to  $\Delta$ OPD=2.7. This may be solved by using more diluted plasma, but this would sacrifice even more the sensitivity, so we decided to work with 25%.



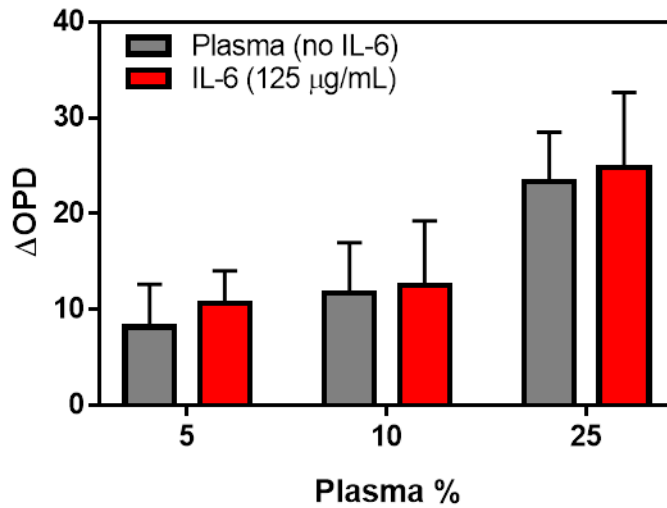


**Figure 5.22:**  $\Delta$ OPD signals obtained for diluted plasma with IL-6 at 0 and 125  $\mu$ g/mL

Different concentrations of IL-6 were incubated but we did not observe a consistent concentration-dependent signal, thus, making impossible a reliable quantification. Also, in almost all cases the  $\Delta$ OPD was smaller than the SDs. In this case, this could be indicative that somehow the interaction of IL-6 with the antibody was more severely hindered than with the previous protein (see **Figure 5.23**, green line).

The addition of Tween 20 to the dilution buffer was also considered as this is a common additive used to minimize non-specific adsorptions. High concentrations of detergent are not advisable as they can break protein-protein associations or even denature them. It is normally used between 0.05 and 0.5% in PBS or Tris-buffer. This reagent is commonly employed in immunoassays like ELISAs and Western blots as it prevents non-specific adsorption and removes unbound moieties, especially antibodies that can be present in plasma. Upon addition of this reagent to the PBS used for diluting the plasma, we observed that the  $\Delta$ OPD was reduced in average 12 units in absence of IL-6. This shows the ability of the PBST of preventing non-specific adsorptions. However, as before, the IL-6 detection at several concentrations resulted in no further increase in the OPD, which confirms the difficulty of quantifying this protein under these conditions (see **Figure 5.23**, red line).

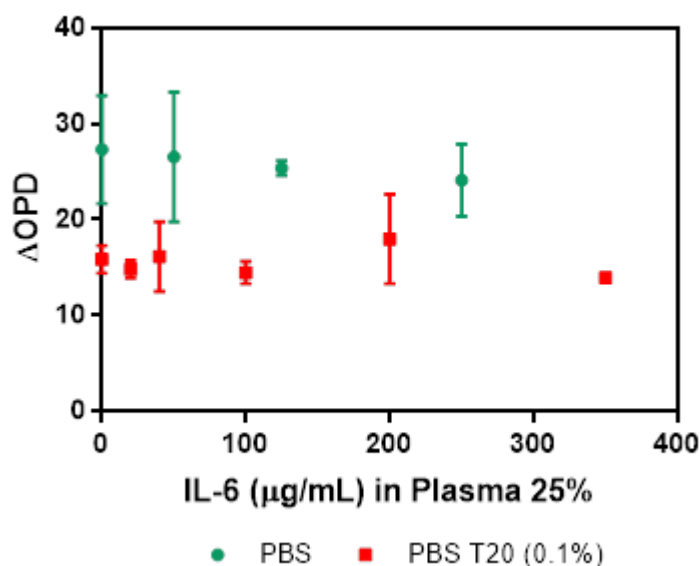


**Figure 5. 23:** IL-6 calibration curves in 25% diluted plasma in PBS (green curve) and PBST (red curve).

As a summary, with the conditions tested we were not able to quantify IL-6 in diluted plasma even when employing additives for preventing non-specific binding. Some alternatives to achieve a proportional and significant signal may be added, as trying other additives that prevent non-specific adsorption or the use of labels to increase the read-out signal.

## 5.5 Validation with real samples

Despite the low sensitivity achieved in the CRP calibration curve in plasma, we decided to attempt the analysis of real samples. For that, we evaluated a set of plasma samples collected from patients at the Vall d’Hebron Hospital (Barcelona, Spain) and stored in the Sepsis Biobank located in the same hospital. We analysed three different types of samples (see **Table 5.7**): healthy donors (4 samples), SIRS patients (4 samples) and sepsis patients (12 samples). Analysis of the CRP levels of the samples was done previously with CRP Latex Kit from Beckam Coulter (USA) at the clinical microbiology and biochemistry Laboratory located in the Hospital. To carry out the evaluation, each sample was diluted to 50% in PBS and then,

incubated for 30 min onto an anti-CRP microarrayed chips. Afterwards, the sensor chips were rinsed, dried and measured at the Hospital with the POC device. Each sample was incubated and analysed in duplicates using two different microarrays to obtain an average value for each concentration. The results are shown in **Figure 5.24A** and **Figure 5.24B** shows the calculated concentrations based on the CRP calibration curve in plasma (**Figure 5.21**) with a comparison between the values obtained at the hospital and the values calculated by the POC.

**Table 5.7:** Summary of the employed patient samples.

Type of Sample	Biobank Code	[CRP] µg/mL
Healthy	BSTC123	0,3
	BSTC124	0,3
	BSTC30	0,4
	BSTC40	0,2
SIRS	BSIRS89	24,3
	BSIRS22	31,7
	BSIRS16	12,8
	BSIRS13	14,3
Sepsis	BSEP51	117
	BSEP68	19,2
	BSEP106	95,4
	BSEP195	306
	BSEP387	469
	BSEP276	549
	BSEP293	445
	BSEP35	456
	BSEP113	434
	BSEP184	130
	BSEP308	123,1
BSEP157	100	

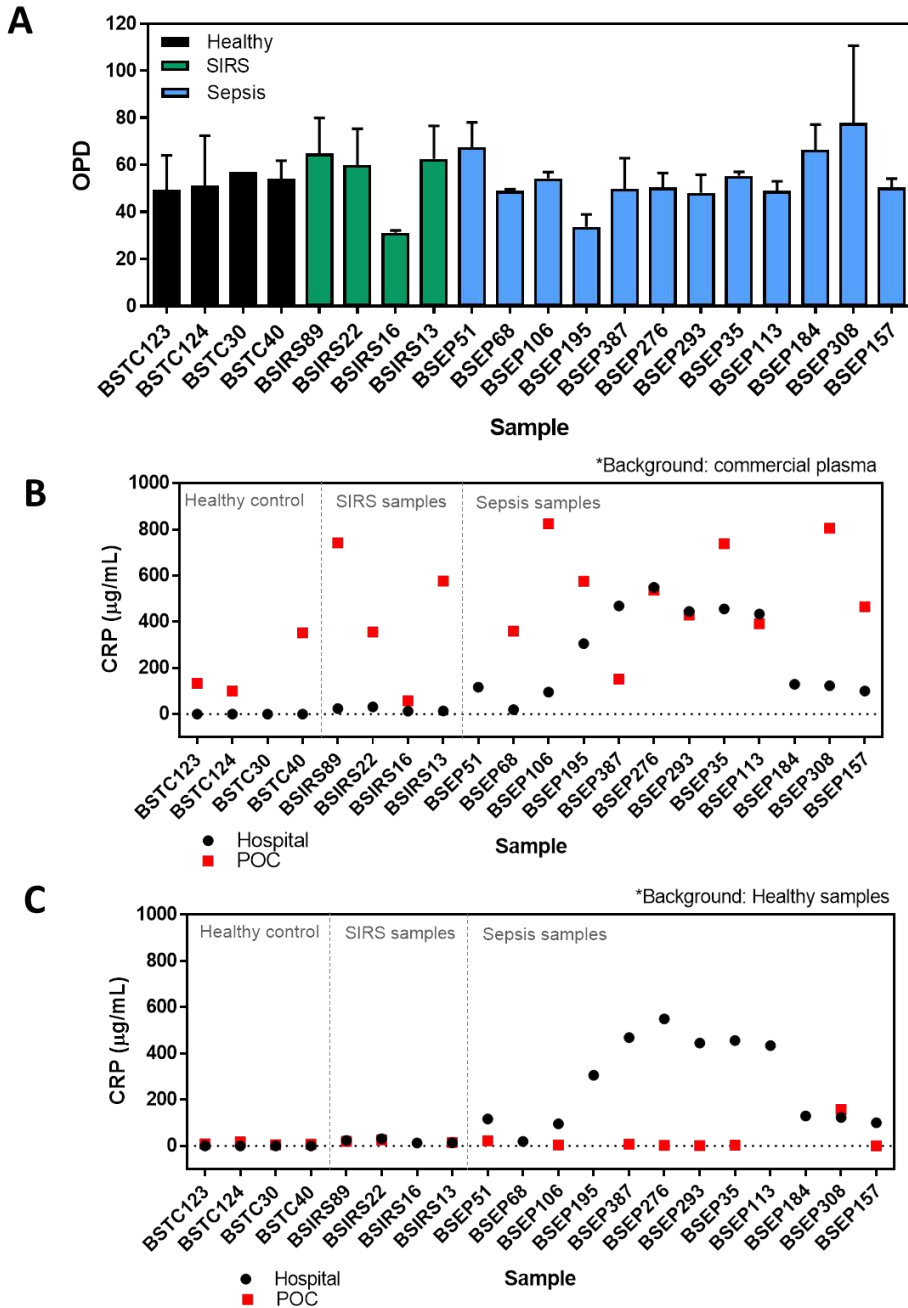


**Figure 5.24:** A: OPD signals obtained after incubation with each plasma sample (diluted 50% in PBS). B: CRP concentrations determined with the POC (by removing the average value of commercial plasma) and with the commercial kit available at the Vall d’Hebron Hospital. C: CRP concentrations determined with the POC (by removing the average value of healthy samples) and with the commercial kit available at the Vall d’Hebron Hospital

As can be concluded from **Figure 5.24A** no significant differences were observed between the three patients group, being not possible to discriminate between the healthy ( $[CRP] < 0.4 \mu\text{g/mL}$ ), the SIRS, ( $[CRP] = 12.8 - 31.7 \mu\text{g/mL}$ ) and the Sepsis samples ( $[CRP] = 19.2 - 549 \mu\text{g/mL}$ ). These results can be due to several reasons. First, the signal of the healthy samples, which can be considered as blank samples, shows a significantly higher signal ( $\Delta\text{OPD}$  around 40-50) compared with the one obtained with the control plasma used in the optimization experiments ( $\Delta\text{OPD} \sim 20$ ), which is a pool of different plasmas from donors. This reflects plasma variability from sample to sample, which inevitably affects the accuracy of the developed assay. A picture of some samples analysed is shown in **Figure 5.25** to illustrate the variability in samples which probably reflects the different composition and affects the global refractive index of the sample.

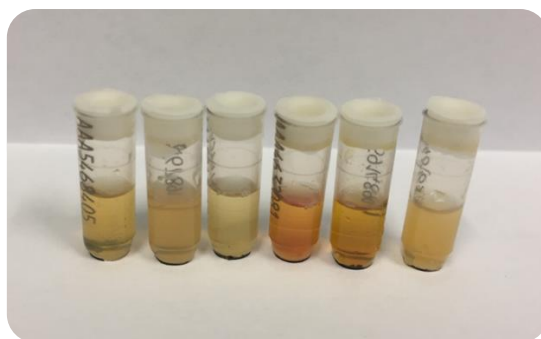


**Figure 5.25:** Picture of some of the human plasma samples employed in the analysis.

In **Figure 5.24B** the concentrations calculated after removing the average background signal from 50% diluted plasma measured in the laboratory are shown. This resulted in a poor quantification as most of the calculated concentrations are far from the value calculated with the commercial kit. We explored another approach to calculate the concentration. Instead of using an average background obtained with the standard commercial plasma, an average signal ( $\text{OPD}=52.42$ ) coming from the 4 healthy samples (considered as a blank sample) was alternatively used. This ended in some values being negatives due to all the OPD signals being higher than the background. These values were not included in **Figure 5.24C** as they were not possible to interpolate. In both cases, sepsis samples showed many discrepancies as most

of them did not match the concentration determined with the commercial kit.

These results confirm the necessity to improve the assay and to remove any variability in the background coming from different plasma samples, in order to ensure a more reliable analysis. As some of the samples from sepsis patients show really high concentrations, a higher dilution of the plasma could also be possible, without falling out of the working range, which in turn would allow minimizing the plasma effect on the assay. These aspects remain as potential experiments to be performed in the future in case the calibration curve can be improved. Nevertheless, although this improvement should be addressed, the limitation of the inherent sensitivity offered by the POC biosensor should also be solved to fully exploit the potential of the device for biosensing.

## 5.6 Conclusions

In this chapter we have attempted the development of direct label-free assays with the novel POC biosensor device for the detection of three sepsis biomarkers; CRP, IL-6 and PCT. Successful quantification of CRP and IL-6 in PBS buffer was done. The LoD achieved was 18  $\mu\text{g/mL}$  for CRP and 88  $\mu\text{g/mL}$  for IL-6. These results are promising especially for CRP because it fits within the clinical range of sepsis diagnosis. Unfortunately, the sensitivity achieved for IL-6 is far from clinical relevance. Besides this, some proof-of-concept multiplexing test were done with IL-6 and CRP. PCT detection was not achieved as the response given by the protein binding had poor sensitivity and non-consistent reproducibility. We believe that the sensitivity offered by the POC biosensor has a main role in these results. The inherent optical resolution of the optical device in this current configuration ( $5 \cdot 10^{-4}$  RIU) has a strong impact on the resultant LoD, and this requires further reconsideration and optimization of the optical components. Besides, the differences in molecular weight of the different protein biomarkers also have an impact because the lower mass the lower refractive index change, thus, less signal and sensitivity.

Also, protein quantification in plasma was studied. Only CRP was possible to be quantified as IL-6 assay did not reach an acceptable sensitivity. So far the detection has been done in diluted plasma and with low accuracy.

The non-specific binding produced by the plasma is still a challenge. Despite this, clinical validation of the technique was done with real patient samples. Quantification of CRP in the samples provided was not successful as there was very high variability on the plasma from patient to patient which ended in very different non-specific bindings which was not compatible with the way the calibration curve was established.

Overall, the results proved the feasibility of using the novel POC biosensor to quantify protein biomarkers in a label-free and direct format. These results are very promising but in order to achieve a more reliable quantification there are still some parameters to improve such as a more anti-fouling surfaces or adding additives to the PBS buffer diluting the plasma to reduce the non-specific binding or to dilute more the plasma. The current stage of the assays does not allow a reliable analysis of CRP levels in septic patients but they open the door for future optimization of the POC device and their prospective applications.

# Chapter 6

## Evaluation of Bacteria Biomarkers for Sepsis diagnosis

In this Chapter we summarize the results obtained for the detection and quantification with the POC of the bacteria *E. coli* and *P. aeruginosa*, which are two of the more prevalent bacteria found in sepsis patients. We detail the detection protocol in buffered solutions, diluted plasma and finally real patients samples. Multiplexed detection of both bacteria has been also explored in buffered conditions and with real samples.





## 6. Evaluation of Bacteria Biomarkers for Sepsis diagnosis

### 6.1 Introduction

Detection of the etiological infectious agent is also an interesting approach for the diagnosis of sepsis. Around 90% of infections are caused by bacteria (being the rest caused by viruses, fungus or other parasites) and the most commonly related to sepsis are *P. aeruginosa* and *E. coli*. Therefore, the detection of both bacteria was attempted.

The effective testing of bacteria requires meeting a number of challenging criteria. Time and sensitivity of analysis are the most important limitations related to the usefulness of microbiological testing. Bacterial detection methods have to be rapid and very sensitive since the presence of even a single pathogenic organism in the body or food may be an infectious dose. Extremely selective detection methodologies are required because low numbers of pathogenic bacteria are often present in a complex biological environment along with many other non-pathogenic organisms.<sup>10</sup>

As stated in Chapter 1, antibodies are very selective to certain antigens. This may be an advantage, for instance, to detect a common structural antigen present in a larger number of bacteria species. However, this also may be a disadvantage if a more deep taxonomical detection is sought because cross-reactivity may arise. It is important to take into account that, ideally, bacteria should be measured without any sample pre-treatment, thus, by direct detection of the whole-cell. This may challenge the specific detection as finding a specific epitope or antigen which is exclusive to single specie is difficult.

### 6.2 Design, optimization and analytical evaluation of *P. aeruginosa*

Initially, the analysis was focused in a gram-negative bacterium, *P. aeruginosa*. The immobilization of the bioreceptors (antibodies) was also based on the use of Protein G, previously spotted onto the sensor chip. However, some conditions of the immobilization and the detection were

modified with respect to the conditions for protein biomarkers. The same Protein G concentration as in protein biomarker assays was used

A specific anti-*P. aeruginosa* polyclonal antibody (anti-Pae) was selected. The specificity of the antibody was tested in a previous work<sup>185</sup> against *E. coli*, showing negligible cross-reactivity, which made it an ideal option to perform these experiments.

**Figure 6.1** shows the three-step biofunctionalization for anti-Pae. As example, three immobilizations steps of 10 microarrays and real pictures can be seen in **Figure 6.1B**. The immobilization resulted in similar OPD enhancements:  $29.3 \pm 4.25$  (CV=14.5%) for Protein G, then the addition of BSA reduces the overall OPD to  $13.0 \pm 3.15$  (CV=24.2%) and finally addition of the antibody increases up to  $66.2 \pm 6.26$  (CV=9.45%) (see **Figure 6.1A**).

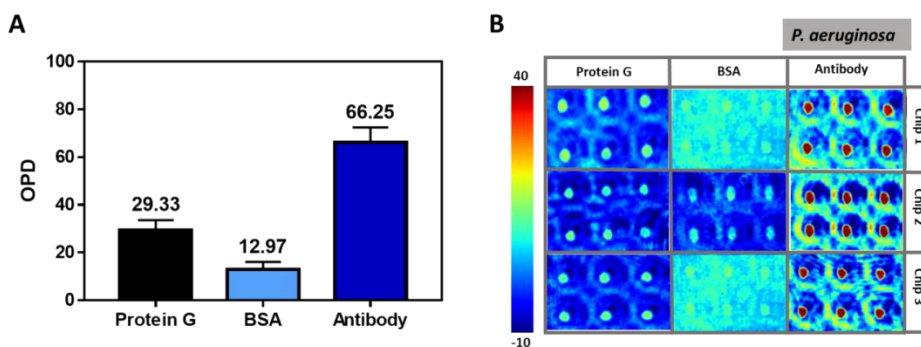


**Figure 6.1:** A: OPD mean values obtained for the three-step anti-Pae immobilization protocol (n=3 chips). B: Representative colour code OPD maps of 2x3 microarrays through the different immobilization steps in three different chips.

Two antibody concentrations were evaluated (250 and 500  $\mu\text{g/mL}$ , see **Figure 6.2A**). This signal is significantly higher than the previous immobilization of antibodies against proteins. Better affinity of Protein G for the antibody may be an explanation for this because the antibodies used in this assay are polyclonal while previously used are monoclonal which may introduce some differences.

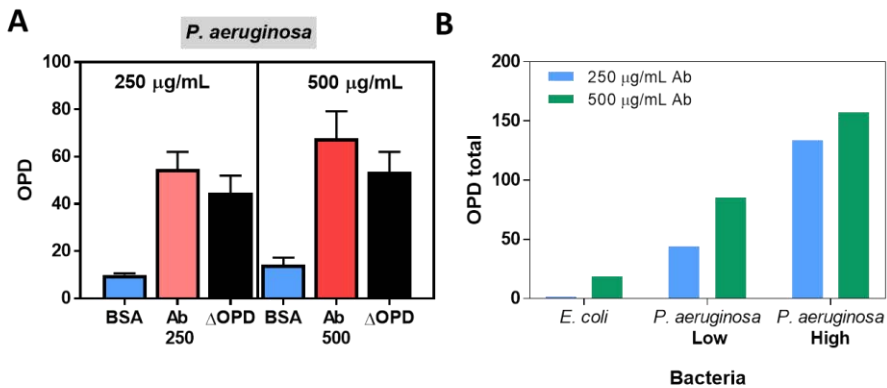


**Figure 6.2:** Antibody immobilization. OPD signals obtained for the immobilization of (A) anti-Pae and B) OPD<sub>total</sub> measured after incubation of both antibody concentrations with two different concentrations of bacteria. Low= 585 cells/mL; High= 5850 cells/mL. [*E. coli*]= 464 cells/mL.

The main goal of the immunoassay is evaluating the lowest possible number of bacteria, ideally between 1 to 10 colony forming units (cfu). To calculate the signal resulting from the binding of bacteria a different approach was considered to overall improve the detectability and the SD. Since bacteria are individual species (discreet entities) the volume of the sample became more critical, especially when gradually decreasing the bacteria concentration (i.e. a concentration of 1000 cfu/mL results in detecting 10 cfu when the sample volume is as low as 10 µL and 500 cfu for a volume of 0.5 mL). In this sense, determining the OPD signal enhancement resultant from averaging an array with several spots (for instance 8x8) is a limitation and can introduce a high variability since at lower concentrations inevitably some spots are not going to have any bacteria captured (see **Figure 6.3** for a representative image).

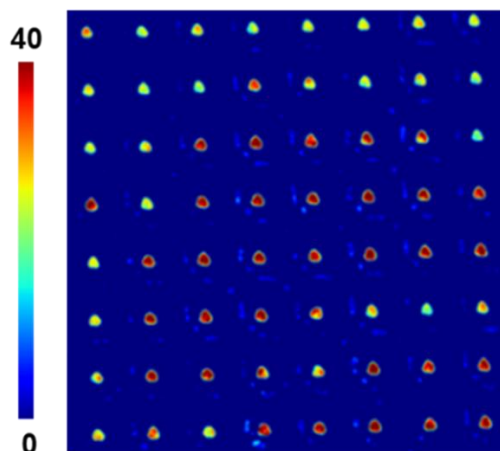


**Figure 6.3:** Colour code OPD map of an 8x8 microarray where a low bacteria concentration has been incubated thus showing the variability of binding from spot-to-spot. From Dey *et al.*<sup>199</sup>

Therefore, in this case we have considered as the detection signal the sum of the  $\Delta OPD$  of each spot individually (considering only the spots with a positive  $\Delta OPD$ ,  $\Delta OPD > 0$ ). This was named:  $OPD_{total}$ , and is expressed with the equation:

$$OPD_{total} = \sum_i^n \Delta OPD_i$$

$$\text{where } \Delta OPD_i = OPD_{sample\ i} - OPD_{antibody\ i}$$

Thus, after applying this calculation to the corresponding signal for the bacteria detection in **Figure 6.2B** also showed higher signals when more antibody was immobilized both for *E.coli* (data not shown) and for *P. aeruginosa*. Two different concentrations of *P. aeruginosa*: 585 cfu/mL (low) and 5850 cfu/mL (high), and 464 cfu/mL *E. coli* were tested for anti-Pae. Nevertheless also a slight recognition of *E.coli* was observed (see **Figure 6.2B**).

At 250  $\mu\text{g/mL}$  antibody concentration, the cross-reactivity was very low (1.10 and 3.35% compared to the low and high *P. aeruginosa* concentrations). This was significantly higher when 500  $\mu\text{g/mL}$  of antibody was present (i.e. 12 and 22.2%). Since bacteria concentrations as high as

≈6000 cells/mL will be hardly seen in an undiagnosed patient (i.e. such concentration will probably have been detected much earlier due to other physical symptoms) we considered this level of cross-reactivity for the high-concentration of antibody would be acceptable and we therefore selected 500 µg/mL .

With these conditions, a calibration curve in PBS was generated after analysing several bacteria concentrations in triplicates (**Figure 6.4A**). The results fitted accurately to an allometric curve with  $R^2 = 0.9226$ ). A wide dynamic range was achieved, from  $10^2$  to  $10^5$  cells/mL. The incubation volume employed was 10 µL, thus, our theoretical LoD is 100 cells/mL, as the minimum concentration that can be used to have at least one single bacterial cell. However, experimentally, the minimum concentration of *P. aeruginosa* which resulted in a significant signal (average  $OPD_{total}$  value = 28) was 146 cells/mL (i.e. 1.5 cells in 10 µL, which can be rounded to 2 cells for a 10 µL sample or 200 cells/mL).

Later, we tested the accuracy of the curve by measuring several blind samples (**Figure 6.4B**) and we found that the slope was 0.9993. Based on this value we can assure that the assay can provide high accuracy in the analysis of sample.

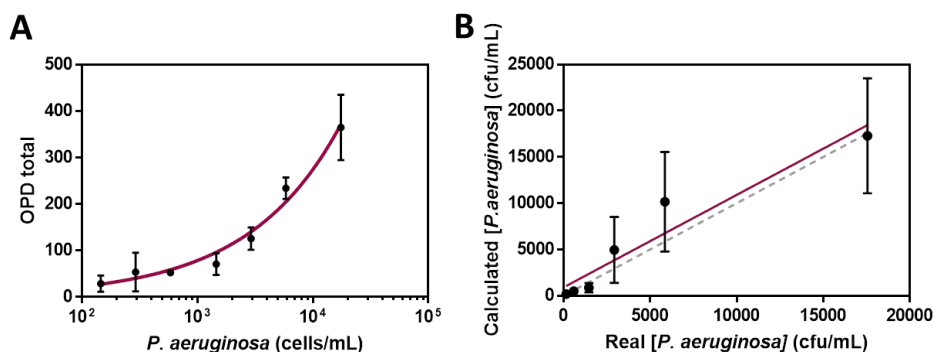


**Figure 6.4:** A: Calibration curve of *P. aeruginosa* in PBS buffer. B: Accuracy study of the immunoassay. The plot shows the correlation between the real value of spiked blind samples and the calculated concentration. Data shows the average of three replicates. Dotted line corresponds to a perfect correlation (slope=1).

### 6.3 *E. coli* detection and quantification with the POC

An immunoassay for the detection of *E. coli* was also developed in our research group for further demonstration of the multiplexing capabilities of the device. **Figure 6.5** shows the three-step biofunctionalization for *E. coli* antibody (anti-Ec). Three representative pictures of an 8x8 microarray are shown through all the steps. Similar OPD signals were achieved for Protein G and BSA in *P. aeruginosa*. The results showed an anti-Ec OPD signal immobilization of  $75 \pm 8.5$  units. This signal is also higher compared to the ones achieved for protein antibodies. This supports the explanation of Protein G having better affinity for polyclonal antibodies. This supports the explanation of Protein G having better affinity for polyclonal antibodies.

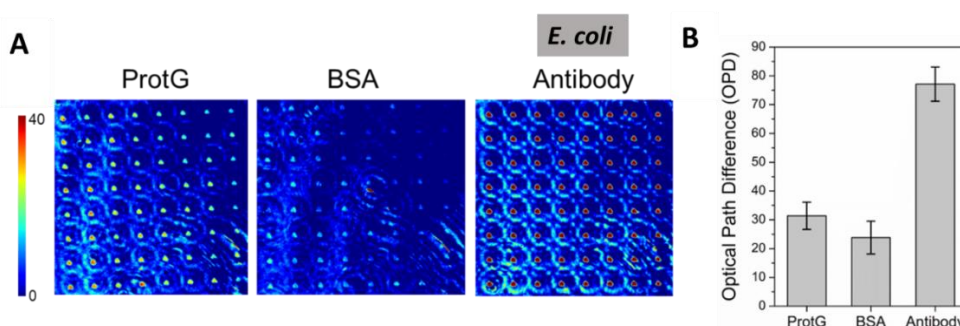


**Figure 6.5:** A: Colour code OPD maps of an 8x8 microarray of the different immobilization steps of anti-Ec specific for *E. coli*. B: The plot shows the OPD numerical values. From Dey et al.<sup>199</sup>

After this, a calibration curve for *E. coli* in PBS buffer with a wide dynamic range of several log orders ( $10^2$  to  $10^6$ ) was obtained with 10  $\mu$ L sample volume (**Figure 6.6A**). Also, accurate fitting was achieved ( $R^2=0.9226$ ). As commented above, the volume of the sample is a key factor for calculating the LoD of the assay. When measuring 150  $\mu$ L of a sample with a concentration of 8 cfu/mL (which correlates to 1 cfu) a significant  $OPD_{total}$  signal could be observed as shown in **Figure 6.6B**. Besides this, correlation of the curve was tested with spiked blind samples and the method showed high accuracy ( $R^2= 0.9841$ , see **Figure 6.6C**)

These results (similarly to what we observed with *P. aeruginosa*) are very promising because they demonstrate that it is feasible to successfully detect only one bacterial cell present in the employed detection volume.

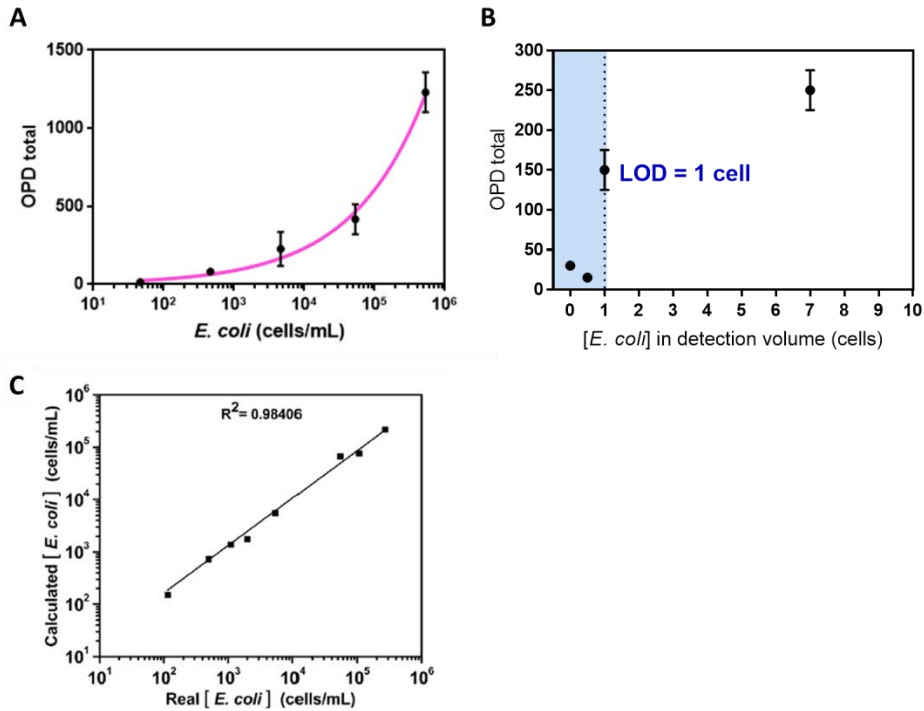


**Figure 6.6:** A: Calibration curve for *E.coli* bacteria detection in PBS buffer B: Plot indicating the experimental LoD in terms of cells in a constant detection volume of 150  $\mu\text{L}$ . C: Correlation plot with spiked samples. From <sup>199</sup>

In addition, evaluation of the specificity of this assay was done as can be seen in **Figure 6.7**. Cross-reactivity against *B. cereus* (a gram-positive bacteria) was tested. For a similar concentration of bacteria (*E. coli* and *B. cereus*), the signal ( $\text{OPD}_{\text{total}}$ ) was much lower for *B. cereus* ( $\text{OPD}_{\text{total}} = 18.9$ ) compared to *E. coli* ( $\text{OPD}_{\text{total}} = 91.1$ ) (blue and purple curves in **Figure 6.7**). ELISA experiments confirmed this signal came from the slight cross-reactivity of the antibody for this bacterium. As *B. cereus* is not a sepsis causing primary bacterium, this slight signal should not be a major problem. Moreover, an ELISA test against *P. aeruginosa* was also done (data not included). Both antibodies (anti-Pae and anti-Ec) showed certain cross-reactivity but the unspecific signal is significantly lower than the specific one (20% of cross-reactivity).



This showed a much lower cross-reactivity with these specific antibodies, even at higher bacteria concentration. On the other hand, when a non-specific antibody was immobilized (**Figure 6.7**, yellow sequence) or no antibody was present (i.e. only Protein G) (**Figure 6.7**, green sequence), the OPD<sub>total</sub> after incubation with bacteria showed no increase, compatible with the absence of bacteria binding. According to these results, we could conclude that the assay is specific for *E. coli* and that the bacteria only bind to the sensor chip when the anti- *E. coli* antibody is present.

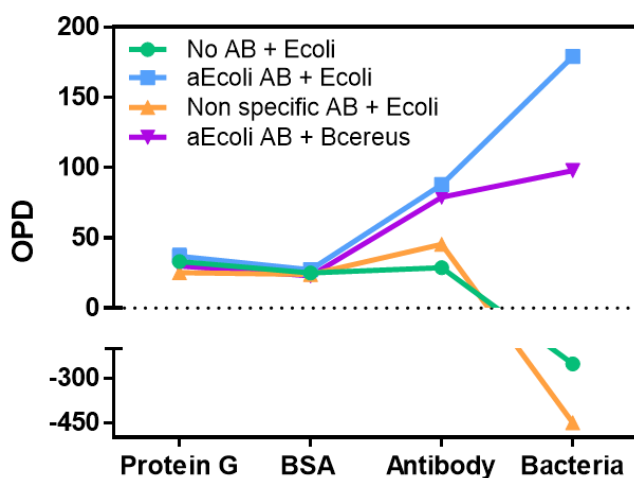


**Figure 6.7:** Specificity tests for *E. coli* assay. The graph shows the OPD values obtained in the successive steps. Green sequence: no antibody immobilized, *E. coli* detection (463 cells/mL in PBS); blue sequence: specific antibody immobilized, *E. coli* detection (463 cells/mL in PBS); yellow sequence: non-specific control antibody immobilized, *E. coli* detection (463 cells/mL in PBS); purple sequence: specific antibody immobilized, control non-specific bacteria (*B. cereus*) detection (590 cells/mL in PBS). From <sup>199</sup>

### 6.3.1 Multiplexed measurements of *P. aeruginosa* and *E. coli* in buffer

The detection of both bacteria was explored in PBS buffer, preparing anti-Ec and anti-Pae microarrays in the same chip (four arrays, two with anti *E. coli* antibodies and the two with anti *P. aeruginosa* antibodies (see **Figures 6.8A** and **6.9A** for illustrative schemes). First, both bacteria were individually incubated with the whole chip, in such way that they would be in contact with specific and non-specific arrays (**Figure 6.8A**). In **Figure 6.8B,C** we

can observe the  $OPD_{total}$  obtained after incubating two different bacteria concentrations (500 and 4000 cells/mL in PBS). Microarrays that were incubated with their specific bacteria showed larger  $OPD_{total}$  signal than when they were incubated with the non-specific bacteria.

This confirmed that the specificity test previously performed for the *P. aeruginosa* assay (summarized in **Figure 6.2B**) was specific for the bacteria, but also showing some cross-reactivity against *E. coli*. If we compare with **Figure 6.2B**, again the cross-signal observed was higher for the lowest bacteria concentration (27.81 and 13.78% for *E. coli* and *P. aeruginosa* at 500 cells/mL) compared to the values obtained for the largest concentration (0.47 and 3.13 for *E. coli* and *P. aeruginosa* at 4000 cells/mL). This reinforces the idea that the antibodies have certain avidity for the non-specific bacteria, but this cross-reactivity becomes less critical when having large concentrations of the specific ones.

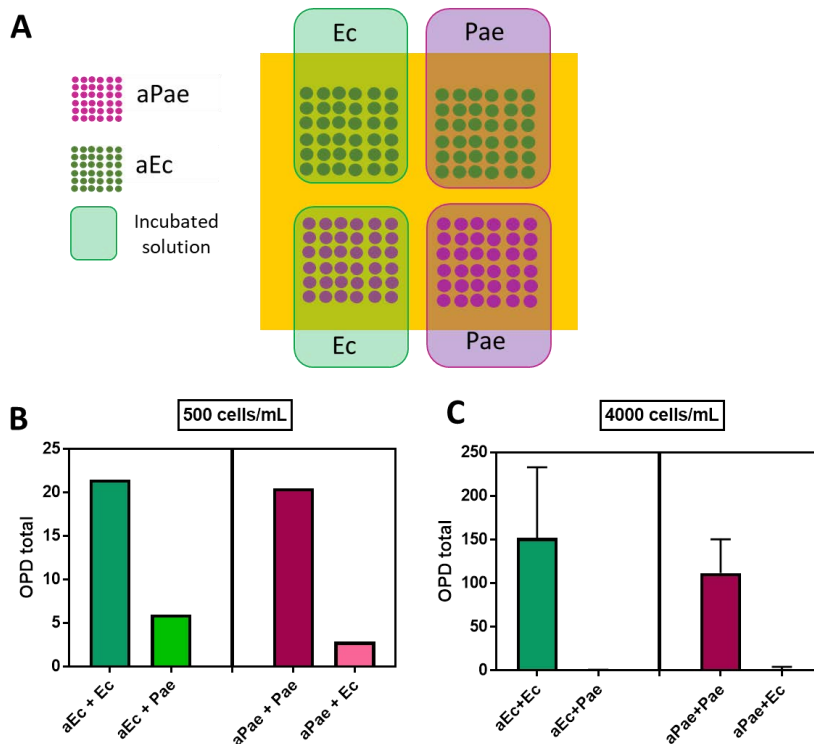


**Figure 6.8:** A: Array design for multiplexed *E. coli* and *P. aeruginosa* detection. Results obtained for B: 500 cells/mL and C:) 4000 cells/mL. anti-Ec: anti *E. coli* antibody. Ec: *E. coli*. anti-Pae: anti *P. aeruginosa* antibody. Pae: *P. aeruginosa*

Then, the effect of incubating both bacteria at the same time on the same solution was explored as this may be valuable for the proper identification of the infectious agent when sepsis is produced by multiple bacteria. To address this, a different design was done (see **Figure 6.9A**). Two microarrays with each type of antibody (four in total) were created. In this case, a mixture of both bacteria (called mix) or a solution with only one type of bacteria (which is incubated over specific antibodies) were incubated. This was tested at two different concentrations, 750 and 4000 cells/mL and the results can be seen in **Figure 6.9BC**.

Similar  $OPD_{total}$  values were achieved for the bacteria being incubated mixed and individually. The concentration of 750 cells/mL resulted in very similar  $OPD_{total}$  signals when incubated both individually and mixed. Also, larger concentrations (i.e. 4000 cells/mL) showed similar results for *P. aeruginosa*. The mixed incubation over anti-Pae gave slightly higher signal compared to single incubation but the SD of that assay was very high.

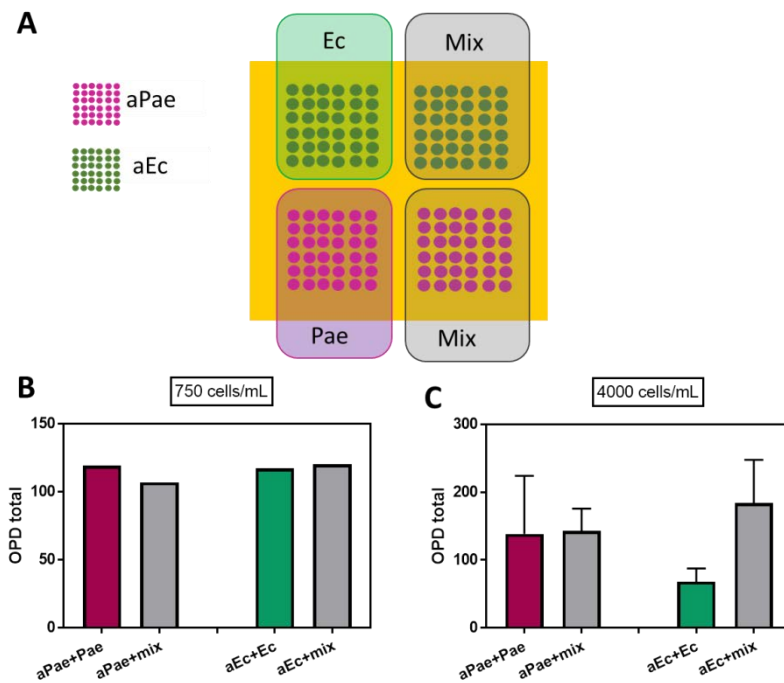


**Figure 6.9:** **A:** Array design for multiplexed *E. coli* and *P. aeruginosa* bacteria biosensing. Incubation of both bacteria alone and mixed in PBS buffer. Results obtained for **(B)** 750 cells/mL and **(C)** 4000 cells/mL. anti-Ec: anti *E. coli* antibody. Ec: *E. coli*. anti-Pae: anti *P. aeruginosa* antibody. Pae: *P. aeruginosa*. Mix: both bacteria.

## 6.4 Analysis of *P. aeruginosa* and *E. coli* in blood plasma

The effect of plasma in the assay features was also evaluated. Although undiluted plasma should be the preferred option in any clinical point-of-care diagnosis, also in this case, a significant enhancement of the  $OPD_{total}$  was observed with whole plasma (such as with protein biomarkers), which was indicative of non-specific binding of the substances present in the fluid, therefore hindering the specific signal coming from bacteria detection. Thus, a dilution step was employed to minimize this effect. Plasma diluted at 25% and 50% showed less background signal than whole plasma.

We tested *E. coli* under these conditions and we found that the bacterium was still recognized by the immobilized antibodies as can be seen in **Figure 6.10A**. Dilution at 25% showed better detectability than 50% diluted plasma. Moreover, the detectability was later improved by the addition of the surfactant Tween 20 at 0.1% in PBS (i.e. PBST). **Figure 6.10B** shows that the detection signal for a given bacteria concentration in plasma diluted in PBST is higher than the one diluted in only PBS.

These conditions were transferred to the *P. aeruginosa* assay. A calibration curve was generated with this plasma dilution as it is shown in **Figure 6.11A** ( $R^2 = 0.9182$ ). Upon incubation with 25% diluted plasma we observed that the average background  $OPD_{total}$  signal obtained is  $254 \pm 97.3$ .

As discussed before, the incubation volume (10  $\mu$ L) limits the theoretical LoD. So, to detect 1 bacterial cell in this volume (1 cell in 10  $\mu$ L, which is 100 cells/mL), implies a plasma concentration of 400 cells/mL (i.e a 1/4 dilution is necessary to have a 25% diluted plasma compatible with the assay). In our case, the minimum concentration measured experimentally in diluted plasma was 146 cells/mL (i.e. 1.46 cells in 10  $\mu$ L), which resulted in a significant  $OPD_{total}$  increase of  $300.5 \pm 21.2$ . This represents an experimental LoD of 584 cells/mL in 100% plasma.

As in the previous assays several blind samples were analysed to evaluate the accuracy (**Figure 6.11B**). The calculated concentration was found by removing the average background signal from the  $OPD_{total}$  signal obtained before interpolating from the calibration curve. As seen in **Figure 6.11B**, the correlation plot shows a good fitting (i.e. a slope of 0.9401) as well as the one obtained in pure buffer.

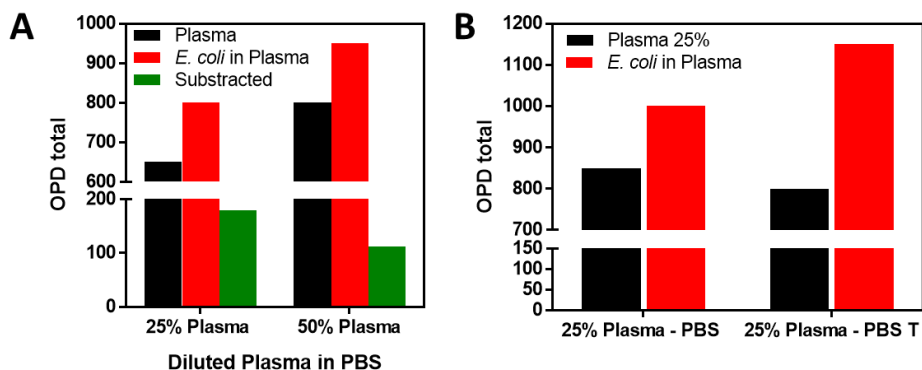


**Figure 6.10:** A: Effect of plasma dilution on the non-specific binding and *E. coli* detection. B: Effect of the buffer (PBS and PBST) used for diluting the plasma on the non-specific binding and *E. coli* detection. From Dey et al.<sup>199</sup>

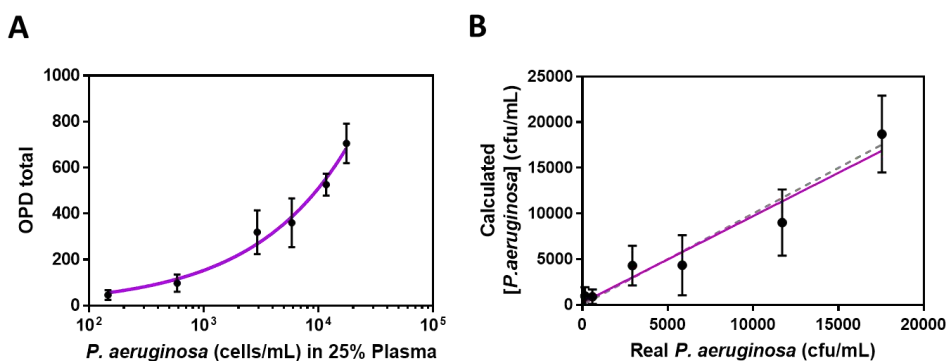


**Figure 6.11:** A: Calibration curve of *P. aeruginosa* in diluted plasma 25% in PBST. Background signal produced by 25% diluted plasma has been subtracted. B: Correlation plot of real and calculated concentrations of blind spiked bacteria samples. Dotted line corresponds to a perfect correlation (slope=1).

*E. coli* assay in plasma also showed good results. The calibration curve obtained in plasma (i.e. 25% diluted plasma in PBST) is shown in **Figure 6.12**. As with *P. aeruginosa*, a good fitting was achieved ( $R^2 = 0.9881$ ) and a wide dynamic range was found. Moreover, a LoD of 1 bacterial cell in diluted plasma (with PBST) corresponding to 4 bacteria cells (400 cells/mL) in undiluted plasma (100% plasma) was achieved.<sup>199</sup> However, in this case, the average background  $OPD_{total}$  signal obtained was  $365.6 \pm 93.3$ . This

slightly higher than the background value observed in the *P. aeruginosa* chips but still acceptable as the SD is around 100.

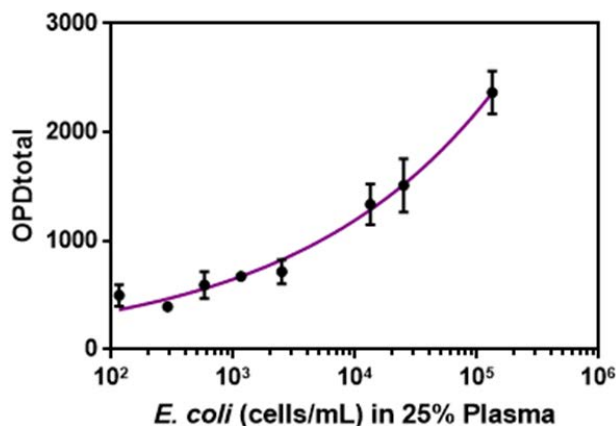


**Figure 6.12:** Calibration curve in plasma diluted at 25% in PBST (with background produced by plasma 25% subtracted).

As a summary, both bacteria have been detected with high sensitivity and achieving very good LoDs both in PBS buffer and diluted plasma. Bacteria are microorganisms with a size of around 1-2  $\mu\text{m}$ . Upon binding to the anti-Pae or anti-Ec, the RI change produced is higher, thus, leading to larger OPD signals changes which lead to better sensitivity.

## 6.5 Validation with Clinical Plasma samples

As all these assays were successful, corroboration and validation with real samples coming from the Sepsis Biobank located at Vall D’Hebron Hospital (Barcelona, Spain) was done. Plasma samples collected from healthy donors and patients admitted in the hospital for SIRS and sepsis category were measured.

In the case of *P. aeruginosa* detection, two sets of samples were provided by the Vall D’Hebron Hospital from the Blood and Tissues Biobank: 4 from healthy patients and 4 from septic patients whose blood culture was positive to *P. aeruginosa* (see **Table 6.1**). The bacteria were identified by cell culture, however, the exact concentration of bacteria (cells/mL) was not known.

**Table 6.1:** List of the patient samples provided by Vall D'hebron for testing *P. aeruginosa*.

	Healthy	Sepsis
Sample	BSTC123	BSEP286
	BSTC124	BSEP407
	BSTC30	BSEP686
	BSTC40	BSEP767

All the samples were diluted (1:3) with PBST to obtain 25% plasma and incubated for 30 min on chips with anti-Pae microarrays. The samples were analysed twice. In order to move closer the device to the clinical settings, the device was placed in the hospital where the samples were stored to perform the analysis. The  $OPD_{total}$  signals measured for each sample were plotted (**Figure 6.13A**) and we observed that there is a clear difference between healthy and sepsis samples, being the latter ones significantly higher than the former. Then, each value was interpolated from the curve in 25% plasma to infer the real bacteria concentration (see **Figure 6.13B** to see final concentration in plasma 100%). As it is not possible to remove the average background because it may vary from sample to sample, we did the interpolation in the curve (**Figure 6.11A**) with the background signal from the diluted plasma included.

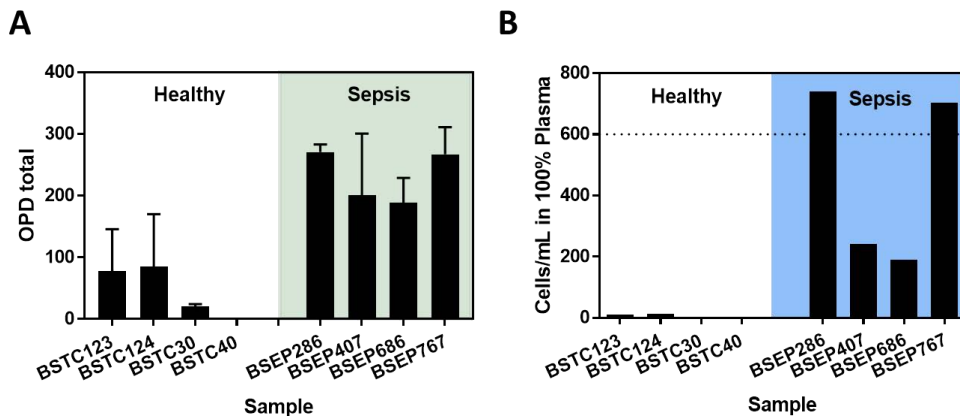


**Figure 6.13:** Clinical evaluation of real patient samples. A:  $OPD_{total}$  values measured for the eight samples (four for healthy individuals and four for sepsis patients positive to *P. aeruginosa*). B: Calculated concentrations from healthy and sepsis patients at the clinical setting. The concentration refers to undiluted 100% plasma.

These results confirm the assay can be used to discriminate healthy and sepsis samples. Nevertheless, **Figure 6.12B** shows that two of the samples (BSEP286 and BSEP767) contain bacteria above the LoD of the assay (600 cells/mL), thus, only those two can be considered properly discriminated. Despite this, the  $OPD_{total}$  signal from healthy samples is very low compared to the signals achieved in sepsis samples.

Besides this, we cannot be sure about the accuracy of the analyses, as the real exact concentration was not quantified by any other conventional method. In addition, as seen in the case of CRP quantification in real samples, there might be some variability due to the different characteristics of the plasma from different individuals. As it was seen in **Figure 5.25** there is high variability in the plasma features among the samples which reflects the differences in the plasma composition and also affects optical properties such as the refractive index which has a big impact in the OPD calculation. We must acknowledge that sample variability from patient-to patient is a factor unresolved which inevitably may affect the accurate quantification.

Similar results were seen with clinical samples containing *E. coli*. Vall D'Hebron selected three sets of samples (**Table 6.2**): healthy, SIRS and septic patients (*E. coli* positive). In this case, the samples provided had been characterized (i.e. bacteria identification) using two different methods: Blood culture and IRIDICA ID test. The IRIDICA platform detects the bacteria present in whole blood. To do so, it first makes a lysis of the clinical sample which is followed by a DNA extraction. These DNA samples were used to carry out a specific PCR (16 wells per sample) to amplify different amplicons in a 96-well plate. Afterwards, this plate was analyzed by means of Mass Spectrometry by calculating the mass of the specific amplicons. By comparing with a data base, there was a correlation of the molecular weight calculated from the amplicons of the sample with the deduced sequences amplified (attaining the nucleotide composition). Depending on the combination of the amplicons amplified and through specific algorithms, IRIDICA provided an ID for each samples. According to the products identified, which could discriminate to the species levels, it could be possible to get a single ID or a multiple ID.



**Table 6.2:** List of the patient samples provided by Vall D'hebron for testing *E. coli*.

	Pathogen Identification		
	Biobank Code	Blood culture	IRIDICA ID
<b>Healthy</b>	BSTC1234	---	---
	BSTC124	---	---
	BSTC43	---	---
<b>SIRS</b>	BSIRS89	---	---
	BSRS35	---	---
	BSIRS40	---	---
	BSIRS78	---	---
<b>Sepsis</b>	BSEP51	BC negative	<i>E. coli</i>
	BSEP68	<i>E. coli</i>	<i>E. coli/Corynebacterium striatum</i>
	BSEP106	<i>E. coli</i>	<i>E. coli</i>
	BSEP195	BC negative	<i>E. coli/Klebsiella pneumoniae</i>
	BSEP276	BC negative	Not performed
	BSEP48	<i>E. coli</i>	<i>E. coli</i>
	BSEP61	<i>E. coli</i>	<i>E. coli</i>
	BSEP342	BC neg	<i>E. coli</i>
	BSEP250	<i>E. coli</i>	<i>E. coli</i>

As before, all the samples were diluted (1:3) with PBST to obtain 25% plasma and incubated for 30 min on chips with anti-Ec microarrays. The samples were analysed twice and the results were plotted (**Figure 6.14A**). This time, all the samples that contained bacteria (i.e. septic samples) showed concentration values above the LoD of the assay (black columns).

The OPD<sub>total</sub> signals measured for each sample were plotted (**Figure 6.13A**) and we observed that there is a clear difference between healthy and sepsis samples, being the latter ones significantly higher than the former. The four samples belonging to SIRS patients also showed levels below the LoD. These results, for *E. coli* and *P. aeruginosa* show the great potential of the POC biosensor for determining the presence of bacteria in blood samples.

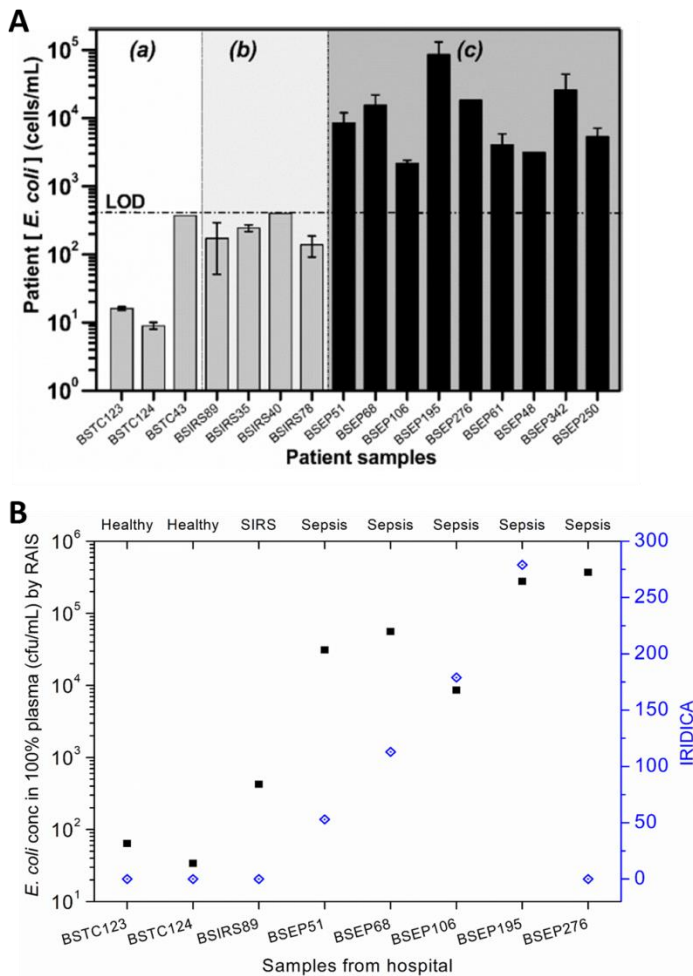


**Figure 6.14:** Clinical evaluation of real patient samples. A:  $OPD_{total}$  values measured for the samples (three for healthy individuals, four for SIRS patients and nine for sepsis patients positive to *E.coli*). From<sup>199</sup>. B: Comparison of the concentrations measured by the POC biosensor and by the IRIDICA ID test.

Moreover, an approximate concentration can be estimated with the IRIDICA ID technique. A comparison between the values measured with the POC biosensor and IRIDICA is included in **Figure 6.14B**. We can observe that the values are similar.

Nevertheless, it is important to mention that despite achieving values below the LoD in healthy and SIRS samples for both *E.coli* and *P. aeruginosa*, the values are still high, as no bacteria is supposed to be present in those samples (i.e. 0 cell/mL). As well as, according to the clinical partner

in the project, the concentrations measured are very high.

It is worth to mention that we have worked with aliquoted frozen bacteria to build the curves and the patient samples were also stored frozen at -80°C. It might be possible that after thawing, some bacteria suffered certain lysis. According to the commercial source, the immunogen used to produce the antibodies consisted of a mixture of intact and lysed (denatured) bacteria. Therefore, it is likely that the antibody is able to detect both viable bacteria (which can grow in the appropriate media, such as in blood culture) and nonviable bacteria (dead, lysed, etc., which remain undetected in blood culture).

Finally, in order to mimic a simple multiplexed experiment, chips arrayed with both anti *P. aeruginosa* and anti *E. coli* antibodies were prepared and the previous samples (together with real plasma sample from patients with *E. coli* infections) were analysed. Moreover, a sample with both bacteria and *Streptococcus constellatus* (BSEP406) was also selected. The sample names are summarised in **Table 6.3**.

**Table 6.3:** Summary of the patient samples provided by Vall D’hebron Hospital

	<i>E. coli</i>	<i>P. aeruginosa</i>	<i>E.coli + P.aeruginosa + S. constellatus</i>
<b>Sample name</b>	BSEP68	BSEP286	
	BSEP106	BSEP407	
	BSEP134	BSEP686	BSEP406
	BSEP274	BSEP767	

**Figure 6.15A** summarises the chips prepared and as can be seen each sample was incubated with both antibodies. Sample containing both bacteria (BSEP406) was incubated twice as depicted in **Figure 6.15B**. The results achieved are summarised in **Figure 6.15C**. All the measurements resulted in signals and concentrations above the LoD which again confirms that the method can discriminate samples containing bacteria from bacteria-free samples. However, the microarrays that were incubated against the non-specific bacteria also showed values above the LoD. Thus, the assay resulted unspecific as we were not able to discriminate if the signal is produced by

one or the other bacteria. The sample BSEP406 showed presence of both bacteria. However, as discussed above, it is not possible to quantify the contribution to the signal from *E.coli* or *P. aeruginosa*. Moreover, the presence of a third bacterium (*S. constellatus*) might also have an effect on the signal as these bacteria have not been individually tested against both *E. coli* and *P. aeruginosa* antibodies.

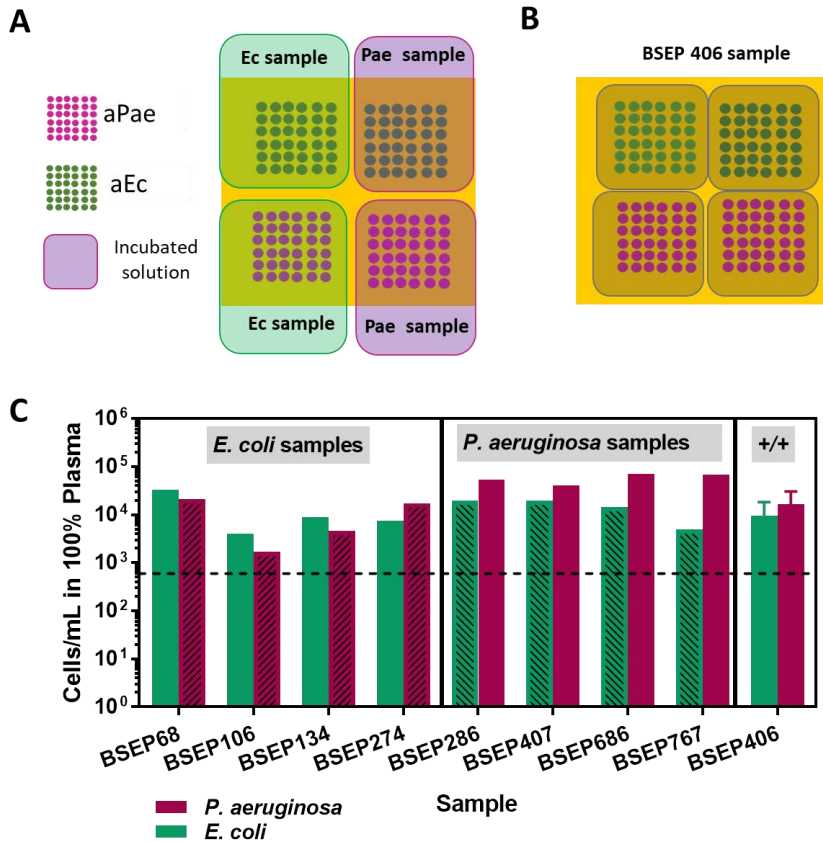


**Figure 6.15:** A: Scheme of the incubation of the samples containing *E. coli* or *P. aeruginosa*. B: Scheme of the incubation of BSEP406 sample, which contains both bacteria. C: Calculated concentrations from sepsis samples containing *E. coli* or *P. aeruginosa*. The concentration refers to undiluted 100% plasma. Horizontal dotted line at 600 cells/mL indicates de LoD in plasma 100%. Patterned columns correspond to non-specific signal produced by the non-specific bacteria over the antibody.

As a summary, the assay above described can discriminate healthy from sepsis samples; however, it is not able to identify the bacteria that produce the infection (at least it cannot differentiate *E. coli* or *P. aeruginosa* with the antibodies used so far). Finding more specific receptors may easily

solve this problem in the future. Besides this, the non-specific binding effect may also play a key role on preventing proper identification. Despite a quantitative test is the best option a qualitative result might also be useful, as conventional bacterial culture exemplifies.

Multiplexed measurements in plasma showed uneven outputs when patient samples were analysed. These results reinforce the fact that a more in depth study should be done to assess the reasons behind the loss of specificity when using diluted plasma. In addition, this study has been conducted with only two types of bacteria and in the future, ideally, this must be done with more bacteria, so cross-reactivity among antibodies must be reviewed in all cases to determine the specificity capability of the assay. Other options to improve the specificity of the assay may be changing the bioreceptor by others available such as aptamers or targeting other biomarkers. Nevertheless, it is mandatory to solve the issue of the non-specific binding produced by plasma as it introduces a lot of variability. This effect varies significantly from sample to sample and increases the RI significantly which ends in higher OPD which do not correspond with the real value.

Taking into account all these factors, it can be concluded that the assay can discriminate healthy from sepsis patients. Although further efforts must be done towards establishing a more accurate analysis conditions and better predicting the effect of plasma variability before implementing such POC device in out-of-the-lab environments, in such a way more reliable results can be obtained to ensure accurate infection diagnosis.

## 6.6 Conclusions

We have shown a method to directly detect and quantify whole bacteria under label-free conditions. *Pseudomonas aeruginosa* and *Escherichia coli* were tested, both in buffer solutions and diluted plasma. The LoDs achieved were 200 cells/mL in PBS buffer and 600 cells/mL in 25% diluted plasma for *P. aeruginosa*, and 8 cells/mL in buffer and 400 cells/mL in 25% diluted plasma for *E. coli*. Besides, we applied both immunoassays (*P. aeruginosa* and *E. coli*) at the same time on the same chip to study the multiplexing capabilities of the method. Finally, the assays were validated with real clinical samples showing good results as both were able to discriminate

between healthy and sepsis (i.e. presence of bacteria) samples. Nevertheless, upon multiplexed measurement of clinical samples the assay showed cross-reactivity which complicated the bacterial identification. We believe that this cross-reactivity is produced mainly due to the antibodies may not be highly specific but also because the signals may be hindered by the unresolved non-specific binding produced by plasma. Therefore, we can conclude that the assay can be used as a qualitative method.

Overall, our approach offers an assay which takes place in only 30 min and in label-free conditions, with good LoD (1 cell and 2 cells for *E. coli* and *P. aeruginosa*, respectively). This improves previous results found in the literature<sup>18,200,201</sup>, where bacteria quantification with biosensors commonly take longer times or need labelling or long sample pre-treatments. We have tested this method with plasma samples but we believe that despite quantification in blood still needs improvement this technology can be currently applied to less complex samples such as waters, urine or saliva. Conventional methods to detect and identify bacteria typically have long processing times, which lack sensitivity and specificity, requiring specialized equipment and trained users, which, in overall, is a costly procedure that is not available in all countries.

Finally, this test is fast (30 min incubation + 1 min readout) so when the POC will be ready to be used in hospitals the physicians will easily and rapidly find if their patient has or not a blood infection thus enabling the early start of the antibiotic therapy.



## General Conclusions and Future Perspectives

The work described in this Doctoral Thesis demonstrates the potential of a recently developed nanophotonic microarray point-of-care biosensor for its use as a clinical diagnosis tool. The combination of the novel LIM technology in a POC format together with nanoplasmonic structures and microarray distribution of bioreceptors creates a unique combination that can be used to study a wide number of biomarkers which allows multiplex detection and quantification. To successfully achieve this system, a multidisciplinary study was needed in the fields of microarray fabrication, surface chemistry and biochemistry combined with an in depth study of the novel optical platform and the custom designed nanoplasmonic sensing structures.

Its multiplex capability was assessed taking sepsis as a representative complex disease process, whose diagnosis remains challenging and requires tracking of different biomarkers. Direct detection assays for protein biomarkers (with different molecular weight) and bacteria were studied to assess the performance of such device for biosensing in terms of sensitivity and specificity in an individual and multiplexed format. Moreover, the analysis of clinical samples has further demonstrated the limits of the proposed technology and also the methodology for their implementation in the biomedical and clinical field.

The main general conclusions that can be drawn from the work done during this thesis are the following:

- The novel LIM technology had been previously demonstrated as potentially useful for inorganic layers thickness measurement and monitoring of current changes. Some preliminary studies shown its capability for the detection of protein mono- and bilayer. We have gone forward to fully characterize its potential and explored its application as a microarrays reader for biosensing purposes. The use of custom-designed nanoplasmonic structures offers a significant improvement in the sensitivity of the device (a 10-fold approximately). Several solutions with different refractive indexes showed that the final measured signal is significantly affected by the



RI of the measuring media. Dry conditions (i.e. air as measuring medium) allowed better sensitivity, thus, drying after incubation of target analyte was chosen.

- As the working surface must allow transmission of the coupled LED light, several biofunctionalization strategies were developed for different transmitting working surfaces: glass, thin gold layers and custom-designed nanoplasmonic chips. Different biofunctionalization strategies were tested showing higher signals when using the gold NHA nanoplasmonic chips. Adsorption of Protein G, surface blocking with BSA and addition of antibodies was the strategy found optimal in terms of sensitivity and analyte detection. Thus, it was selected for the development of all the assays. This immobilization protocol is direct, simple and easy. Besides, it introduces orientation in antibodies and allows detecting the analyte in label-free conditions.
- The selected biofunctionalization strategy was applied to the detection of CRP (120 kDa), IL-6 (24 kDa) and PCT (13 kDa), which are relevant biomarkers for sepsis diagnosis. The detection of the proteins was done directly and in label-free conditions. Standardization of the immobilization protocol showed very good reproducibility (i.e. the antibody immobilization step was  $CV \leq 10\%$  for the three proteins).. The limit of detection in buffer conditions was 18  $\mu\text{g/mL}$  for CRP, which fits within the clinical relevant range for sepsis. Conversely, the LoD of IL-6 was 88  $\mu\text{g/mL}$ , which is not adequate for sepsis determination. PCT showed not reproducible detection neither in direct nor sandwich assay. These results demonstrate the large effect that the MW of the analyte has on the sensitivity of the device. This also illustrates that the sensitivity of  $5 \cdot 10^{-4}$  RIU of the novel POC biosensor limits its performance with small analytes.
- The multiplexed capabilities of the POC with the chosen immobilization protocol were explored in a proof-of-concept test. This demonstrated the ability of the POC device for performing 2-analyte tests to quantify protein biomarkers in a label-free and direct format. Besides, this assay design allows to extend to 4 different targets (as four  $8 \times 8$  microarrays fit on a  $1 \text{cm}^2$  nanoplasmonic chip).

- The POC biosensor was employed for evaluating real sepsis samples, thus, protein detection in plasma was explored before. Despite blocking the surface with BSA, evaluation in plasma was very challenging due to the strong interference from non-specific binding. Successful detection in diluted plasma was achieved with CRP but not with IL-6 although the reliability is low due to unresolved non-specific binding of the fluid. The validation with real clinical samples showed that there is high plasma variability from sample to sample which also makes difficult to quantify CRP in plasma. These results currently hinder the application of the POC device for the quantification of CRP levels.
- We have also applied the selected immunoassay to the detection and quantification of two common bacteria causing in sepsis infections: *E. coli* and *P. aeruginosa*. As bacteria cells are large (0.5-2  $\mu\text{m}$ ) compared to proteins, a remarkable better sensitivity was achieved. The LoDs measured were 200 and 600 cells/mL for *P. aeruginosa* in buffer and in 25% diluted plasma, whereas for *E. coli* the LoD was 8 cells/mL in buffer and 400 cells/mL in 25% diluted plasma. These values can be simplified to detection of 1 cell and 2 cells for *E. coli* and *P. aeruginosa*, respectively. This improves significantly previous results found in the literature. Moreover, this methodology has been clinically validated obtaining a reliable discrimination of septic samples and samples coming from healthy individuals. We have also tested the feasibility of multiplex detection. However, quantification was complex due to some cross-reactivity was found on the antibodies.

The protocol followed in these assays show that the time required to analyse one sample is 30 min of incubation plus 1 min of measuring. This reduces significantly the time currently needed in hospitals to assess if a blood sample contains or not bacteria (which is commonly done by blood culture or PCR) or to evaluate the concentration of a particular protein clinical biomarker. The implementation of this POC may drastically improve sepsis diagnosis and later monitoring of the effectivity of the antibiotic treatment in hospital and other clinical scenarios.

Future perspectives to improve these immunoassays are to find other antibody immobilization protocols to allow fitting more antibodies on the nanoplasmonic chips. This is desirable for scalability purposes (i.e. measuring hundreds of biomarkers simultaneously). Also, more robust and controlled biofunctionalization strategies should be re-evaluated in order to achieve a better sensitivity. It would be advisable to avoid adsorption as immobilization method because it commonly introduces variability.

From a technical-optical point of view, the novel POC biosensor may also improve its sensitivity by, for instance, achieving novel algorithms that enhance the measured signal. This may be also applied to the custom-made nanoplasmonic working surface as they are a key point on the measuring procedure. Novel nanostructures with better transmission and signal enhancement should be designed, fabricated and implemented.

Nowadays there are more than 170 possible biomarkers for sepsis. Many efforts are being done in clinical research in order to establish a reliable panel of biomarkers for the detection of Sepsis. In our experiments, the sensor chip surface is  $1\text{ cm}^2$  and the separation between spots is  $250\text{ }\mu\text{m}$ . Therefore, we can place 1.600 spots on one single sensor chip. In the future we foresee that the POC device could have the potential to be applied to other diseases by switching bioreceptors to other specific biomarkers. Also it will be possible to examine other human fluids such as urine or even used it in other fields such as environmental monitoring. In conclusion, this thesis shows the enormous potential of such developed novel nanophotonic POC device for future clinical applications just by specifically designing customized microarrays of bioreceptors for specific disease biomarkers.





## Abbreviations and Acronyms

$\Delta$ OPD	Change in Optical Path Difference
Ab	Antibody
AFM	Atomic Force Microscopy
anti-Ec	antibody against <i>E. coli</i>
anti-Pae	antibody against <i>P. aeruginosa</i>
Au-	Gold Periodically-ordered sub-wavelength nanohole arrays
NHA	
BSA	Bovine Serum Albumin
BSEPS	Sepsis Sample
BSIRS	SIRS samples
BSTC	Sample from <i>Banc de Sang i Teixits de Catalunya</i> (Blood and Tissue Bank)
CCD	charge-coupled camera
CMOS	complementary metal–oxide–semiconductor
CRP	C-reactive protein
CV	Coefficient of Variance
DUVL	Deep Ultra-Violet lithography
Ec	<i>E. coli</i>
EDC	1-ethyl-3(3-dimethylaminopropyl)carbodiimide hydrochloride
ELISA	Enzyme-Linked Immunosorbent Assay
FOV	field-of-view
HEPES	4-(hydroxyethyl)-1-piperazineethanesulfonic acid
HPDP	EZ-Link™ HPDP-Biotin
ICU	Intensive Care Units
IL-6	Interleukin 6
LFM	lens-free microscopes
LIM	large-FOV interferometric microscope
LoD	Limit of detection
MHDA	16-mercaptohexadecanoic acid
MW	Molecular Weight
NA	NeutrAvidin
NHS	N-hydroxysulfosuccinimide
o.n.	overnight
OPD	Optical Path Difference

Pae	<i>P. aeruginosa</i>
PBS	Phosphate Buffered Saline
PBST	Phosphate Buffered Saline with Tween 20
PCR	Polymerase Chain Reaction
PCT	Procalcitonin
POC	point-of-care or nanophonotonic point-of-care biosensor
ProtG	Protein G
RI	Refractive Index
RT	Room Temperature
SA	strptavidin
SAM	Self-assembled monolayer
SD	standard deviation
SIRS	Systemic inflammatory response syndrome
SP	Savart Plates







## List of publications

### Journal articles

#### **Label-free Bacteria Quantification in Blood Plasma by a Bioprinted Microarray Based Interferometric Point-of-Care Device.**

P. Dey, N. Fabri-Faja, O. Calvo-Lozano, R. Terborg, A. Belushkin, F. Yesilkoy, A. Fàbrega, J.C. Ruiz-Rodriguez, R. Ferrer, J.J. González-López, M.C. Estévez, H. Altug, V. Pruneri and L.M. Lechuga  
**2019 ACS Sensors** – 4 (1), 52-60

#### **Early Sepsis Diagnosis via Protein and miRNA Biomarkers using a novel Point-of-Care Photonic Biosensor.**

N. Fabri-Faja, O. Calvo-Lozano, P. Dey, R. A. Terborg, M.-C. Estévez, A. Belushkin, F. Yesilköy, L. Duempelmann, H. Altug, V. Pruneri and L. M. Lechuga  
**2019 Analytica Chimica Acta**

#### **Label-free, scalable and point-of-care imaging platform for rapid analysis of biomarker.**

L. Duempelmann, R.A Terborg, J. Pello, I. Mannelli, F. Yesilkoy, A.A. Belushkin, Y. Jahani, N. Fabri-Faja, P. Dey, O. Calvo-Lozano, M.-C. Estevez, L.M. Lechuga, H. Altug and V. Pruneri.  
Proceed. SPIE **2019**

### Relevant Oral presentations and poster contributions

#### **Rapid detection of sepsis with a point-of care and label free microarray platform - Poster**

N. Fabri-Faja, O. Calvo-Lozano, M.C. Estévez, J. Pello, R. A. Terborg, A. Belushkin, F. Yesilköy, P. Soetaert, M. Rabaey, H. Altug, V. Pruneri and L.M. Lechuga  
**2017 VIII International Congress on Analytical Nanoscience and Nanotechnology** – Barcelona, Spain

#### **RAIS: Scalable, point-of-care and label free microarray platform for rapid detection of Sepsis - WP5: Laboratory Validation – Poster**

N. Fabri-Faja, O. Calvo-Lozano, P. Dey, M.C. Estévez and L.M. Lechuga  
**2017 RAIS open workshop H2020** – Barcelona, Spain

**Use of a microarray reader for the fast, label-free and multiplexed measurement of biomarkers for Sepsis – Oral**

N. Fabri-Faja, R.A. Terborg, F. Yesilköy, O. Calvo, P. Dey, M.C. Estévez, J. Pello, A. Fàbrega, J.C. Ruiz-Rodríguez, A. Belushkin, J. Götzen, P. Soetaert, M. Rabaey, J.J. González-López, H. Altug, V. Pruneri and L.M. Lechuga  
**2018 Europtrode XIV Conference on Optical Chemical Sensors and Biosensors** - Naples, Italy

**Fast, multiplex and label-free quantification of sepsis biomarkers with an innovative optical point-of-care platform – Oral**

N. Fabri-Faja, O. Calvo, P. Dey, R. A. Terborg, M.C. Estévez, F. Yesilköy, J. Pello, A. Fàbrega, J. C. Ruiz-Rodríguez, A. Belushkin, J. González-López, H. Altug, V. Pruneri and L. M. Lechuga  
**2018 Ibersensors 11<sup>th</sup> Ibero-American Congress on Sensors** – Barcelona, Spain

**Label-free, scalable and point-of-care imaging platform for rapid analysis of biomarker**

L. Duempelmann, R.A Terborg, J. Pello, I. Mannelli, F. Yesilkoy, A.A. Belushkin, Y. Jahani, N. Fabri-Faja, P. Dey, O. Calvo-Lozano, M.-C. Estevez, L.M. Lechuga, H. Altug and V. Pruneri  
**2019 SPIE Photonics West**, San Francisco, USA

**Label-free imaging platform for rapid analysis of biomarker**

L. Duempelmann, R.A Terborg, J. Pello, I. Mannelli, F. Yesilkoy, A.A. Belushkin, Y. Jahani, N. Fabri-Faja, P. Dey, O. Calvo-Lozano, M.-C. Estevez, Anna Fàbrega, Juan J. González-López, L.M. Lechuga, H. Altug and V. Pruneri  
**2019 45th International Conference on Micro & Nano Engineering** - Rhodes, Greece

**Lens-free Interferometric Microscope for Point-of-Care Label-free Detection of Sepsis Biomarkers**

R.A. Terborg, L. Duempelmann, J. Pello, A. Noyan, F. Yesilkoy, A. Belushkin, Y. Jahani, N. Fabri-Faja, P. Dey, O. Calvo-Lozano, M.-C. Estevez, A. Fàbrega, J.J. González-López, L.M. Lechuga, H. Altug, V. Pruneri.  
Frontiers in Optics and Laser Science- Washington DC, USA





## References

1. Sinha, M. *et al.* Emerging Technologies for Molecular Diagnosis of Sepsis. *Clin. Microbiol. Rev.* **31**, (2018).
2. Quesada-González, D. & Merkoçi, A. Nanomaterial-based devices for point-of-care diagnostic applications. *Chem. Soc. Rev.* (2018).
3. Xu, D., Huang, X., Guo, J. & Ma, X. Automatic smartphone-based microfluidic biosensor system at the point of care. *Biosens. Bioelectron.* **110**, 78–88 (2018).
4. Zarei, M. Infectious pathogens meet point-of-care diagnostics. *Biosens. Bioelectron.* **106**, 193–203 (2018).
5. Swierczewska, M., Liu, G., Lee, S. & Chen, X. High-sensitivity nanosensors for biomarker detection. *Chemical Society Reviews* **41**, 2641–2655 (2012).
6. Luque-Garcia, J. L. & Neubert, T. A. Sample preparation for serum/plasma profiling and biomarker identification by mass spectrometry. *J. Chromatogr. A* **1153**, 259–276 (2007).
7. Salzman, G., Singham, S.B., Johnston, R.G., Bohren, C. F. *Light scattering and cytometry - Flow cytometry and sorting*. (John-Wiley, 1990).
8. Pinder, A.C., Purdy, P.W., Poulter, S.A.G., Clark, D. C. Validation of flow cytometry for rapid enumeration of bacterial concentrations in pure cultures. *J. Appl. Bacteriol.* **69**, 92–100 (1990).
9. Lloyd, D. *Flow Cytometry in Microbiology*. (Springer- Verlag London Limited, 1991).
10. Ivnitski, D., Abdel-Hamid, I., Atanasov, P. & Wilkins, E. *Biosensors for detection of pathogenic bacteria*. *Biosensors & Bioelectronics* **14**, (1999).
11. Bunn, T. W. & Sikarwar, A. S. Diagnostics: conventional vs. Modern Methods. *J. Adv. Med. Pharm. Sci.* **8**, 1–7 (2016).
12. Opota, O., Jatou, K. & Greub, G. Microbial diagnosis of bloodstream infection: towards molecular diagnosis directly from blood. *Clin. Microbiol. Infect.* **21**, 323–331 (2015).

13. Opota, O., Croxatto, A., Prod'hom, G. & Greub, G. Blood culture-based diagnosis of bacteraemia: state of the art. *Clin. Microbiol. Infect.* **21**, 313–322 (2015).
14. Masson, J.-F. Surface Plasmon Resonance Clinical Biosensors for Medical Diagnostics. *ACS Sensors* **2**, 16–30 (2017).
15. Thevenot, D. R., Toth, K., Durst, R. A. & Wilson, G. S. Electrochemical biosensors: Recommended definitions and classification. *Pure Appl. Chem* **71**, 2333–2348 (1999).
16. Yoon, J.-Y. Introduction. in *Introduction to Biosensors* 229–255 (Springer International Publishing, 2016).
17. Estevez, M. C., Alvarez, M. & Lechuga, L. M. Integrated optical devices for lab-on-a-chip biosensing applications. *Laser Photon. Rev.* **6**, 463–487 (2012).
18. Ahmed, A., Rushworth, J. V, Hirst, N. A. & Millner, P. A. Biosensors for whole-cell bacterial detection. *Clin. Microbiol. Rev.* **27**, 631–646 (2014).
19. Clark, L. & Lyons, C. Electrode Systems for Continuous Monitoring in Cardiovascular Surgery. *Ann. N. Y. Acad. Sci.* **102**, 29–45 (1962).
20. Kadish, A. H. & Hall, D. A. A New Method for the Continuous Monitoring of Blood Glucose by Measurement of Dissolved Oxygen. *Clin. Chem.* **11**, (1965).
21. Clark, L.C., J. 539,455. (1970).
22. Freedberg, K. A. *et al.* Diagnostic point-of-care tests in resource-limited settings. *Lancet Infect. Dis.* **14**, 239–249 (2013).
23. Meagher, R. J., Hatch, A. V., Renzi, R. F. & Singh, A. K. An integrated microfluidic platform for sensitive and rapid detection of biological toxins. *Lab Chip* **8**, 2046–2053 (2008).
24. Schudel, B. R., Tanyeri, M., Mukherjee, A., Schroeder, C. M. & Kenis, P. J. A. Multiplexed detection of nucleic acids in a combinatorial screening chip. *Lab Chip* **11**, 1916–1923 (2011).
25. Gubala, V., Harris, L. F., Ricco, A. J., Tan, M. X. & Williams, D. E. Point of care diagnostics: Status and future. *Anal. Chem.* **84**, 487–515 (2012).

26. Dincer, C., Bruch, R., Kling, A., Dittrich, P. S. & Urban, G. A. Multiplexed Point-of-Care Testing – xPOCT. *Trends Biotechnol.* **35**, 728–742 (2017).
27. Wang, J. *et al.* A self-powered, one-step chip for rapid, quantitative and multiplexed detection of proteins from pinpricks of whole blood. *Lab Chip* **10**, 3157–3162 (2010).
28. Jönsson, C. *et al.* Silane-dextran chemistry on lateral flow polymer chips for immunoassays. *Lab Chip* **8**, 1191–1197 (2008).
29. Madou, M. *et al.* Lab on a Cd. *Annu. Rev. Biomed. Eng.* **8**, 601–628 (2006).
30. Ducrée, J. *et al.* The centrifugal microfluidic Bio-Disk platform. *J. Micromechanics Microengineering* **17**, (2007).
31. Lehman, C. A., Price, C. P., St. John, A. & Hicks, J. *Point-of-care testing*. (American Association for Clinical Chemistry Inc., 2004).
32. Laurence, C. O., Moss, J. R., Briggs, N. E. & Beilby, J. J. The cost-effectiveness of point of care testing in a general practice setting: Results from a randomised controlled trial. *BMC Health Serv. Res.* **10**, (2010).
33. Response Biomedical Corp. Available at: <http://responsebio.com/>. (Accessed: 10th August 2018)
34. Gallegos, D. *et al.* Label-free biodetection using a smartphone. *Lab Chip* **13**, 2124 (2013).
35. Breslauer, D. N., Maamari, R. N., Switz, N. A., Lam, W. A. & Fletcher, D. A. Mobile Phone Based Clinical Microscopy for Global Health Applications. *PLoS One* **4**, 6320 (2009).
36. Smith, Z. J., Chu, K., Espenson, A. R., Rahimzadeh, M. & Gryshuk, A. Cell-Phone-Based Platform for Biomedical Device Development and Education Applications. *PLoS One* **6**, 17150 (2011).
37. Bandodkar, A. J. & Wang, J. Non-invasive wearable electrochemical sensors: A review. *Trends Biotechnol.* **32**, 363–371 (2014).
38. Graf, H. & Mühlemann, H. R. Oral telemetry of fluoride ion activity. *Arch. Oral Biol.* **14**, 259-IN3 (1969).
39. Graf, H. & Mühlemann, H. R. Telemetry of plaque pH from interdental area. *Helv. Odontol. Acta* **10**, 94–101 (1966).



40. Kumar, S., Rai, P., Sharma, J. G., Sharma, A. & Malhotra, B. D. PEDOT:PSS/PVA-Nanofibers-Decorated Conducting Paper for Cancer Diagnostics. *Adv. Mater. Technol.* **1**, 1–8 (2016).
41. Modali, A., Vanjari, S. R. K. & Dendukuri, D. Wearable Woven Electrochemical Biosensor Patch for Non-invasive Diagnostics. *Electroanalysis* **28**, 1276–1282 (2016).
42. Ren, K., Zhou, J. & Wu, H. Materials for microfluidic chip fabrication. *Acc. Chem. Res.* **46**, 2396–2406 (2013).
43. Mabey, D., Peeling, R. W., Ustianowski, A. & Perkins, M. D. Diagnostics for the developing world. *Nat. Rev. Microbiol.* **2**, 231–240 (2004).
44. ASSURED diagnostics | i-sense. Available at: <https://www.i-sense.org.uk/infectious-diseases/assured-diagnostics>. (Accessed: 10th August 2018)
45. Narayanaswamy, R. & Wolfbeis, O. S. *Optical sensors*. (Springer Berlin Heidelberg, 2004).
46. Ligler, F. S. & Taitt, C. A. R. *Optical biosensors: Today and Tomorrow*. (Elsevier, 2011).
47. Schmit, K. & Hoffman, C. High-Refractive-Index Waveguide Platforms for Chemical and Biosensing. in *Optical Guided-wave Chemical and Biosensors I* (ed. Urban, G. A.) 21–54 (Springer Berlin Heidelberg, 2010).
48. Lopez, G. A., Estevez, M. C., Soler, M. & Lechuga, L. M. Recent advances in nanoplasmonic biosensors: Applications and lab-on-a-chip integration. *Nanophotonics* **6**, 123–136 (2017).
49. Passaro, Vittorio M. N Dell’Olio, Francesco Casamassima, Biagio De Leonardi, F. Guided-Wave Optical Biosensors. *sensors* **7**, 508–536 (2007).
50. Homola, J. Surface Plasmon Resonance Biosensors for Food Safety. in *Optical Sensors* (ed. Wolfbeis, O. S.) 145–172 (Springer Berlin Heidelberg, 2004).
51. Brolo, A. G., Gordon, R. & Sinton, D. Nanohole Arrays in Metal Films at Integrated Chemical Sensors and Biosensors. in *Optical Guided-wave Chemical and Biosensors I* (ed. Urban, G. A.) 155–179 (Springer Berlin Heidelberg, 2010).

52. Barnes, W. L., Dereux, A. & Ebbesen, T. W. Surface plasmon subwavelength optics. *insight Rev. Artic.* **424**, (2003).
53. Liedberg, B., Nylander, C. & Lunström, I. Surface plasmon resonance for gas detection and biosensing. *Sensors and Actuators* **4**, 299–304 (1983).
54. Kambhampati, D. K. & W. Knoll. Surface-plasmon optical techniques. *Curr. Opin. Colloid Interface Sci.* **4**, (1999).
55. Homola, J., Yee, S. & Gauglitz, G. Surface plasmon resonance sensors: review. *Sensors Actuators B* **54**, 3–15 (1999).
56. Thammacharoen, C., Yu, F., Ekgasit, S. & Knoll, W. Influence of the Metal Film Thickness on the Sensitivity of Surface Plasmon Resonance Biosensors. *Appl. Spectrosc.* **59**, 661–667 (2005).
57. Piliarik, M. & Homola, J. Surface plasmon resonance (SPR) sensors: approaching their limits? *Opt. Express* **17**, 16505–16517 (2009).
58. Willets, K. A. & Van Duyne, R. P. Localized Surface Plasmon Resonance Spectroscopy and Sensing. *Annu. Rev. Phys. Chem.* **58**, 267–297 (2007).
59. Jackman, J. A., Ferhan, A. R. & Cho, N.-J. Nanoplasmonic sensors for biointerfacial science. *Chem. Soc. Rev.* **46**, 3485–3865 (2017).
60. Mazzotta F, Johnson TW, Dahlin AB, Shaver J, O. S.-H. et al. Influence of the evanescent field decay length on the sensitivity of plasmonic nanodisks and nanoholes. *ACS Photonics* **2**, 256–262 (2015).
61. Guo, L. *et al.* Strategies for enhancing the sensitivity of plasmonic nanosensors. *Nano Today* **10**, 213–239 (2015).
62. Willets, K. A. & Van Duyne, R. P. Localized Surface Plasmon Resonance Spectroscopy and Sensing. *Annu. Rev. Phys. Chem.* **58**, 267–297 (2007).
63. Christ, A. *et al.* Controlling the interaction between localized and delocalized surface plasmon modes: Experiment and numerical calculations. *Phys. Rev. B* **74**, (2006).
64. Nau, D. *et al.* Correlation Effects in Disordered Metallic Photonic Crystal Slabs. *Phys. Rev. Lett.* 133902. (2007).

65. Rockstuhl, C., Lederer, F., Zentgraf, T. & Giessen, H. Enhanced transmission of periodic, quasiperiodic, and random nanoaperture arrays. *Appl. Phys. Lett.* **91**, 151109 (2007).
66. Gordon, R., Sinton, D., Kavanagh, K. L. & Brolo, A. G. A New Generation of Sensors Based on Extraordinary Optical Transmission. *Acc. Chem. Res.* **41**, 1049–1057 (2008).
67. Ebbesen, T. W., Lezec, H. J., Ghaemi, H. F., Thio, T. & Wolff, P. A. Extraordinary optical transmission through sub-wavelength hole arrays. *Nature* **391**, 667–669 (1998).
68. Zhu, X. *et al.* Oblique-incidence reflectivity difference microscope for label-free high-throughput detection of biochemical reactions in a microarray format. *Appl. Opt.* **46**, 1890 (2007).
69. Duer, R., Lund, R., Tanaka, R., Christensen, D. A. & Herron, J. N. In-plane parallel scanning: A microarray technology for point-of-care testing. *Anal. Chem.* **82**, 8856–8865 (2010).
70. Mace, C. R., Striemer, C. C. & Miller, B. L. Theoretical and experimental analysis of arrayed imaging reflectometry as a sensitive proteomics technique. *Anal. Chem.* **78**, 5578–5583 (2006).
71. Kemmler, M., Sauer, U., Schleicher, E., Preininger, C. & Brandenburg, A. Biochip point-of-care device for sepsis diagnostics. *Sensors Actuators, B Chem.* **192**, 205–215 (2014).
72. Zhu, X. *et al.* Oblique-incidence reflectivity difference microscope for label-free high-throughput detection of biochemical reactions in a microarray format. *Appl. Opt.* **46**, 1890 (2007).
73. Scarano, S., Mascini, M., Turner, A. P. F. F., Minnuni, M. & Minunni, M. Surface Plasmon resonance imaging for affinity-based biosensors. *Biosens. Bioelectron.* **25**, 957–966 (2010).
74. Puiu, M. & Bala, C. SPR and SPR Imaging: Recent Trends in Developing Nanodevices for Detection and Real-Time Monitoring of Biomolecular Events. *sensors* **16**, 1–15 (2016).
75. Mace, C. R., Striemer, C. C. & Miller, B. L. Detection of human proteins using arrayed imaging reflectometry. *Biosens. Bioelectron.* **24**, 334–337 (2008).
76. Bucukovski, J. *et al.* Label-free microarray-based detection of autoantibodies in human serum. *J. Immunol. Methods* **459**, 44–49 (2018).

77. Carter, J. A., Triplett, E., Striemer, C. C. & Miller, B. L. A label-free, multiplex competitive assay for small molecule pollutants. *Biosens. Bioelectron.* **77**, 1–6 (2016).
78. Jeong, M. L. *et al.* Direct immobilization of protein G variants with various numbers of cysteine residues on a gold surface. *Anal. Chem.* **79**, 2680–2687 (2007).
79. Gorodkiewicz, E. E. *et al.* Surface plasmon resonance imaging biosensor for cathepsin G based on a potent inhibitor: Development and applications. *Anal. Biochem.* **423**, 218–223 (2012).
80. Nelson, B. P., Grimsrud, T. E., Liles, M. R., Goodman, R. M. & Corn, R. M. Surface Plasmon Resonance Imaging Measurements of DNA and RNA Hybridization Adsorption onto DNA Microarrays. *Anal. Chem.* **73**, 1–7 (2001).
81. Angenendt, P. Progress in Protein and Antibody microarray technology. *Drug Discov. Today* **10**, 503–511 (2005).
82. Tang, C. K., Vaze, A. & Rusling, J. F. Fabrication of immunosensor microwell arrays from gold compact discs for detection of cancer biomarker proteins. *Lab Chip* **12**, 281–286 (2012).
83. Arnandis-Chover, T., Morais, S., Ángel González-Martínez, M., Puchades, R. & Maquieira, Á. High density MicroArrays on Blu-ray discs for massive screening. *Biosens. Bioelectron.* **51**, 109–114 (2013).
84. Romanov, V. *et al.* A critical comparison of protein microarray fabrication technologies. *Analyst* **139**, 1303–1326 (2014).
85. Aguilar-Mahecha, A., Hassan, S., Ferrario, C. & Basik, M. Microarrays as Validation Strategies in Clinical Samples: Tissue and Protein Microarrays. *Omi. A J. Integr. Biol.* **10**, 311–326 (2006).
86. Berrade, L., Garcia, A. E. & Camarero, J. A. Protein Microarrays: Novel Developments and Applications. *Pharm. Res* **28**, 1480–1499 (2011).
87. Wu, P. & Grainger, D. W. Toward immobilized antibody microarray optimization: print buffer and storage condition comparisons on performance. *Biomed. Sci. Instrum.* **40**, 243–8 (2004).
88. Wu, P., Castner, D. G. & Grainger, D. W. Diagnostic devices as biomaterials: a review of nucleic acid and protein microarray surface performance issues. *J. Biomater. Sci. Polym. Ed.* **19**, 725–753 (2008).

89. Gong, P. & Grainger, D. W. Nonfouling Surfaces: a review of principles and applications for microarray capture assay designs. in *Microarrays* **381**, 59–92 (Humana Press, 2007).
90. Wu, P. & Grainger, D. W. Comparison of Hydroxylated Print Additives on Antibody Microarray Performance. *J. Proteome Res.* **5**, 2956–2965 (2006).
91. Sokolik, C. W., Walker, A. S. & Nishioka, G. M. A simple and sensitive Assay for Measuring Very small Volumes of Microprinted solutions. *Anal. Chem. Insights* **6**, 61–66 (2011).
92. Arrabito, G. & Pignataro, B. Solution Processed Micro- and Nano-Bioarrays for Multiplexed Biosensing. *Anal. Chem.* **84**, (2012).
93. Barbulovic-Nad, I. *et al.* Bio-Microarray Fabrication Techniques—A Review. *Crit. Rev. Biotechnol.* **26**, 237–259 (2006).
94. Piner, R. D., Zhu, J., Xu, F., Hong, S. & Mirkin, C. A. “Dip-Pen” Nanolithography. *Science* (80-. ). **283**, 661–664 (1999).
95. Ginger, D. S., Zhang, H. & Mirkin, C. A. The Evolution of Dip-Pen Nanolithography. *Angew. Chemie Int. Ed.* **43**, 30–45 (2004).
96. Rozhok, S., Piner, R. & Mirkin, C. A. Dip-Pen Nanolithography : What Controls Ink Transport? *J. Phys. Chem. B* **107**, 751–757 (2003).
97. Mrksich, M. What can surface chemistry do for cell biology? *Curr. Opin. Chem. Biol.* **6**, 794–797 (2002).
98. Joyce, G. F. Toward an Alternative Biology. *Science* (80-. ). **336**, 307–308 (2012).
99. Campbell, M. A. & Wengel, J. Locked vs. unlocked nucleic acids (LNA vs. UNA): contrasting structures work towards common therapeutic goals. *This J. is Cite this Chem. Soc. Rev* **40**, 5680–5689 (2011).
100. Appella, D. H. Non-natural Nucleic Acids for Synthetic Biology. *Curr Opin Chem Biol* **13**, 687–696 (2009).
101. Hasegawa, H., Savory, N., Abe, K. & Ikebukuro, K. Methods for improving aptamer binding affinity. *Molecules* **21**, (2016).
102. Lippa, P. B., Sokoll, L. J. & Chan, D. W. Immunosensors—principles and applications to clinical chemistry. *Clin. Chim. Acta* **314**, 1–26 (2001).

103. Bazin, I., Tria, S. A., Hayat, A. & Marty, J. L. New biorecognition molecules in biosensors for the detection of toxins. *Biosens. Bioelectron.* **87**, 285–298 (2017).
104. Conroy, P. J., Hearty, S., Leonard, P. & O’Kennedy, R. J. Antibody production, design and use for biosensor-based applications. *Semin. Cell Dev. Biol.* **20**, 10–26 (2009).
105. Srivastava, A., O’Connor, I. B., Pandit, A. & Gerard Wall, J. Polymer-antibody fragment conjugates for biomedical applications. *Prog. Polym. Sci.* **39**, 308–329 (2014).
106. Byrne, B., Stack, E., Gilmartin, N. & O’Kennedy, R. Antibody-based sensors: Principles, problems and potential for detection of pathogens and associated toxins. *sensors* **9**, 4407–4445 (2009).
107. Essandoh, K. & Fan, G.-C. C. Role of extracellular and intracellular microRNAs in sepsis. *Biochim. Biophys. Acta - Mol. Basis Dis.* **1842**, 2155–2162 (2014).
108. Tupchong, K., Koyfman, A. & Foran, M. Sepsis, severe sepsis, and septic shock: A review of the literature. *African J. Emerg. Med.* **5**, 127–135 (2015).
109. Caserta, S. *et al.* Circulating Plasma microRNAs can differentiate Human Sepsis and Systemic Inflammatory Response Syndrome (SIRS). *Sci. Rep.* **6**, 1–13 (2016).
110. Zhang, J., Cheng, Y., Duan, M., Qi, N. & Liu, J. Unveiling differentially expressed genes upon regulation of transcription factors in sepsis. *3 Biotech* **7**, 1–8 (2017).
111. Prucha, M., Bellingan, G. & Zazula, R. Sepsis biomarkers. *Clin. Chim. Acta* **440**, 97–103 (2015).
112. Epstein, L., Dantes, ; Ray, Magill, S. & Fiore, A. Varying Estimates of Sepsis Mortality Using Death Certificates and Administrative Codes- United States, 1999-2014. *Morb. Mortal. Wkly. Rep.* **65**, 342–345 (2016).
113. Álvaro-Meca, A. *et al.* Epidemiological trends of sepsis in the twenty-first century (2000-2013): an analysis of incidence, mortality, and associated costs in Spain. *Popul. Health Metr.* **16**, 1–11 (2018).
114. Markets and Markets. *Sepsis Diagnostics Market by Technology, Product, Method, Test type, Pathogen and End User - 2023.*

115. Faix, J. d. Biomarkers of Sepsis. *Crit. Rev. Clin. Lab. Sci.* **50**, 23–26 (2013).
116. Huang, J. *et al.* Identification of MicroRNA as sepsis biomarker based on miRNAs regulatory network analysis. *Biomed Res. Int.* **2014**, (2014).
117. Shapiro, N. I. *et al.* A prospective, multicenter derivation of a biomarker panel to assess risk of organ dysfunction, shock, and death in emergency department patients with suspected sepsis. *Crit. Care Med.* **37**, 96–104 (2009).
118. Jekarl, D. W. *et al.* Procalcitonin as a diagnostic marker and IL-6 as a prognostic marker for sepsis. *Diagn. Microbiol. Infect. Dis.* **75**, 342–347 (2013).
119. Clyne, B. & Olshaker, J. S. The C-reactive protein. *J. Emerg. Med.* **17**, 1019–1025 (1999).
120. Sierra, R. *et al.* C-reactive protein used as an early indicator of infection in patients with systemic inflammatory response syndrome. *Intensive Care Med* **30**, 2038–2045 (2004).
121. Riedel, S. & Carroll, K. C. Early Identification and Treatment of Pathogens in Sepsis Molecular Diagnostics and Antibiotic Choice. *Clin. Chest Med.* **37**, 191–207 (2016).
122. Petti, C. A. *et al.* Utility of Extended Blood Culture Incubation for Isolation of Haemophilus, Actinobacillus, Cardiobacterium, Eikenella, and Kingella Organisms: a Retrospective Multicenter Evaluation. *J. Clin. Microbiol.* **44**, 257–259 (2006).
123. Baron, E. J., Scott, J. D. & Tompkins, L. S. Prolonged Incubation and Extensive Subculturing Do Not Increase Recovery of Clinically Significant Microorganisms from Standard Automated Blood Cultures. *Clin. Infect. Dis.* **41**, 1677–1680 (2005).
124. Fauci, A. S. & Marston, H. D. The Perpetual Challenge of Antimicrobial Resistance. *JAMA* **311**, 1853 (2014).
125. Ventola, C. L. The Antibiotic Resistance Crisis. *Pharm. Ther.* **40**, 278–283 (2015).
126. Dellinger, R. P. *et al.* Surviving Sepsis Campaign. International guidelines for Management of severe sepsis and sepsis shock: 2012. *Crit. Care Med.* **41**, 580–637 (2013).

127. Kollef, M. H., Sherman, G., Ward, S. & Fraser, V. J. Inadequate Antimicrobial Treatment of Infections. *Chest* **115**, 462–474 (2003).
128. Garnacho-Montero, J. *et al.* Impact of adequate empirical antibiotic therapy on the outcome of patients admitted to the intensive care unit with sepsis. *Crit. Care Med.* **31**, 2742–2751 (2003).
129. Vallés, J., Rello, J., Ochagavía, A., Garnacho, J. & Alcalá, M. A. Community-Acquired Bloodstream Infection in Critically Ill Adult Patients: Impact of Shock and Inappropriate Antibiotic Therapy on Survival. *Chest* **123**, 1615–1624 (2003).
130. Weiss, S. L. *et al.* Delayed Antimicrobial Therapy Increases Mortality and Organ Dysfunction Duration in Pediatric Sepsis. *Crit Care Med* **42**, 2409–2417 (2014).
131. Kumar, A. *et al.* Initiation of Inappropriate Antimicrobial Therapy Results in a Fivefold Reduction of Survival in Human Septic Shock. *Chest* **136**, 1237–1248 (2009).
132. Kofoed, K. *et al.* Use of plasma C-reactive protein, procalcitonin, neutrophils, macrophage migration inhibitory factor, soluble urokinase-type plasminogen activator receptor, and soluble triggering receptor expressed on myeloid cells-1 in combination to diagnose infections. *Crit. Care* **11**, 1–10 (2007).
133. Andaluz-Ojeda, D. *et al.* A combined score of pro- and anti-inflammatory interleukins improves mortality prediction in severe sepsis. *Cytokine* **57**, 332–336 (2012).
134. Yesilkoy, F. *et al.* Phase-sensitive plasmonic biosensor using a portable and large field of view interferometric microarray imager. *Light Sci. Appl.* (2018).
135. Zernike, F. Phase contrast, a new method for the microscopic observation of transparent objects. *Physica* **9**, 686–698 (1942).
136. Fürhapter, S., Jesacher, A., Bernet, S. & Ritsch-Marte, M. Spiral phase contrast imaging in microscopy. *Opt. Express* **13**, 689–694 (2005).
137. Gabor, D. Microscopy by Reconstructed Wave-Fronts. *Proc. R. Soc. A Math. Phys. Eng. Sci.* **197**, 454–487 (1949).
138. Vanligten, R. F. & Osterberg, H. Holographic microscopy. *Nature* **211**, 282–283 (1966).



139. Zhang, T. & Yamaguchi, I. Three-dimensional microscopy with phase-shifting digital holography. *Opt. Lett.* **23**, 1221 (1998).
140. Allen, R. D., David, G. B. & Nomarski, G. The Zeiss-Nomarski differential interference equipment for transmitted-light microscopy. *Z. Wiss. Mikrosk.* **69**, 193–221 (1969).
141. Mudanyali, O. *et al.* Wide-field optical detection of nanoparticles using on-chip microscopy and self-assembled nanolenses. *Nat. Photonics* **7**, 247–254 (2013).
142. Greenbaum, A. *et al.* Imaging without lenses: achievements and remaining challenges of wide-field on-chip microscopy. *Nat. Methods* **9**, 889–895 (2012).
143. Repetto, L., Piano, E. & Pontiggia, C. Lensless digital holographic microscope with light-emitting diode illumination. *Opt. Lett.* **29**, 1132 (2004).
144. Cui, X. *et al.* Lensless high-resolution on-chip optofluidic microscopes for *Caenorhabditis elegans* and cell imaging. *Proc. Natl. Acad. Sci.* **105**, 10670–10675 (2008).
145. Isikman, S. O. *et al.* Lens-free optical tomographic microscope with a large imaging volume on a chip. *Proc. Natl. Acad. Sci.* **108**, 7269–7301 (2011).
146. Cetin, A. E. *et al.* Handheld high-throughput plasmonic biosensor using computational on-chip imaging. *Light Sci. Appl.* **3**, e122 (2014).
147. Pérez, J. M. *et al.* An image cytometer based on angular spatial frequency processing and its validation for rapid detection and quantification of waterborne microorganisms. *Analyst* **140**, 7734 (2015).
148. Illumination in Microscopy. Phase Contrast Illumination. Available at: <http://www.microscopy-uk.org.uk/mag/artmar06/go-phase.html>. (Accessed: 19th May 2019)
149. Egelberk. File:Phase-Phase Contrast.jpg - Wikimedia Commons. Available at: [https://commons.wikimedia.org/wiki/File:Phase-Phase\\_Contrast.jpg](https://commons.wikimedia.org/wiki/File:Phase-Phase_Contrast.jpg). (Accessed: 19th May 2019)
150. Lang, W. Nomarski differential interference-contrast microscopy. *ZEISS Inf.* **70**, 114–120 (1968).

151. Terborg, R. A., Pello, J., Mannelli, I., Torres, J. P. & Pruneri, V. Ultrasensitive interferometric on-chip microscopy of transparent objects. *Sci. Adv.* **2**, e1600077 (2016).
152. Barbarossa, G., Pruneri, V., Jore Cruanyes, M., Martinez Cordero, P. A. & Luca Janer, D. Apparatus and Method for Optical Interrogation. (2011).
153. Ekşioğlu, Y., Cetin, A. E. & Petráček, J. Optical Response of Plasmonic Nanohole Arrays: Comparison of Square and Hexagonal Lattices. *Plasmonics* **11**, 851–856 (2016).
154. Lin, B. J. Deep uv lithography. *J. Vac. Sci. Technol.* **12**, 1317–1320 (1975).
155. Dunbar, L. A. *et al.* Talbot Lithography as an Alternative for Contact Lithography for Submicron Features. *Proc. SPIE* **8974**, (2014).
156. Solak, H. H., Dais, C. & Clube, F. Displacement Talbot lithography: a new method for high-resolution patterning of large areas. *Opt. Express* **19**, 10686–10691 (2011).
157. Homola, J. Surface Plasmon Resonance Sensors for Detection of Chemical and Biological Species. *Chem. Rev.* **108**, 462–493 (2008).
158. Cottier, K., Wiki, M., Voirin, G., Gao, H. & Kunz, R. E. Label-free highly sensitive detection of (small) molecules by wavelength interrogation of integrated optical chips. *Sensors Actuators B* **91**, 241–251 (2003).
159. Lambeck, P. V. Integrated optical sensors for the chemical domain. *Meas. Sci. Technol.* **17**, R93–R116 (2006).
160. Zinoviev, K. *et al.* Silicon Photonic Biosensors for Lab-on-a-Chip Applications. *Adv. Opt. Technol.* **2008**, 1–6 (2008).
161. Zinoviev, K. E., Gonzalez-Guerrero, A. B., Dominguez, C. & Lechuga, L. M. Integrated Bimodal Waveguide Interferometric Biosensor for Label-Free Analysis. *J. Light. Technol.* **29**, 1926–1930 (2011).
162. Schmitt, K., Schirmer, B., Hoffmann, C., Brandenburg, A. & Meyrueis, P. Interferometric biosensor based on planar optical waveguide sensor chips for label-free detection of surface bound bioreactions. *Biosens. Bioelectron.* **22**, 2591–2597 (2007).

163. Ymeti, A. *et al.* Realization of a multichannel integrated Young interferometer chemical sensor. *Appl. Opt.* **42**, 5649–5660 (2003).
164. De Vos, K. *et al.* Nanophotonic Waveguides in Silicon-on-Insulator Fabricated with CMOS Technology. *Opt. Express* **15**, (2007).
165. Iqbal, M. *et al.* Label-Free Biosensor Arrays Based on Silicon Ring Resonators and High-Speed Optical Scanning Instrumentation. *IEEE J. Sel. Top. Quantum Electron.* **16**, 654–661 (2010).
166. Luchansky, M. S., Washburn, A. L., Martin, T. A., Gunn, L. C. & Bailey, R. C. Characterization of the evanescent field profile and bound mass sensitivity of a label-free silicon photonic microring resonator biosensing platform. *Biosens. Bioelectron.* **26**, 1283–1291 (2010).
167. De Vos, K. *et al.* Multiplexed antibody detection with an array of silicon-on-insulator microring resonators. *IEEE Photonics J.* **1**, 225–235 (2009).
168. Benesch, J., Askendal, A. & Tengvall, P. The determination of thickness and surface mass density of mesothick immunoprecipitate layers by null ellipsometry and protein<sup>125</sup>Iodine labeling. *J. Colloid Interface Sci.* **249**, 84–90 (2002).
169. Jung, L. S., Campbell, C. T., Chinowsky, T. M., Mar, M. N. & Yee, S. S. Quantitative Interpretation of the Response of Surface Plasmon Resonance Sensors to Adsorbed Films. *Langmuir* **14**, 5636–5648 (1998).
170. Vörös, J. The density and refractive index of adsorbing protein layers. *Biophys. J.* **87**, 553–561 (2004).
171. Rabe, M., Verdes, D. & Seeger, S. Understanding protein adsorption phenomena at solid surfaces. *Adv. Colloid Interface Sci.* **162**, 87–106 (2011).
172. Jonkheijm, P., Weinrich, D., Schröder, H., Niemeyer, C. M. & Waldmann, H. Chemical strategies for generating protein biochips. *Angew. Chemie - Int. Ed.* **47**, 9618–9647 (2008).
173. Sassolas, A., Blum, L. J. & Leca-Bouvier, B. D. Immobilization strategies to develop enzymatic biosensors. *Biotechnol. Adv.* **30**, 489–511 (2012).

174. Ericsson, E. Biosensor surface chemistry for oriented protein immobilization and biochip patterning. (Linköping University, Sweden, 2013).
175. Makaraviciute, A. & Ramanaviciene, A. Site-directed antibody immobilization techniques for immunosensors. *Biosens. Bioelectron.* **50**, 460–471 (2013).
176. Tsougeni, K. *et al.* Three-dimensional (3D) plasma micro-nanotextured slides for high performance biomolecule microarrays: Comparison with epoxy-silane coated glass slides. *Colloids Surfaces B Biointerfaces* **165**, 270–277 (2018).
177. Bain, C. D. *et al.* Formation of Monolayer Films by Spontaneous Assembly of Organic Thiols from solution onto Gold. *J. Chem. Soc., Chem. Commun* **111**, 3559–3568 (1989).
178. Schaeferling, M. *et al.* Application of self-assembly techniques in the design of biocompatible protein microarray surfaces. *Electrophoresis* **23**, 3097–3105 (2002).
179. Hermanson, G. T. *Bioconjugate techniques*. (Elsevier Science Publishing Co Inc, 2013).
180. Arrabito, G., Pignataro, B. & Arrabito, G. Solution Processed Micro- and Nano-Bioarrays for Multiplexed Biosensing. (2012). doi:10.1021/ac300621z
181. Gau, J.-J., Lan, E. H., Dunn, B., Ho, C.-M. & Woo, J. C. S. A MEMS based amperometric detector for E. Coli bacteria using self-assembled monolayers. *Biosens. Bioelectron.* **16**, 745–755 (2001).
182. Tisone, T. C. & Tonkinson, J. L. Non-contact dispensing for protein microarrays. in *Protein Microarrays* (M. Schena M, Jones & Bartlett Learning, 2005).
183. Chen, Z., Dodig-Crnković, T., Schwenk, J. M. & Tao, S.-C. Current applications of antibody microarrays. *Clin. Proteomics* **15**, 7 (2018).
184. Angenendt, P., Glökler, J., Murphy, D., Lehrach, H. & Cahill, D. J. Toward optimized antibody microarrays: a comparison of current microarray support materials. *Anal. Biochem.* **309**, 253–260 (2002).
185. Soler, M. *et al.* Direct Detection of Protein Biomarkers in Human Fluids Using Site-Specific Antibody Immobilization Strategies. *Sensors* **14**, 2239–2258 (2014).

186. Rhodes, B., Fürnrohr, B. G. & Vyse, T. J. C-reactive protein in rheumatology: Biology and genetics. *Nat. Rev. Rheumatol.* **7**, 282–289 (2011).
187. Meynaar, I. A., Droog, W., Batstra, M., Vreede, R. & Herbrink, P. In Critically Ill Patients, Serum Procalcitonin Is More Useful in Differentiating between Sepsis and SIRS than CRP, Il-6, or LBP. *Crit. Care Res. Pract.* **2011**, (2011).
188. Wacker, C., Prkno, A., Brunkhorst, F. M. & Schlattmann, P. Procalcitonin as a diagnostic marker for sepsis: a systematic review and meta-analysis. *Lancet Infect. Dis.* **13**, 426–435 (2013).
189. Georgopoulou, A.-P. *et al.* Early changes of procalcitonin may advise about prognosis and appropriateness of antimicrobial therapy in sepsis. *J. Crit. Care* **26**, 331.e1-331.e7 (2011).
190. Rodríguez-Gaspar, M. *et al.* Prognostic value of cytokines in SIRS general medical patients. *Cytokine* **15**, 232–236 (2001).
191. Messer, J., Donato, L., Gallati, H., Matis, J. & Simeoni, U. Evaluation of interleukin-6 and soluble receptors of tumor necrosis factor for early diagnosis of neonatal infection. *J. Pediatr.* **129**, 574–80 (1996).
192. Aznar-Oroval, E. *et al.* Diagnostic value of procalcitonin, interleukin 8, interleukin 6, and c-reactive protein for detecting bacteremia and fungemia in cancer patients. *Enferm. Infecc. Microbiol. Clin.* **28**, 273–277 (2010).
193. Brodská, H. *et al.* Significantly higher procalcitonin levels could differentiate Gram-negative sepsis from Gram-positive and fungal sepsis. *Clin Exp Med* **13**, 165–170 (2013).
194. Charles, P. E. *et al.* Serum procalcitonin elevation in critically ill patients at the onset of bacteremia caused by either gram negative or gram positive bacteria. *BMC Infect. Dis.* **8**, 1–8 (2008).
195. Shrivastava, A. & Gupta, V. B. Methods for the determination of limit of detection and limit of quantitation of the analytical methods. *Chronicles Young Sci.* **2**, 21–25 (2011).
196. Buchegger, P. & Preininger, C. Four assay designs and on-chip calibration: Gadgets for a sepsis protein array. *Anal. Chem.* **86**, 3174–3180 (2014).

197. Tengvall, P., Lundström, I. & Liedberg, B. Protein adsorption studies on model organic surfaces: an ellipsometric and infrared spectroscopic approach. *Biomaterials* **19**, 407–422 (1998).
198. Wang, Z.-H., Viana, A. S. & Abrantes, L. M. Immunosensor interface based on physical and chemical immunoglobulin G adsorption onto mixed self-assembled monolayers. *Bioelectrochemistry* **69**, 180–186 (2006).
199. Dey, P. *et al.* Label-free Bacteria Quantification in Blood Plasma by a Bioprinted Microarray Based Interferometric Point-of-Care Device. *ACS Sensors* **4**, 52–60 (2018).
200. Yoo, S. M. & Lee, S. Y. Optical Biosensors for the Detection of Pathogenic Microorganisms. *Trends Biotechnol.* **34**, (2016).
201. Pang, P. *et al.* Detection of *Pseudomonas aeruginosa* using a wireless magnetoelastic sensing device. *Biosens. Bioelectron.* **23**, 295–299 (2007).

